Contents

Chapter 1

Introduction

The inverse scattering problem has been the subject of several mathematical investigations in the past [1]–[9] and it is nowadays a book material [10]–[11]. Its historical evolution can be found in Refs. [12]–[14] while its applications can be found mainly in Refs. [5]. [7], [10] and [15]. Frodberg [16] and Hylleraas [17] were the pioneers of the study of the inverse scattering problem and suggested a formal expansion for the potential with the S-wave phase shift being used as input data. The problem of different phase-equivalent potentials with the same bound state energy has been solved by Bargmann [18]–[19]. The ambiguity in the potential when related to the existence of a discrete spectrum was pointed out by Levinson [20] and discussed by Marchenko [21]–[22] as well as by Jost and Kohn [23], Borg [24] and Holmberg [25]. Gel'fand and Levitan [26] gave an alternative method to that of the S-matrix for the reconstruction of the potential from the spectral function. The method was applied by Jost and Kohn [27] who reached the same conclusion as Marchenko.

The quantum inverse scattering problem can be regarded nowadays as essential for developing techniques which can be used in non-destructive evaluation of materials, image science, remote sensing, plasma and nuclear physics, medical diagnostics, geophysics, seismology, astrophysics and radar [28]. Although the quantum inverse scattering problem is important for the development of a variety of techniques in diverse areas [6], not enough progress has been made in practical applications because the phase problem always was the major obstacle in using it. This is because one needs to know both the absolute value as well as the phase of the reflection coefficient $R(k)$, the latter being not easily measurable. Thus, in most instances only the reflectivity $|R(k)|$ can be obtained from measurements but not the phase δ. This is the famous age-old phase problem in diffraction analysis (see, for example, [29] and references therein) which has until now not been satisfactorily solved. Furthermore, the determination of the input kernel requires the knowledge from experiment of $R(k)$ for sufficiently large values of k so that the remainder of the Fourier integral can be neglected. Although the Fourier transform requires values of $R(k)$ also on the negative k axis, this problem can be solved by using the relation $R(-k) = R(k)^*$. Yet, another reason for the lack of progress can be attributed to the underlying numerical difficulties in solving the problem and it was only in recent years that accurate numerical solutions were obtained [29]–[32]. Sofianos *et. al* [32] used an efficient and accurate numerical algorithm employing Romberg integration to solve the one-dimensional coupled channel Marchenko integral equation (MIE) in the presence of thresholds.

In the present thesis we shall concentrate mainly on two aspects of the inverse scattering problem in one dimension. The first concerns the solution of the quantum inverse scattering problem; the second is related to seismic inversion and its application. We numerically treat scattering of an incident wave by a known potential and then reconstruct this potential from the calculated scattering data, namely, the reflection and transmission coefficients. These scattering data are obtained by solving the Schrödinger equation with the given boundary conditions by using the fourth-order Runge-Kutta method [33]–[36] to obtain the required reflection coefficient $R(k)$. The fast Fourier transform [37] is then used to calculate the input kernel to the Marchenko integral equation, the solution of which provides us with the scattering profiles.

We also apply the knowledge gained from the quantum inverse scattering problem to seismic reflection travel-time data in reflection seismology. This is known as the seismic inverse scattering problem. The seismic inverse scattering procedure became a popular method for the oil and gas exploration and motivated efforts to extract more information from the seismic reflection data [38]. Seismic surveys provide information about the subsurface layers and measure the time taken by the seismic waves to travel through the layers of the Earth and to be reflected back to the surface. This time is called the two-way travel-time.

The seismic reflection data can be used to gain some understanding of the characteristics of bottom layers. The seismic impedance of each layer, which is determined by the product of the velocity and density, is among the characteristics of the medium. In the case where the seismic impedance, reflectivity sequence and seismic wavelet are

not known, the inversion method is the suitable choice when only the seismic reflection data are available. In order to apply the seismic inverse scattering method to seismic reflection data, the one-dimensional classical wave equation can be transformed into a Schrödinger-like equation, the solution of which can provide the information about the scatterer or reflector by using the Marchenko integral equation. Assuming that the seismic wavelet remains unchanged during transmission through the medium (this is only valid for a limited range of frequencies) [39], then from the solution of the Marchenko integral equation we can obtain the seismic impedances of the reflecting layers of the medium.

To test the reliability of our approach, marine data from a deep water location in the North sea are considered. As the reflectivity sequence and seismic wavelet are unavailable, we obtain them by assuming that the seismic reflection data are the result of the reflectivity sequence convolved with the seismic wavelet plus noise. Thus, the extraction of the seismic wavelet and reflectivity sequence can be executed by applying a blind deconvolution technique with the reflectivity sequence assumed to be white in order for the random variables to be mutually independent [40]–[41]. Probabilistic models for the reflectivity sequence such as the Bernoulli-Gaussian white sequence model have been successfully used [40]–[43]. The Bernoulli-Gaussian model can simulate the reflectivity sequence when parameters are properly chosen. For our purpose, the blind deconvolution approach is based on the Bayesian procedure [44] which treats the unknown quantities as random variables. Thus, we apply a Markov Chain Monte Carlo (MCMC) procedure [45, 46, 47, 48] which, in our case, uses the Gibbs sampler.

This thesis is organized in the following manner: In Chapter 2, we briefly discuss the quantum scattering for single and coupled channels in one dimension. We consider three potentials by way of example, namely, Gaussian potential, smooth square-type potential and multi-layered potential to test our model. Chapter 3 treats the seismic scattering in layered media. The reflection and transmission coefficients for normally incident waves are derived. The solution of the quantum inverse scattering problem using the Marchenko integral equation is discussed in Chapter 4. Seismic inversion is also considered. In Chapter 5 we discuss the computational analysis needed for this study. We also discuss the blind deconvolution problem by applying the MCMC method in terms of the Gibbs sampler algorithm. The Bayesian probabilistic approaches are explored. Applications are handled in Chapters 6 through 8. Conclusions and directions for future work are given in Chapter 9.

Chapter 2

Quantum scattering in 1-D

In this chapter we shall discuss the Schrödinger equation for single and coupled channels.

2.1 Single channel Schrödinger equation

In the quantum scattering problem, knowing the potential one can obtain the wave function from which all physical information can be extracted. There are cases, however, in which the potential is not known and the relevant information about the system comes from the scattering and spectral data. Using these data one may reconstruct the potential profile and thus the physical information is again available. This is known as the inverse scattering problem.

We start by considering the x-axis divided into three regions where in region I : $x < 0$, in region II: $0 \leq x \leq a$ and in region III: $a < x$, a being the range of the potential. The time-independent Schrödinger equation can be written as

$$\frac{-\hbar^2}{2m}\frac{\partial^2\Psi(x)}{\partial x^2} + W(x)\Psi(x) = E\psi(x)\,, \tag{2.1}$$

where $W(x)$ denotes the potential function satisfying $W(x) = 0$ for $x < 0$ and $W(x) = 0$ for $x \geq a$ which is assumed to be time-independent. If the relations $k^2 = \frac{2m}{\hbar^2}E$ and $V(x) = \frac{2m}{\hbar^2}W(x)$ are substituted into Eq. (2.1), then the equation we obtain is

$$\frac{d^2\psi(x)}{dx^2} + (k^2 - V(x))\psi(x) = 0\,, \quad 0 \leq x \leq a\,. \tag{2.2}$$

For $x < 0$ and $x > a$ the potential is assumed to be zero and therefore

$$\frac{d^2\psi(x)}{dx^2} + k^2\psi(x) = 0\,, \quad x < 0\,, \quad x > a. \tag{2.3}$$

The asymptotic scattering solutions of Eq. (2.2) may be expressed in the form

$$\psi_I(k,x) = \mathrm{e}^{ikx} + R(k)\mathrm{e}^{-ikx}\,, \quad -\infty < x < 0\,, \tag{2.4}$$

and

$$\psi_{III}(k,x) = T(k)\mathrm{e}^{ikx}\,, \quad a < x < \infty\,, \tag{2.5}$$

where $R(k)$ and $T(k)$ are the reflection and transmission coefficients respectively.

2.1.1 Potentials used

In our investigation we shall consider the following potentials:

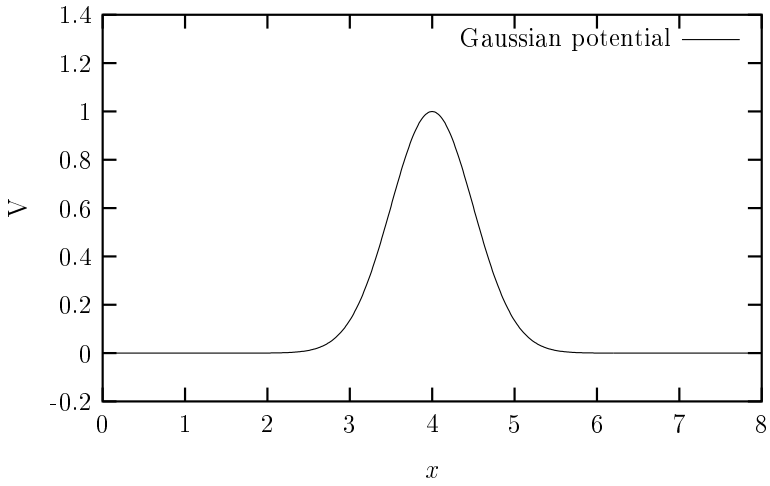

Figure 2.1: The Gaussian potential of Eq. (2.6).

(a) Gaussian potential

This is given by

$$V(x) = V_0 \mathrm{e}^{-b(x-\frac{a}{2})^2}\,, \tag{2.6}$$

where $a = 8$, $b = 2$ and $V_0 = 1$. Graphically, this potential is depicted in Fig. (2.1). If b is chosen large enough then the potential will effectively vanish for $x < 0$ and $x > a$.

(b) Smooth square-type potential

This potential has the form

$$V(x) = V_0 \frac{1 + \mathrm{e}^{d(3-x)})}{1 + \mathrm{e}^{d(x-5)}}\,, \tag{2.7}$$

where $V_0 = 1$ and $d = 20$. Its graphical representation is depicted in Fig. (2.2).

(c) Multi-layered potential

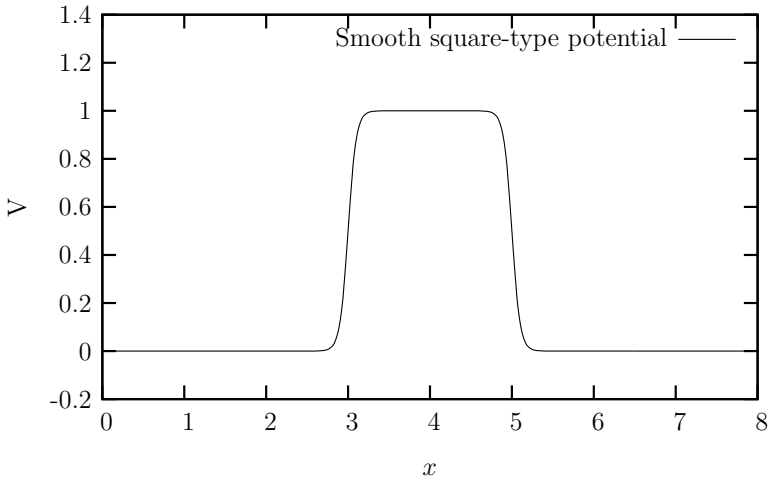

Figure 2.2: The smooth square-type potential of Eq. (2.7).

This potential corresponds to a multi-layered scatterer. We have constructed this potential by adding a number of square-type potentials of Fig. (2.2) together as in Fig. (2.3) with some modifications. Thus, it is a scatterer consisting of a finite number of homogeneous layers.

2.1.2 Reflection and transmission coefficients

Since the potential vanishes for $x < 0$ and $x > a$, the Schrödinger equation, Eq. (2.2), only needs to be solved in the interval $[0, a]$ and the two linear independent solutions outside this region are analytically given by

$$\psi^{+}(k, x) = \mathrm{e}^{ikx}\,, \tag{2.8}$$

and

$$\psi^{-}(k, x) = \mathrm{e}^{-ikx}\,, \tag{2.9}$$

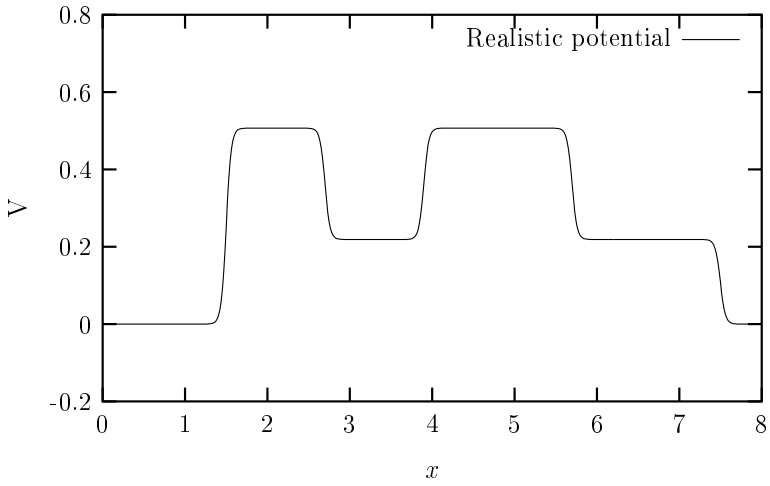

Figure 2.3: The multi-layered potential.

where ψ^+ represents a plane wave of unit amplitude traveling to the right and ψ^- a plane wave of unit amplitude traveling to the left. The solutions $\psi^\pm$ are the Jost solutions and therefore at the origin they are the Jost functions. Dividing Eqs. (2.4) and (2.5) by T(k), it follows that

$$\widetilde{\psi}_I(k,x) = \frac{1}{T(k)}\left[\psi^+ + R(k)\psi^-\right] = \frac{1}{T(k)}\left[\mathrm{e}^{ikx} + R(k)\mathrm{e}^{-ikx}\right], \tag{2.10}$$

and

$$\widetilde{\psi}_{III}(k,x) = \psi^+ = \mathrm{e}^{ikx}\,. \tag{2.11}$$

The derivative of Eq. (2.10) with respect to x can be written as

$$\frac{d\psi_I}{dx}(k,x) = \frac{ik}{T(k)}\left[\mathrm{e}^{ikx} - R(k)\mathrm{e}^{-ikx}\right]. \tag{2.12}$$

Thus, for $x = 0$

$$\widetilde{\psi}_I(k,0) = \frac{1}{T(k)}[1 + R(k)]\,, \tag{2.13}$$

and

$$\frac{d\widetilde{\psi_I}(k,0)}{dx} = \frac{ik}{T(k)}[1 - R(k)]\,, \tag{2.14}$$

from which we obtain

$$R(k) = \frac{T(k)}{2k}\left[k\widetilde{\psi}_I(k,0) + i\frac{d\widetilde{\psi_I}(k,0)}{dx}\right], \tag{2.15}$$

and

$$T(k) = \frac{2k}{k\widetilde{\psi}_I(0) - i\widetilde{\psi}_I(0)}, \tag{2.16}$$

respectively. Thus, the coefficients $R(k)$ and $T(k)$ are related to the properties of $\widetilde{\psi_I}$ and $\frac{d\widetilde{\psi_I}}{dx}$ at the origin.

2.2 Coupled channel problem

For the coupled-channel problem, the Schrödinger equation can be written in the form

$$\frac{d^2\mathcal{F}(k,x)}{dx^2} + \Big(k^2 - V(x)\Big)\mathcal{F}(k,x) = 0\,, \quad 0 \le x \le a\,, \tag{2.17}$$

where $V(x)$ is a real symmetric $n_c \times n_c$ potential matrix with matrix elements $v_{\alpha\beta}$ for $\alpha,\ \beta = 1, ..., n_c$ with n_c denoting the number of channels. $\mathcal{F}(k,x)$ is a matrix whose columns consist of the n_c linear independent solution vectors and k is the incident momentum. The potential matrix elements $v_{\alpha\beta}(x)$ are zero outside the interval $[0,a]$ and the scattering solutions are given by

$$\mathcal{F}(k,x) = \mathrm{e}^{ikx}\mathcal{G}(k) + \mathrm{e}^{-ikx}\mathcal{H}(k)\,, \quad x < 0\,, \tag{2.18}$$

and

$$\mathcal{F}(k,x) = \mathrm{e}^{ikx}\mathcal{S}(k)\,, \quad a < x < \infty\,, \tag{2.19}$$

where $\mathcal{G}(k)$, $\mathcal{H}(k)$ and $\mathcal{S}(k)$ are matrices [49].

2.2.1 Reflection coefficient matrix

The derivative of Eq. (2.18) yields

$$\mathcal{F}^{'}(k,x) = ik\mathrm{e}^{ikx}\mathcal{G}(k) - ik\mathrm{e}^{-ikx}\mathcal{H}(k)\,, \tag{2.20}$$

or

$$\frac{\mathcal{F}^{'}(k,x)}{ik} = \mathrm{e}^{ikx}\mathcal{G}(k) - \mathrm{e}^{-ikx}\mathcal{H}(k)\,. \tag{2.21}$$

On adding Eqs. (2.18) and (2.21) we find

$$\mathcal{F}(k,x) + \frac{\mathcal{F}^{'}(k,x)}{ik} = 2\mathrm{e}^{ikx}\mathcal{G}(k)\,. \tag{2.22}$$

Upon solving for $\mathcal{G}(k)$ at x=0, Eq. (2.22) reduces to

$$\mathcal{G}(k) = \frac{1}{2}\left(\mathcal{F}(k,0) - \frac{i\mathcal{F}^{'}(k,0)}{k}\right)\,. \tag{2.23}$$

Similarly, on subtracting Eq. (2.21) from Eq. (2.18) the equation

$$\mathcal{F}(k,x) - \frac{\mathcal{F}^{'}(k,x)}{ik} = 2\mathrm{e}^{-ikx}\mathcal{H}(k)\,, \tag{2.24}$$

is obtained and results in

$$\mathcal{H}(k) = \frac{1}{2}\left(\mathcal{F}(k,0) + \frac{i\mathcal{F}^{'}(k,0)}{k}\right)\,, \tag{2.25}$$

at $x = 0$. Thus, the reflection coefficient can be defined such that

$$\mathcal{R}(k) = \mathcal{H}(k)\mathcal{G}^{-1}(k)\,, \tag{2.26}$$

where $\mathcal{H}(k)$ is given by Eq. (2.25) and $\mathcal{G}^{-1}(k)$ stands for the inverse matrix of Eq. (2.23).

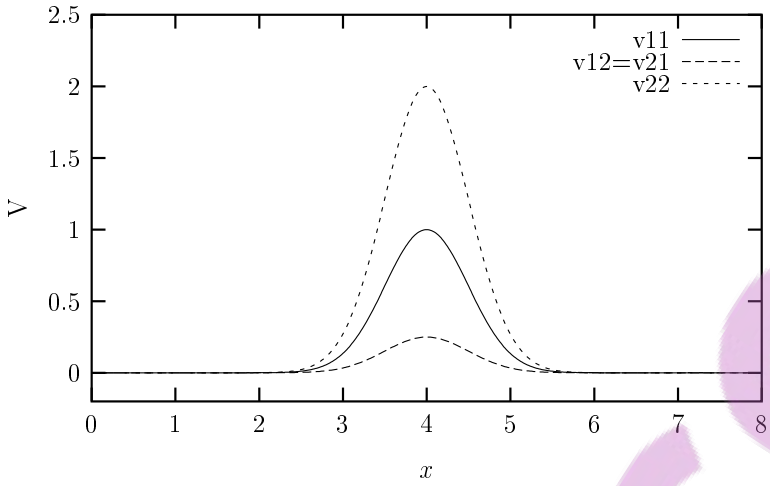

Figure 2.4: The Gaussian potential matrix.

2.2.2 Scattering potential matrix

In the present work, we consider 2×2 potential matrices which will be used to test our inversion method by recovering them from the Fourier transformed reflection coefficient. For a potential with Gaussian elements, we use

$$V(x) = \begin{pmatrix} 1.0\mathrm{e}^{-2(x-4)^2} & 0.25\mathrm{e}^{-2(x-4)^2} \\ 0.25\mathrm{e}^{-2(x-4)^2} & 2.0\mathrm{e}^{-2(x-4)^2} \end{pmatrix},$$

shown in Fig. (2.4) while for the smooth square-type potential matrix we use the form

$$V_{\alpha\beta}(x) = V_{0(\alpha\beta)} \frac{1 + \mathrm{e}^{d(3-x)}}{1 + \mathrm{e}^{d(x-5)}}, \tag{2.27}$$

where $V_{0(\alpha\beta)}$ is a constant and $b = 20$. This potential is depicted in Fig. (2.5). Lastly, the multi-layered potential is shown in Fig. (2.6).

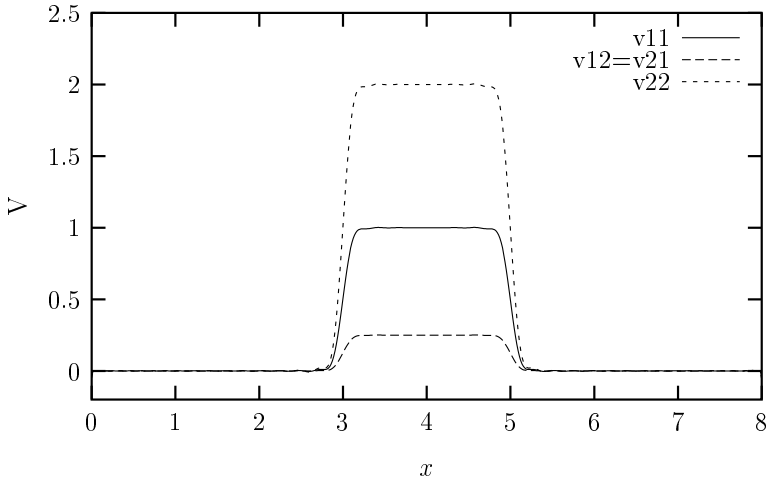

Figure 2.5: The smooth square-type potential matrix.

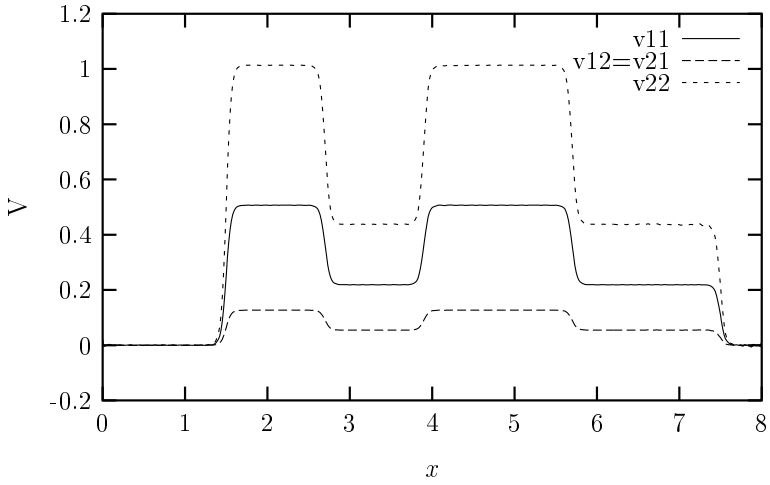

Figure 2.6: The multi-layered potential matrix.

Chapter 3

Seismic scattering in layered media

In marine oil exploration, a seismic wavelet sent from the source (for example, airgun) passes through the water column into the sea bottom. At the first interface the seismic wavelet is partly reflected and partly transmitted and continues through to the second interface. At the second interface, the seismic wavelet is again partly reflected and partly transmitted and continues into the third layer and so on. The change in the amplitude depends on the change in impedance while the change in phase is the result of dispersion. In most practical situations in the seismic reflection method, the Earth can be considered, to a good approximation, as an elastic medium.

In what follows we shall discuss the various reflection and transmission coefficients appearing in the multiple scattering processes. We shall also briefly discuss the seismic wave equation and its transformation into the Schrödinger-type equation.

3.1 Two-layered medium

We assume that a seismic wave is normally incident on the interface. We consider reflection at the interface separating two homogeneous media with density ρ_i and speed c_i for $i = 1, 2$. We also assume the incident plane wave to have unit amplitude with the reflected and transmitted waves having the amplitudes represented by R_p and T_p respectively. Thus, for the normal incidence, we can express the seismic pressure in the form [50]–[51]

$$p_i = \mathrm{e}^{ik_1 z}\,, \tag{3.1}$$

$$p_r = R_p \mathrm{e}^{-ik_1 z}\,, \tag{3.2}$$

and

$$p_t = T_p \mathrm{e}^{ik_2 z}\,, \tag{3.3}$$

where $k_1 = \omega c_1$ and $k_2 = \omega c_2$. For simplicity we have omitted a common time factor $\mathrm{e}^{-i\omega t}$. Thus, the total pressure in medium 1 is given by

$$p_1 = p_i + p_r = \mathrm{e}^{ik_1 z} + R_p \mathrm{e}^{-ik_1 z}\,, \tag{3.4}$$

and the total pressure in medium 2 by

$$p_2 = p_t = T_p \mathrm{e}^{ik_2 z}\,. \tag{3.5}$$

The first boundary condition states that

$$p_1 = p_2\,, \tag{3.6}$$

which reduces to

$$1 + R_p = T_p\,, \tag{3.7}$$

when the requirement of continuity of pressure at $z = 0$ is used. The second boundary condition states that

$$\frac{1}{i\omega\rho_1}\frac{\partial p_1}{\partial z} = \frac{1}{i\omega\rho_2}\frac{\partial p_2}{\partial z}\,, \tag{3.8}$$

which becomes

$$1 - R_p = T_p\frac{\rho_1 c_1}{\rho_2 c_2}\,, \tag{3.9}$$

when Eqs. (3.4) and (3.5) are used at $z = 0$. From the above the reflection and transmission coefficients can be obtained as

$$R_p = \frac{\rho_2 c_2 - \rho_1 c_1}{\rho_2 c_2 + \rho_1 c_1}\,, \tag{3.10}$$

and

$$T_p = \frac{2\rho_2 c_2}{\rho_2 c_2 + \rho_1 c_1}\,. \tag{3.11}$$

The reflection coefficient is negative if the seismic impedance of the incident layer is greater than that of the refracting layer. The free-surface reflection coefficient is $R_p = -1$. The seismic impedance of air is equal to zero. Thus, the total pressure field value on the free surface is zero.

Alternatively, if the vertical component of particle velocity is recorded instead of pressure then the reflection and transmission coefficients take the following forms [51]

$$R_c = \frac{\rho_1 c_1 - \rho_2 c_2}{\rho_1 c_1 + \rho_2 c_2}\,, \tag{3.12}$$

and

$$T_c = \frac{2\rho_1 c_1}{\rho_1 c_1 + \rho_2 c_2}\,, \tag{3.13}$$

where the subscript c represents the vertical particle velocity. However, it must be noted that Eq. (3.12) has the opposite polarity as compared to the pressure reflection

coefficient of Eq. (3.10). Thus, the particle velocity reflection coefficient is equal to +1 at the free surface. The value of the reflection coefficient relates to the magnitude of reflection from interface between two media with different properties. Thus, the seismic impedance of the two media involved is defined by [52]

$$\eta = \rho c\,. \tag{3.14}$$

Now from Eqs. (3.10–3.14) we can write $\eta_1 = \rho_1 c_1$ for the first layer and $\eta_2 = \rho_2 c_2$ for the second layer. Thus, $R_p \longrightarrow R_{12}$ and $R_c \longrightarrow R_{12}$ from Eqs. (3.10) and (3.12). Similarly, $T_p \longrightarrow T_{12}$ and $T_c \longrightarrow T_{12}$ from Eqs. (3.11) and (3.13). If the pressure has been recorded, then we have from Eq. (3.10)

$$R_{12} = \frac{\eta_2 - \eta_1}{\eta_2 + \eta_1}\,, \tag{3.15}$$

and from Eq. (3.11)

$$T_{12} = \frac{2\eta_2}{\eta_1 + \eta_2}\,, \tag{3.16}$$

or if the vertical component of velocity is recorded, we find from Eq. (3.12)

$$R_{12} = \frac{\eta_1 - \eta_2}{\eta_1 + \eta_2}\,, \tag{3.17}$$

and from Eq. (3.13)

$$T_{12} = \frac{2\eta_1}{\eta_1 + \eta_2}\,. \tag{3.18}$$

3.2 Three-layered medium

The medium usually consists of N layers and therefore we may have multiple reflections. An incident signal with a unit amplitude in a three-layered medium, Fig. (3.1),

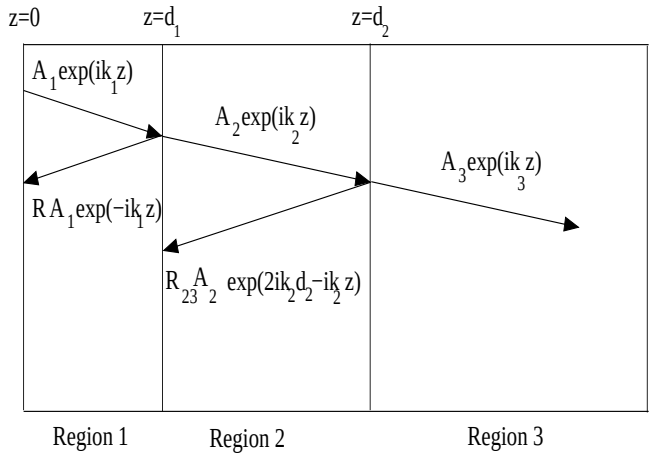

Figure 3.1: The reflection-transmission problem for the medium with three layers(regions). Although the pulse motion is for normal incidence, ray paths are drawn at oblique incidence for clarity.

is considered in which the third layer is assumed to be extended all the way to $z = \infty$, that is, no reflections are generated beyond the point $z = d_2$. It is further assumed that no reflections are created at $z = 0$, or alternatively, that they have been removed from the signal. The receiver and the source are located on the surface of the first layer.

The waves in the layers 1, 2,and 3 are given by Chew [54]

$$\psi_1 = A_1(\mathrm{e}^{ik_1 z} + \tilde{R}_{12}\mathrm{e}^{ik_1(2d_1 - z)})\,, \tag{3.19}$$

$$\psi_2 = A_2(\mathrm{e}^{ik_2 z} + R_{23}\mathrm{e}^{ik_2(2d_2 - z)})\,, \tag{3.20}$$

and

$$\psi_3 = A_3\mathrm{e}^{ik_3 z}\,. \tag{3.21}$$

$\widetilde{R_{12}}$ is the generalized reflection coefficient due to reflections on interfaces 2 and 3.

Matching the various waves as usual we obtain

$$\tilde{R}_{12} = R_{12} + \frac{T_{12}R_{23}T_{21}\mathrm{e}^{2ik_2(d_2-d_1)}}{1 - R_{21}R_{23}\mathrm{e}^{2ik_2(d_2-d_1)}}\,, \tag{3.22}$$

which can be expanded in a geometric series (see also, [54], [50] and [55])

$$\tilde{R}_{12} = R_{12} + T_{12}R_{23}T_{21}\mathrm{e}^{2ik_2(d_2-d_1)} + T_{12}R_{23}^2R_{21}T_{21}\mathrm{e}^{4ik_2(d_2-d_1)} + \ldots\,, \tag{3.23}$$

in which the $n-th$ term represents the $n-th$ reflection or

$$\tilde{R}_{12} = R_{12} + T_{12}R_{23}T_{21}\mathrm{e}^{2ik_2(d_2-d_1)}\sum_{n=0}^{\infty}\left(R_{23}R_{21}\mathrm{e}^{2ik_2(d_2-d_1)}\right)^n\,, \tag{3.24}$$

where $\tilde{R}_{12}$ combines the effect of subsurface reflections and the reflection from the first interface. $\tilde{R}_{12}$ is the generalized reflection coefficient for the three-layer medium. R_{12} on the right hand of Eq. (3.23) is the result of a single scattering off the first interface. The first two terms in the series Eq. (3.23) are the primary waves and multiples respectively. The spike R_{12} takes place at the time of the source spike while the spike train $T_{12}R_{23}T_{21}$ happens at a delay of the two-way travel-time through the first layer. The spike train $T_{12}R_{23}^2R_{21}T_{21}$ takes place at a delay of double the two-way travel-time and so on. By using the identities [50]–[54] $R_{21} = -R_{12}$ and $T_{12}T_{21} = 1 - R_{12}^2$, Eq. (3.22) can be written as

$$\tilde{R}_{12} = \frac{R_{12} + R_{23}\mathrm{e}^{2ik_2(d_2-d_1)}}{1 + R_{12}R_{23}\mathrm{e}^{2ik_2(d_2-d_1)}}\,. \tag{3.25}$$

It can be deduced that the numerator of Eq. (3.25) gives the effect of the front and back surfaces while the denominator gives the actual multiple reflections. Eq. (3.25) indicates the fact that the reflection coefficients are introduced at the first and second interfaces where the equation

$$R_{23} = \frac{\eta_2 - \eta_3}{\eta_2 + \eta_3}\,, \tag{3.26}$$

and Eq. (3.15) can be used.

The main modification as compared to Chew's formalism [54], Eq. (3.19), is that, in the Marchenko formalism we need to work with the overall reflection coefficient $R(k)$ for the whole half-space which is defined via

$$\psi_1 = A_1 \left(\mathrm{e}^{ik_1 z} + R(k) \mathrm{e}^{-ik_1 z} \right) . \tag{3.27}$$

Thus, by comparison with Eq. (3.19), we obtain

$$R(k) = \mathrm{e}^{2ikd_1} \left(R_{12} + \frac{T_{12} R_{23} T_{21} \mathrm{e}^{2ik_2(d_2 - d_1)}}{1 - R_{21} R_{23} \mathrm{e}^{2ik_2(d_2 - d_1)}} \right) . \tag{3.28}$$

In the travel-time coordinate ξ, the interfaces are located at

$$\xi_1 = \frac{d_1}{c_1} , \tag{3.29}$$

and

$$\xi_2 = \frac{d_1}{c_1} + \frac{d_2 - d_1}{c_2} = \frac{d_1}{c_1} + \frac{k_2}{k_1} \frac{d_2 - d_1}{c_1} , \tag{3.30}$$

where c_i is the velocity in the $i - th$ layer. Since the frequency is constant, that is, $\omega = kc$ it is evident that $k_1 c_1 = k_2 c_2 = k_3 c_3$. As an example, we consider the total reflection coefficient for the multiple scattering contributions. Thus, the $k-$dependent reflection coefficient can be given as

$$R_{12}(k) = R_{12} \mathrm{e}^{-\frac{b^2 k^2}{4}} , \tag{3.31}$$

where R_{12} is given in terms of the impedances of the medium, namely, Eq. (3.15). The corresponding transformation for the $k-$dependent classical transmission coefficient is given by

$$T_{12}(k) = 1 + R_{12}(k) . \tag{3.32}$$

Due to the $k-$dependent of the reflection and transmission coefficients we can express Eq. (3.28) in the form

$$\begin{aligned} R(k) &= R_{12}(k)\mathrm{e}^{2ik\xi_1} + T_{12}(k)R_{23}(k)T_{21}(k)\mathrm{e}^{2ik\xi_2} \\ &+ T_{12}(k)R_{23}^2(k)R_{21}(k)T_{21}(k)\mathrm{e}^{4ik\xi_2-2ik\xi_1} \\ &+ T_{12}(k)R_{23}^3(k)R_{21}^2(k)T_{21}(k)\mathrm{e}^{6ik\xi_2-4ik\xi_1} \\ &+ T_{12}(k)R_{23}^4(k)R_{21}^3(k)T_{21}(k)\mathrm{e}^{8ik\xi_2-6ik\xi_1} \\ &+ \cdots , \end{aligned} \tag{3.33}$$

which can be summed as

$$R(k) = \sum_{i=1}^{\infty} R_i(k)\,, \tag{3.34}$$

where

$$R_1(k) = R_{12}(k)\mathrm{e}^{2ik\xi_1}\,, \tag{3.35}$$

$$R_2(k) = T_{12}(k)R_{23}(k)T_{21}(k)\mathrm{e}^{2ik\xi_2}\,, \tag{3.36}$$

$$R_3(k) = T_{12}(k)R_{23}^2(k)R_{21}(k)T_{21}(k)\mathrm{e}^{4ik\xi_2-2ik\xi_1}\,, \quad \text{etc}\,. \tag{3.37}$$

If more than two layers are present the subsequent multiple scattering contributions of the series of Eq. (3.33) contain a product of reflection coefficients describing the multiple scattering each with a Gaussian dependence starting from the second term of Eq. (3.33). That is

$$T_{12}(k)T_{21}(k) = 1 - R_{12}^2 e^{-\frac{2b^2k^2}{4}}\,. \tag{3.38}$$

Thus, the total reflection coefficient $R(k)$ in Eq. (3.33) becomes

$$\begin{aligned}
R_1(k) &= R_{12}\mathrm{e}^{-\frac{b^2k^2}{4}}\mathrm{e}^{2ik\xi_1}\,, && (3.39)\\
R_2(k) &= \left(1-R_{12}^2\,\mathrm{e}^{-\frac{2b^2k^2}{4}}\right)R_{23}\,\mathrm{e}^{-\frac{2b^2k^2}{4}}\,\mathrm{e}^{2ik\xi_2}\,, && (3.40)\\
R_3(k) &= \left(1-R_{12}^2\mathrm{e}^{-\frac{2b^2k^2}{4}}\right)R_{23}^2R_{21}\mathrm{e}^{-\frac{3b^2k^2}{4}}\,\mathrm{e}^{4ik\xi_2-2ik\xi_1}\,, && (3.41)\\
R_4(k) &= \left(1-R_{12}^2\mathrm{e}^{-\frac{2b^2k^2}{4}}\right)R_{23}^3R_{21}^2\mathrm{e}^{-\frac{5b^2k^2}{4}}\,\mathrm{e}^{6ik\xi_2-4ik\xi_1}\,, && (3.42)\\
R_5(k) &= \left(1-R_{12}^2\mathrm{e}^{-\frac{2b^2k^2}{4}}\right)R_{23}^4R_{21}^3\mathrm{e}^{-\frac{7b^2k^2}{4}}\,\mathrm{e}^{8ik\xi_2-6ik\xi_1}\,, && (3.43)\\
&\text{etc}\,.
\end{aligned}$$

In seismic inversion it is customary to assume that the various reflection coefficients R_{ij} are constant. Thus, by taking the Fourier transform of Eq. (3.33) we obtain for a δ-function impulse,

$$B(\xi) = B_1 + B_2 + B_3 + \cdots\,, \tag{3.44}$$

where

$$\begin{aligned}
& && (3.45)\\
B_1(\xi) &= R_{12}\delta(\xi-2\xi_1)\,, && (3.46)\\
B_2(\xi) &= T_{12}R_{12}T_{21}\delta(\xi-2\xi_1)\,, && (3.47)\\
B_3(\xi) &= T_{12}R_{12}^2R_{21}T_{21}\delta(\xi-(4\xi_2-2\xi_1))\,, && (3.48)\\
&\text{etc}\,.
\end{aligned}$$

3.3 Multi-layered medium

In Eq. (3.23), R_{23} is the reflection coefficient from the space under layer 2. The space may consist of any number of layers. Since R_{23} is the reflection coefficient in layer 2,

any subsurface layer added below layer 3 will cause it to change to $\tilde{R}_{23}$ which indicates reflections from an interface between layers 2 and 3. This description can be applied to an N-layered medium. In general terms, the transmission coefficients are given by [56]

$$T_{i,i+1} = 1 + R_{i,i+1} = \frac{2\eta_i}{\eta_i + \eta_{i+1}}\,, \tag{3.49}$$

or

$$T_{i+1,i} = 1 - R_{i,i+1} = \frac{2\eta_{i+1}}{\eta_i + \eta_{i+1}}\,, \tag{3.50}$$

where $R_{i,i+1} = -R_{i+1,i}$. Hence, the product of $T_{i,i+1}$ and $T_{i+1,i}$ above yields

$$T_{i+1,i}T_{i,i+1} = 1 - R_{i,i+1}^2\,. \tag{3.51}$$

On using Eqs. (3.49) and (3.50), the quotient of η_{i+1} and η_i takes the form

$$\frac{\eta_{i+1}}{\eta_i} = \frac{T_{i+1,i}}{T_{i,i+1}} = \frac{1 - R_{i,i+1}}{1 + R_{i,i+1}}\,. \tag{3.52}$$

Eq. (3.52) is used to calculate the seismic impedance through the medium if the seismic impedance at the first interface and the $i-th$ reflection coefficients are known.

This equation (Eq. (3.52)) reduces to

$$R_{i,i+1} = \frac{\eta_i - \eta_{i+1}}{\eta_i + \eta_{i+1}}\,, \quad 1 \le i \le N\,, \tag{3.53}$$

which is the general formula for Eqs. (3.15) and (3.26). Eq. (3.53) is used when the medium is divided into a series of layers. The generalized reflection coefficient $R_{i,i+1}$ at the interface between layers i and $i+1$ is given by the general recursive relation [54]

$$\tilde{R}_{i,i+1} = R_{i,i+1} + \frac{T_{i,i+1}\tilde{R}_{i+1,i+2}T_{i+1,i}\mathrm{e}^{2ik_{i+1}(d_{i+1}-d_i)}}{1 - R_{i+1,i}\tilde{R}_{i+1,i+2}\mathrm{e}^{2ik_{i+1}(d_{i+1}-d_i)}}\,, \tag{3.54}$$

where the reflection coefficients $R_{i,i+1}$ represent the ordinary half-space reflection coefficients and $\tilde{R}_{i,i+1}$ denote the effects of subsurface reflections from the N-layered medium.

Eq. (3.54) is the general recursive relation used to calculate the reflection from any number of layers. On using $T_{i,i+1} = 1 + R_{i,i+1}$ and the fact that $R_{i,i+1} = -R_{i+1,i}$, Eq. (3.54) simplifies to [54]

$$\tilde{R}_{i,i+1} = \frac{R_{i,i+1} + \tilde{R}_{i+1,i+2} \mathrm{e}^{2ik_{i+1}(d_{i+1}-d_i)}}{1 + R_{i,i+1}\tilde{R}_{i+1,i+2}\mathrm{e}^{2ik_{i+1}(d_{i+1}-d_i)}}\,, \tag{3.55}$$

which can be solved recursively for $\tilde{R}_{i,i+1}$ in all layers because $\tilde{R}_{N,N+1} = 0$. Thus, Eqs. (3.19) and (3.20) are generalized as

$$\psi_i = A_i(\mathrm{e}^{ik_i z} + \tilde{R}_{i,i+1}\mathrm{e}^{2ik_i d_i - ik_i z})\,. \tag{3.56}$$

3.4 A simulated reflected seismic signal

A synthetic reflected signal generated by a seismic source placed in the surface of a layer can be simulated by assuming that the reflecting layer is situated at travel time ξ_1. Then an ideal reflected pulse would take the form $R_{12}\delta(\xi - 2\xi_1)$. Since, however, the reflecting interfaces are not sharply defined, $B(\xi)$ is stretched over a time interval $\triangle\xi$ and it can be modeled by the Gaussian form

$$B(\xi) = R_{12}\beta \mathrm{e}^{-\frac{(\xi-2\xi_1)^2}{b^2}}\,, \tag{3.57}$$

where b is the width of the Gaussian (of the order $c\triangle\xi$) and $\beta = 1/b\sqrt{\pi}$ is the normalization constant. If we identify the factor $\exp(2ik\xi_1)$ with the one already present in Eq. (3.33), the signal, Eq. (3.57), corresponds to the $k-$dependent reflection coefficient given by Eq. (3.31).

3.5 Seismic wave equation

The one-dimensional linearized elastic theory is governed by a simple partial differential equation whose general solution can be determined analytically for homogeneous media. The following discussion is in the spirit of Refs. [57, 58]. The free vibration of an infinitely long, linear elastic rod is considered. The rod has a cross-sectional area A, Young's modulus $\mathcal{Y}$ and density ρ. The area is regarded as constant. A small displacement of a disk of thickness dz at the coordinate z is denoted by $u(z)$ and is also considered constant over the whole cross-section. The rate of change of momentum is equal to the resultant force and is analytically given by

$$\frac{\partial}{\partial t}\left(\rho A dz \frac{\partial u}{\partial t}\right) = \left(\sigma + \frac{\partial \sigma}{\partial z} dz\right) A - \sigma A \,, \tag{3.58}$$

where

$$m = \rho A dz \,, \tag{3.59}$$

$$F_1 = \sigma A \,, \tag{3.60}$$

and

$$F_2 = \left(\sigma + \frac{\partial \sigma}{\partial z} dz\right) A \,, \tag{3.61}$$

with σ representing stress on the rod.

Eq. (3.58) reduces to

$$\rho \frac{\partial^2 u}{\partial t^2} = \frac{\partial \sigma}{\partial z} \,, \tag{3.62}$$

where u is the elastic displacement. If the half-space subjected to uniform surface tractions is assumed then any plane parallel to the z-axis is a plane of symmetry and thus transverse displacements are not possible. This allows the motion of the half-space

to be described by the displacements $u(z,t)$. Thus, the half-space is a one-dimensional deformation which can be described by a single strain component given by

$$\gamma = \frac{\partial u}{\partial z}\,. \tag{3.63}$$

Eq. (3.63) is a one-dimensional longitudinal strain from which the relationship between stress σ and strain γ can be given by

$$\sigma = \mathcal{Y}\gamma\,, \tag{3.64}$$

where $\mathcal{Y}$ is the Young's modulus of elasticity expressed in the form

$$\mathcal{Y} = \rho c^2\,, \tag{3.65}$$

where c is the speed of the wave. On substituting for the strain Eq. (3.63) and stress Eq. (3.64) into Eq. (3.62) we obtain

$$\rho\frac{\partial^2 u}{\partial t^2} = \frac{\partial}{\partial z}\left(\mathcal{Y}\frac{\partial u}{\partial z}\right). \tag{3.66}$$

Thus, the one-dimensional wave equation is given by [52, 59]

$$\rho\frac{\partial^2 u}{\partial t^2} = \frac{\partial}{\partial z}\left(\rho c^2\frac{\partial u}{\partial z}\right). \tag{3.67}$$

3.6 Transformation of seismic wave equation

Eq. (3.67) can also be written as

$$\rho\frac{\partial u}{\partial t^2} - \frac{\partial}{\partial z}\left(\rho c^2\frac{\partial u}{\partial z}\right) = 0\,, \tag{3.68}$$

where t is the time and z is the one space coordinate. As a function of z the density of the medium becomes $\rho = \rho(z)$ and the seismic wave speed takes the form $c = c(z)$. If u represents the transverse displacement perpendicular to the z-direction then $c_s(z)$ is defined by [52]

$$c_s = \sqrt{\frac{\mu(z)}{\rho}}\,, \tag{3.69}$$

where c_s represents the secondary wave velocity. If u represents the longitudinal displacement in the z-direction then $c_p(z)$ can be given as [52]

$$c_p = \sqrt{\frac{\lambda(z) + 2\mu(z)}{\rho}}\,, \tag{3.70}$$

where c_p denotes the primary wave velocity, λ and μ are the Lamé parameters. For the purpose of this study, Eq. (3.68) is transformed to the Schrödinger-type equation. A new space variable ξ is defined via

$$\partial z = c\partial\xi\,, \tag{3.71}$$

which upon integration yields

$$\xi = \int_0^z \frac{1}{c(z')}\partial z'\,. \tag{3.72}$$

The variable ξ is the travel time for the seismic waves from the origin to position z. From Eq. (3.71) it follows that

$$\frac{\partial}{\partial z} = \frac{1}{c}\frac{\partial}{\partial\xi}\,, \tag{3.73}$$

and the right-hand side of Eq. (3.68) simplifies to

$$\frac{\partial}{\partial z}\left(\rho c^2\frac{\partial u_z}{\partial z}\right) = \frac{\partial}{\partial z}\left(\rho c\frac{\partial u_\xi}{\partial\xi}\right) = \frac{1}{c}\frac{\partial}{\partial\xi}\left(\rho c\frac{\partial u_\xi}{\partial\xi}\right). \tag{3.74}$$

Thus, from Eqs. (3.68) and (3.74), we obtain the equation

$$\rho c\frac{\partial^2 u}{\partial t^2} - \frac{\partial}{\partial\xi}\left(\rho c\frac{\partial u_\xi}{\partial\xi}\right) = 0\,. \tag{3.75}$$

For the one-dimensional equation, data at z=0 cannot allow the recovery of ρ and c independently, but only in the product form ρc [52, 60]. The seismic impedance can now be written, using Eq. (3.14) as [59]

$$\eta(\xi) = \rho(z)c(z)\,, \tag{3.76}$$

which must be real and positive. From Eq. (3.70) the seismic impedance can also be expressed in terms of Lamé parameters such that

$$\eta(\xi) = \sqrt{\rho(z)(\lambda(z) + 2\mu(z))}\,. \tag{3.77}$$

Thus, Eq. (3.75) can be rewritten in terms of the seismic impedance as

$$\eta\frac{\partial^2 u}{\partial t^2} - \frac{\partial}{\partial \xi}\left(\eta\frac{\partial u_\xi}{\partial \xi}\right) = 0\,. \tag{3.78}$$

If a new dependent variable u is defined by

$$\psi = \eta^{\frac{1}{2}} u\,, \tag{3.79}$$

then after dropping the subscript ξ from Eq. (3.78), we obtain

$$\eta\frac{\partial u}{\partial \xi} = \eta^{\frac{1}{2}}\frac{\partial \psi}{\partial \xi} - \frac{\partial \eta^{\frac{1}{2}}}{\partial \xi}\psi\,, \tag{3.80}$$

$$\frac{\partial}{\partial \xi}\left(\eta\frac{\partial u}{\partial \xi}\right) = \eta^{\frac{1}{2}}\frac{\partial^2 \psi}{\partial \xi^2} - \frac{\partial^2 \eta^{\frac{1}{2}}}{\partial \xi^2}\psi\,, \tag{3.81}$$

and

$$\eta\frac{\partial^2 u}{\partial t^2} = \eta^{\frac{1}{2}}\frac{\partial^2 \psi}{\partial t^2}\,. \tag{3.82}$$

By substituting Eqs. (3.81) and (3.82) into Eq. (3.75) we obtain the relation

$$\eta^{\frac{1}{2}}\frac{\partial^2 \psi}{\partial t^2} - \eta^{\frac{1}{2}}\frac{\partial^2 \psi}{\partial \xi^2} + \frac{\partial^2 \eta^{\frac{1}{2}}}{\partial \xi^2}\psi = 0\,. \tag{3.83}$$

Finally, dividing Eq. (3.83) by $\eta^{\frac{1}{2}}$, the classical wave equation

$$\frac{\partial^2\psi}{\partial t^2} - \frac{\partial^2\psi}{\partial\xi^2} + V(\xi)\psi = 0\,, \tag{3.84}$$

is obtained where

$$V(\xi) = \frac{1}{\eta^{\frac{1}{2}}}\frac{\partial^2\eta^{\frac{1}{2}}}{\partial\xi^2}\,. \tag{3.85}$$

From the definition of the scattering potential V in Eq. (3.85) we can write

$$\frac{d^2\eta^{\frac{1}{2}}}{d\xi^2} - V(\xi)\eta^{\frac{1}{2}} = 0\,, \tag{3.86}$$

which is a reduced form of

$$\frac{d^2\eta^{\frac{1}{2}}}{d\xi^2} + (k^2 - V(\xi))\eta^{\frac{1}{2}} = 0\,, \tag{3.87}$$

when $k = 0$. Once Eq. (3.68) is transformed into the form of the Schrödinger-type equation, the inversion procedure can take its course through the Marchenko integral equation.

Chapter 4

Marchenko inversion method

In what follows we shall briefly describe the Marchenko integral equation which can be used to solve the inverse scattering problem. Our objective is to find the potential $V(x)$ from the reflected waves.

4.1 Marchenko integral equation

The time-dependent wave equation for the classical amplitude U is given by [61]

$$\frac{\partial^2 U(x,y)}{\partial x^2} - \frac{\partial^2 U(x,y)}{\partial y^2} = V(x)U(x,y)\,, \tag{4.1}$$

where $y = vt$, v is the velocity of the wave and $V(x)$ is the scattering potential. For our purpose we choose the ansatz

$$U = \psi(x,k)\mathrm{e}^{-iky}\,. \tag{4.2}$$

Thus, we can construct solutions of Eq. (4.1) by linear superposition

$$U(x,y) = \int_{-\infty}^{+\infty} C(k)\psi(x,k)\mathrm{e}^{-iky}\mathrm{d}k\,, \tag{4.3}$$

which will then be a solution of the wave equation. A delta function pulse impinging on a potential from the left and reaching the origin at $y = 0$ can be described by

$$\delta(x-y) = \frac{1}{2\pi}\int_{-\infty}^{+\infty} \mathrm{e}^{-ik(x-y)}\mathrm{d}k\,. \tag{4.4}$$

Since we have assumed that $V(x) = 0$ for $x < 0$, it is clear that scattering under those boundary conditions will only affect the solution of the wave equation for the region $y > |x|$. By choosing $\psi(x,k) = \psi_I$ as given by Eq. (2.4), and $C(k) = 1/(2\pi)$ in Eq. (4.3), it can be shown that for $x < 0$, the solution of Eq. (4.1) is given by

$$U_0(x,y) = \delta(x-y) + B(x+y)\,, \tag{4.5}$$

where $\delta(x-y)$ is the incident wave and B stands for the input kernel which can be expressed as the Fourier transform of the reflection coefficient

$$B(x+y) = \frac{1}{2\pi}\int_{-\infty}^{+\infty} R(k)\mathrm{e}^{-ik(x+y)}\mathrm{d}k\,. \tag{4.6}$$

Due to the causality argument given above, $B(x+y)$ will vanish for $x+y < 0$ and we thus, have obtained a solution for $x < 0$ consistent with our boundary condition. If we assume that the wave amplitude $U(x,y)$ in the region $x > 0$ can be related with the amplitude $U_0(x,y)$ for $x < 0$ by the linear transformation ansatz

$$U(x,y) = U_0(x,y) + \int_{-\infty}^{+x} K(x,z)U_0(z,y)\mathrm{d}z, \tag{4.7}$$

then we obtain, by substituting the expression for $U_0(x,y)$, the integral equation [6]

$$K(x,y) + B(x+y) + \int_{-x}^{+x} \mathrm{d}z K(x,z)B(y+z) = 0, \qquad -x \le y \le x\,, \tag{4.8}$$

for which $K(x,y) = 0$ where $x < |y|$. The lower limit is now $-x$ since the input kernel B is of finite support. $K(x,y)$ is a non-causal and an auxiliary function. Eq. (4.8) is known as the Marchenko integral equation (MIE) and has to be solved for the function $K(x,y)$. Conditions on K are found by substituting the expression, Eq. (4.7), for $U(x,y)$ in the differential equation, Eq. (4.1); applying certain algebraic manipulations, the function $K(x,y)$ is found to satisfy the same differential equation as $U(x,y)$ subject to the conditions [62]

$$K(x,-x) = 0, \tag{4.9}$$

and

$$V(x) = 2\frac{\mathrm{d}K(x,x)}{\mathrm{d}x}, \qquad 0 \leq x \leq a\,, \tag{4.10}$$

where a is the range of the potential. Thus, the solution of the inverse scattering problem requires the knowledge of the kernel K which in turn requires the evaluation of B. The latter can be obtained using the fast Fourier transform [37]. It should be noted that the input kernel B needs to be calculated only on the interval $[0, 2a]$ since the reflected wave travels the distance a twice and the potential is only non-vanishing in interval $[0, a]$. However, two points must be emphasized:

(a) The determination of B requires the knowledge from experiment (or theory in the case of a model problem) of $R(k)$ for sufficiently large values of $|k|$ such that the remainder of the Fourier integral can be neglected.

(b) For large values of $x + y$, this results in a rapidly oscillating behavior of the integrand of Eq. (4.6) .

Once more, we stress that the experimental measurement of $R(k)$ is problematic since only the reflectivity $|R(k)|$ can be normally measured which means that the phase

information is lost. This is the phase problem that we encounter in Quantum inversion. However, for applications in seismology, measurements can be carried out in the time-domain in order to measure B and in this way no phase problem is encountered.

4.2 Obtaining impedance from the Marchenko kernel

In this section we shall briefly discuss an alternative form of the seismic impedance used in the numerical treatment.

The inverse problem for a one-dimensional seismic wave equation involves the transformation of the seismic wave equation into the Schrödinger equation and the reconstruction of the seismic impedance from the reflectivity sequence which is estimated from the observed reflection data. This reflectivity sequence is then used as an input to the Marchenko integral equation. Since it is not possible to recover the density ρ and the velocity c separately, we show that the quantity which can be evaluated is the seismic impedance given by Eq. (3.76) and it is recovered as a function of travel-time ξ. The higher the seismic impedance the larger the amount of reflection. This effect is an indication that the rock layers have various mineral density or porosity characteristics that generate strong reflections.

The objective of seismic inverse problem is to find the seismic impedance profile for $z > 0$. Such an impedance profile will be recovered as a function of one-way travel-

time. By using Eq. (3.85), the seismic impedance can be determined as a function of the travel-time ξ in the form [54]

$$\eta^{\frac{1}{2}}(\xi) = \eta^{\frac{1}{2}}(0)\left[1 + \int_{-\xi}^{+\xi} K(\xi,\tau)\,\mathrm{d}\tau\right], \tag{4.11}$$

which relates $\eta^{\frac{1}{2}}(\xi)$ with the output kernel $K(\xi,\tau)$. Eq. (4.11) can be simplified to

$$\eta(\xi) = \eta(0)\left[1 + \int_{-\xi}^{+\xi} K(\xi,\tau)\,\mathrm{d}\tau\right]^2, \tag{4.12}$$

which is related to the Marchenko integral equation via the kernel $K(\xi,\tau)$ which satisfies Eq. (4.8).

Chapter 5

Computational analysis

In the present chapter we shall briefly outline certain aspects of the numerical and computational methods used. Furthermore we shall present the statistical approach used in the simultaneous extraction of the reflectivity sequence and seismic wavelet.

5.1 Single channel inversion

The Marchenko integral equation will be solved for the kernel $K(x, y)$ on the triangular region $-x \leq y \leq x$ in the xy - plane by applying the orthogonal collocation method. Given a value of x, $K(x, y)$ can be expanded in terms of N localized functions. The building blocks of our expansion are the Hermite interpolation polynomials that allow us to fix the value of the function to be interpolated and its derivative at the beginning and the end of any interval. For the unit interval, these polynomials are defined in

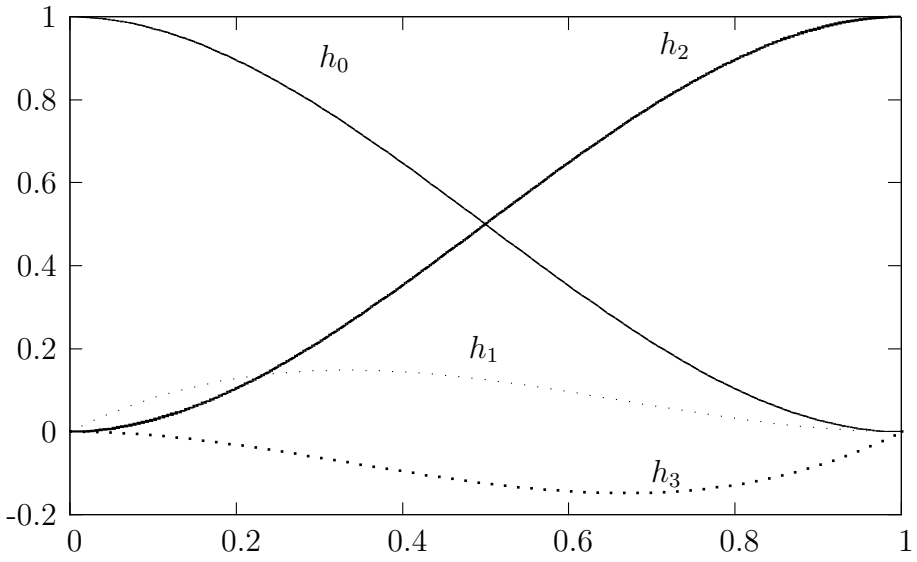

Figure 5.1: Hermite interpolation polynomials on the interval [0,1]

.

Eqs. (5.1–5.4) and depicted in Fig. (5.1)

$$h_0(s) = (1-s)^2(1+2s)\,, \tag{5.1}$$

$$h_1(s) = (1-s)^2 s\,, \tag{5.2}$$

$$h_2(s) = s^2(3-2s)\,, \tag{5.3}$$

$$h_3(s) = s^2(s-1)\,. \tag{5.4}$$

By subdividing the interval $[-x, x]$ into n equidistant sub-intervals, we can expand the output kernel in terms of the above interpolation polynomials adapted to each of those sub-intervals. Due to the requirements of continuity, this is equivalent to expanding K in terms of functions $g_j(y)$ that are spliced together by joining interpolation polynomials on adjacent sub-intervals, as shown in Fig. (5.2). The splicing together of the

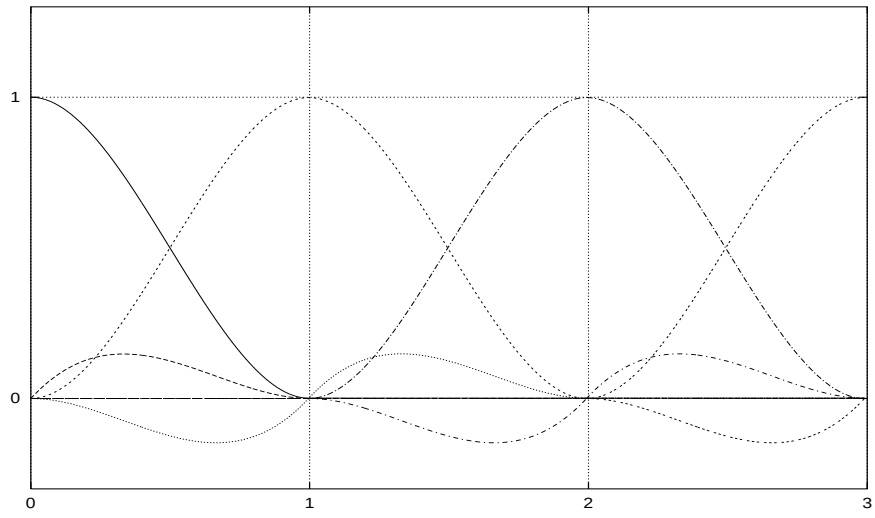

Figure 5.2: Spliced functions for the case of three sub-intervals

.

interpolation polynomials can be efficiently handled by creating an index array $j_{i,\nu}$. This array will indicate to which g_j, the local Hermite interpolation polynomial with index ν in the $i-th$ sub-interval, belongs. Due to the boundary condition given in Eq. (4.9), we do not use the function which equals unity at the left boundary $y = -x$, instead we use only $2(n+1) - 1 = 2n + 1$ functions. Therefore

$$K(x, y) = \sum_{j=1}^{N} c_j g_j(y)\,, \tag{5.5}$$

where c_j are coefficients and g_j are functions. Orthogonal collocation is then effected by requiring Eq. (4.8) to be satisfied at $N = 2n + 1$ collocation points y_i, chosen to be the Gauss-Legendre integration points of order 2 for the sub-intervals of the grid and $y_N = x$.

A solution of the quantum inverse scattering problem is generally a two step process. The first step handles the calculation of the $B-$function from the reflection coefficient by employing the Fast Fourier transform. The second step is the actual inversion process which uses the $B-$function as the input kernel to the Marchenko integral equation. The results are the reconstructed potentials. This is illustrated in the following discussion. For a numerical treatment, the Marchenko integral equation Eq. (4.8), has to be discretized such that the following linear system of equations are obtained

$$\sum_{j=1}^{N} c_j g_j(y_i) + B(x+y_i) + \sum_{i=1}^{N} c_j \int_{-x}^{+x} dz g_j(z) B(z+y_i) = 0\,. \tag{5.6}$$

In matrix form this set of equations may be written as

$$(U+K)\mathbf{c} = -\mathbf{b}, \tag{5.7}$$

where the matrices U and K and the vector b are respectively defined by the following equations

$$u_{ij} = g_j(y_j)\,, \tag{5.8}$$

$$k_{ij} = \int_{-x}^{+x} dz g_j(z) B(z+y_i)\,, \tag{5.9}$$

$$b_i = B(x+y_i)\,. \tag{5.10}$$

The integral required in Eq. (5.9) is evaluated via repeated Gauss-Legendre integration over the sub-intervals of our discretization. We solve for the coefficient vector $\mathbf{c}$ in Eq. (5.7) via LU-decomposition using the subroutines from LAPACK [63]. To achieve our goal, that is, to obtain the potential, we need to take a derivative according to Eq. (4.10). Thus, another numerical procedure is required to evaluate this derivative. To this end we calculate $K(x,x)$ on the grid points suitable for applying interpolation via Chebyshev polynomials. Those grid points are with respect to the interval $[x_{min}, x_{max}]$

given by

$$x_i = \frac{(x_{min} + x_{max})}{2} + \cos\left(\frac{i - 0.5}{n_{ch}}\pi\right)\frac{(x_{max} - x_{min})}{2}\,, \tag{5.11}$$

where n_{ch} is the number of Chebyshev grid points used. In our case $x_{min} = 0$ and $x_{max} = a$ where a is the range of the potential. Once the coefficients of this interpolation are known, we can easily obtain the required derivatives since the coefficients of the Chebyshev interpolation of the derivative can be recursively calculated from the interpolation coefficients for $K(x, x)$.

5.2 Coupled channel inversion

The Marchenko fundamental equation Eq. (4.8), can be generalized to a system of coupled channel integral equations [49]

$$K_{\alpha\beta}(x, y) + B_{\alpha\beta}(x + y) + \sum_{\gamma}\int_{-x}^{+x} K_{\alpha\gamma}(x, z)B_{\gamma\beta}(z + y)dz = 0, \;\; -x \leq y \leq x\,, \tag{5.12}$$

where α, β and γ are channel indices of the matrices. It is therefore observed that the input and output kernels of the Marchenko integral equation have been replaced by the matrix kernels as seen in Eq. (5.12). The input kernel $B_{\alpha\beta}(x + y)$ and the output kernel $K_{\alpha\beta}(x, y)$ are $n_c \times n_c$ matrices. Thus, the potential matrix becomes

$$V_{\alpha\beta} = 2\frac{dK_{\alpha\beta}(x, x)}{dk}\,, \quad 0 \leq x \leq a \tag{5.13}$$

in analogy to Eq. (4.10). The symmetrical input kernel of Eq. (4.6) now has the form

$$B_{\alpha\beta}(x + y) = \frac{1}{2\pi}\int_{-\infty}^{+\infty} R_{\alpha\beta}(k)\mathrm{e}^{-ik(x+y)}dk\,, \tag{5.14}$$

where $R_{\alpha\beta}(k)$ is the reflection coefficient matrix. The scattering data $R_{\alpha\beta}$(k) determine the input kernel $B_{\alpha\beta}$ which are needed to solve the Marchenko integral matrix equation. For a constant value of x at a collocation point y_i, Eq. (5.12) can be written as

$$K_{\alpha\beta}(x,y_i)+B_{\alpha\beta}(x+y_i)+\sum_{\gamma}\int_{-x}^{+x}dzK_{\gamma\alpha}(x,z)B_{\beta\gamma}(z+y_i)=0\,,\quad -x\leq y_i\leq x\,. \tag{5.15}$$

The Marchenko integral matrix equation should be satisfied at N points. Thus, the kernel can then be expanded in terms of $g_{j,x}$

$$K_{\alpha\beta}(x,y_i)=\sum_{j=1}^{N}c_{j,\alpha\beta}^{(x)}g_{j,x}(y_i)\,, \tag{5.16}$$

where j numbers the splines and x denotes the dependence of c_j and g_j on it. Inserting this expansion in Eq. (5.15) and requiring the equation to be fulfilled for all y_i we obtain

$$\sum_{\gamma=1}^{n_c}\sum_{j=1}^{N}c_{j,\alpha\gamma}\;\delta_{\beta\gamma}\;g_j(y_i)+B_{\alpha\beta}(x+y_i)+\sum_{\gamma=1}^{n_c}\sum_{j=1}^{N}c_{j,\alpha\gamma}\int_{-x}^{+x}dzg_j(z)B_{\gamma\beta}(z+y_i)=0\,, \tag{5.17}$$

where x has been dropped for the sake of simplicity and $\delta_{\beta\gamma}$ is the Kronecker delta. Now let

$$k_{\beta i,\gamma j}=\delta_{\beta\gamma}\,g_j(y_i)\,, \tag{5.18}$$

$$\widetilde{c}_{\gamma j,\alpha}=c_{j,\alpha\gamma}\,, \tag{5.19}$$

$$b_{\beta i,\alpha}=B_{\alpha\beta}(x+y_i)\,, \tag{5.20}$$

and

$$d_{\beta i,\gamma j}=\int_{-x}^{+x}dz\;B_{\gamma\beta}(z+y_i)\,g_i(z)\,. \tag{5.21}$$

Thus, from the contributions of Eqs. (5.18–5.21), the Marchenko integral matrix equation, Eq. (5.17), reduces to

$$\sum_{\gamma j}(d_{\beta i,\gamma j}+k_{\beta i,\gamma j})\widetilde{c}_{\gamma j,\alpha}=-b_{\beta i,\alpha}\,, \tag{5.22}$$

which may then be further simplified to

$$\sum_{\gamma j} a_{\beta i,\gamma j}\widetilde{c}_{\gamma j,\alpha} = -b_{\beta i,\alpha}\,, \tag{5.23}$$

in the $(N \times n_c) \times (N \times n_c)$ space, where

$$a_{\beta i,\gamma j} = d_{\beta i,\gamma j} + k_{\beta i,\gamma j}\,. \tag{5.24}$$

For the LU - decomposition, Eq. (5.23) can be written in matrix form as

$$\mathcal{A}\mathcal{C} = -\mathcal{B}\,, \tag{5.25}$$

where

$$\mathcal{A} = \left(a_{\beta i,\gamma j}\right), \tag{5.26}$$

$$\mathcal{B} = \left(b_{\beta i,\alpha}\right), \tag{5.27}$$

and

$$\mathcal{C} = \left(\widetilde{c}_{\gamma j,\alpha}\right). \tag{5.28}$$

5.3 Reconstruction of impedance from synthetic data

Knowing $\eta(0)$ in Eq. (4.12) the seismic impedance profile $\eta(\xi)$, for $\xi > 0$ can be recovered from the solution $K(\xi,\tau)$ of the Marchenko integral equation. In order to reconstruct the seismic impedance profile from the output kernel $K(\xi,\tau)$ in the Marchenko integral equation, the expansion in terms of N localized functions can be considered. Thus,

$$K(\xi,\tau) = \sum_{j=1}^{N} c_j(\xi) g_j(\tau)\,. \tag{5.29}$$

Upon integrating Eq. (5.29), we find

$$\int_{-\xi}^{+\xi} K(\xi,\tau)\,\mathrm{d}\tau = \sum_{j=1}^{N} \int_{-\xi}^{+\xi} c_j(\xi) g_j(\tau)\,\mathrm{d}\tau\,. \tag{5.30}$$

Thus, for a given value of ξ, the seismic impedance $\eta(\xi)$ can be obtained such that

$$\eta(\xi) = \eta(0)\left[1 + \sum_{j=1}^{N} c_j \kappa_j\right]^2, \tag{5.31}$$

where

$$\kappa_j = \int_{-\xi}^{+\xi} g_j(\tau)\,\mathrm{d}\tau\,. \tag{5.32}$$

5.4 Blind deconvolution method

5.4.1 Deconvolution process

Before discussing the deconvolution process we present a brief description of the convolution model. This model [41] can be described schematically as

$$\text{measured output} = \text{output} + \text{noise} = \text{wavelet} * x + \text{noise}\,,$$

where x is the reflectivity sequence or reflector series. Mathematically, it can be written as

$$z_t = \sum_{k=1}^{\min(N,t)} h_k x_{t-k+1} + n_t\,, \qquad t = 1, ..., N+M-1\,, \tag{5.33}$$

where z is an observed seismic trace of length $N+M-1$, h represents the seismic wavelet of length N, x stands for the white reflectivity sequence of the medium of

length M and n is a zero-mean white noise of Gaussian type. The noise sequence is characterized by its variance σ^2 [41]. Eq. (5.33) can be written in a convolutional form

$$z = h * x + n\,, \tag{5.34}$$

or in a matrix form we have

$$z = Hx + n\,, \tag{5.35}$$

where H is a convolution matrix associated with the finite seismic wavelet $h = [h_1, \cdots, h_N]^T$. that is,

$$H = \begin{bmatrix} h_1 & 0 & \cdots & & 0 \\ h_N & \cdots & h_1 & 0 & \cdots & 0 \\ 0 & \ddots & & \ddots & \ddots & \\ \vdots & \ddots & & & & 0 \\ 0 & \cdots & & 0 & h_N & \cdots & h_1 \\ \vdots & & & & \ddots & \ddots & \vdots \\ 0 & \cdots & & & & 0 & h_N \end{bmatrix}. \tag{5.36}$$

Our objective is to separate the reflectivity sequence and seismic wavelet from each other by applying the blind deconvolution procedure.

In the literature the system's unit response is called the reflectivity sequence. In our model it will also include multiple reflections (only a finite number is needed) effected by the system provided the seismic wavelet is shorter than the travel-time distance between the consecutive interfaces. For our numerical computations we identify the reflectivity sequence up to a scaling factor with the unit response of the medium and call it the $B-$function.

Deconvolution of the seismic reflection data series z when the source wavelet h is known, is a well-understood problem. However, in some investigations such as ours, only the marine seismic reflection data have been provided from which both reflectivity sequence and seismic wavelet have to be retrieved. For this purpose, we apply the blind deconvolution method to estimate the reflectivity sequence and seismic wavelet.

We assume the sea floor to consist of several homogeneous layers that are separated by interfaces. Such an assumption makes it possible to express the reflectivity sequence in terms of a Bernoulli-Gaussian (BG) sequence [64, 65]. Thus, the reflectivity sequence that defines the generalized BG sequence can be modeled by using two random sequences in the form [41]

$$x_k = r_k q_k \,, \tag{5.37}$$

where $r = (r_k)$ denotes a zero-mean Gaussian white sequence with variance σ_r^2 and $q = (q_k)$ stands for the Bernoulli sequence with the probability parameter λ being equal to its mean value [66]. For the probabilities associated with this sequence we have

$$P(q_k = 1) = \lambda \,, \tag{5.38}$$

or

$$P(q_k = 0) = 1 - \lambda \,, \tag{5.39}$$

that is, the random variable q_k is one with probability λ and zero with probability $1 - \lambda$. The probability of the whole sequence q reads

$$P(q|\lambda) = \prod_k P(q_k) = \lambda^n (1-\lambda)^{M-n}, \tag{5.40}$$

where n is the number of ones in the sequence.

5.4.2 Markov Chain Monte Carlo method

The Markov Chain Monte Carlo (MCMC) method is concerned with the simulation via a Markov chain. It is a Monte Carlo integration procedure in which the random samples are generated by evolving a Markov chain. We are concerned with the MCMC method in a pure Bayesian approach. Upon using the Bayes' rule, we can write the probability distribution as [44]

$$P(\theta|z) = \frac{P(z|\theta)P(\theta)}{P(z)}\,, \tag{5.41}$$

where θ stands for all parameters of the problem [67], that is,

$$\theta \equiv (h, x, \lambda, \sigma^2)\,, \tag{5.42}$$

and h, x, λ, and σ^2 have the same meaning as above. $P(\theta|z)$ is the posterior probability of the model conditional on the observed data z, $P(\theta)$, and $P(z)$ describe the prior knowledge and data respectively while $P(z|\theta)$ describes the discrepancy between the model and observation.

The complete joint probability distribution is expressed in the form [44]

$$P(\theta|z) \propto P(z|\theta)P(\theta)\,, \tag{5.43}$$

since $P(z)$ is in this case a normalizing constant. The MCMC algorithm is iterative and may require a number of iterations before the first sample from the correct distribution can be provided. These initial iterations are called burn-in iterations and should not be used in the statistical analysis. Thus, the estimation of the reflectivity sequence and

seismic wavelet is determined by the simulation of random variables via the MCMC algorithms based on the Gibbs sampler [46], which is regarded as the best known and most popular of the MCMC algorithms [47]. It is an algorithm in which the vector $\theta^{(k+1)}$ is obtained from $\theta^{(k)}$ by updating the vector elements one at a time. The prior distribution in Eq. (5.43) can be written as

$$P(\theta) = P(x|\lambda)P(\lambda)P(h)P(\sigma^2)\,, \tag{5.44}$$

where $P(h) = P(\sigma^2) = P(\lambda) = 1$ are flat prior probability densities and $P(x|\lambda)$ is described by a Bernoulli-Gaussian distribution. Upon using Eq. (5.44), we can write Eq. (5.41) in the form

$$P(\theta|z) = \frac{P(z|\sigma^2, x, \lambda)P(x|\lambda)P(h)}{P(z)}\,. \tag{5.45}$$

The assumption of a white Gaussian noise sequence n of variance σ^2 leads to

$$P(z|\sigma^2, x, \lambda) = (2\pi\sigma^2)^{-(N+M-1)/2} \exp\left(-\frac{\|z - h * x\|^2}{2\sigma^2}\right). \tag{5.46}$$

For our purpose, we need to calculate the distributions $P(h|z, x, \sigma^2, \lambda)$, $P(x|z, h, \lambda, \sigma^2)$, $P(\sigma^2|z, x, h, \lambda)$, and $P(\lambda|z, x, h, \sigma^2)$. Thus, Eq. (5.45) can be employed to handle the relevant re-sampling processes.

(a) Re-sampling of the amplitude of the reflectivity sequence

The reflectivity sequence x contains information about the Earth's structure. In order to statistically separate it from the seismic wavelet we use the BG white sequence model [65]

$$P(x) = \prod_m P(x_m)\,, \tag{5.47}$$

with

$$P(x_m) \sim (1-\lambda)\delta(x_m = 0) + \lambda\mathcal{N}(0, \varrho^2)\,, \tag{5.48}$$

where $\mathcal{N}$ is a Gaussian distribution with specified mean and variance and where $\lambda \in (0,1)$ is the probability that $x_m = 1$, and both λ and ϱ^2 are unknown.

It can be shown [65] that the posterior probabilities involving single components of the vector x remain Gaussian mixtures with a structure comparable to that of Eq. (5.48). More precisely,

$$P(x_m|\lambda, h, z, x_{-m},) \sim (1-\lambda_m)\delta(x_m = 0) + \lambda_m\mathcal{N}(x_m^*, \sigma_m^2)\,, \tag{5.49}$$

where $x_{-m} = (x_1, \ldots, x_{m-1}, x_{m+1}, \ldots, x_M)$ and

$$\sigma_m^2 = \frac{\sigma^2\varrho^2}{\sigma^2 + \varrho^2\|h\|^2}\,, \tag{5.50}$$

$$x_m^* = \frac{\sigma_m^2}{\sigma^2}(h^T e_m)\,, \tag{5.51}$$

$$\lambda_m = \left[1 + \frac{\lambda}{1-\lambda}\frac{\sigma_m}{\varrho}\exp\left(\frac{{x_m^*}^2}{2\sigma_m^2}\right)\right]^{-1}\,, \tag{5.52}$$

and

$$e_m = z - h * x^{(m)} \tag{5.53}$$

where $x^{(m)}$ is identical to x except for $x_m^{(m)} = 0$. Using Eqs. (5.49)-(5.52), the components x_m of the reflectivity sequence can be re-sampled, one at a time.

(b) Re-sampling of the seismic wavelet

In order to re-sample the seismic wavelet h, we deduce from the Bayes' rule that $P(h|\sigma^2, x, z) \propto P(z|\sigma^2, x, h)$, given $P(h) = 1$, where $P(z|\sigma^2, x, h)$ is given by Eq.

(5.46). Moreover, it is easy to check the following identity:

$$-\frac{\|z - h * x\|^2}{2\sigma^2} = -\frac{1}{2}(h-\mu)^T R^{-1}(h-\mu), \tag{5.54}$$

where

$$\mu = (X^T X)^{-1} X^T z\,, \tag{5.55}$$

and

$$R = (X^T X)^{-1}\sigma^2 \mathbf{1}\,, \tag{5.56}$$

where X is the Toeplitz matrix of size $(N + M - 1, N)$ such that

$$Xh = h * x = Hx\,, \tag{5.57}$$

that is,

$$X = \begin{bmatrix} x_1 & 0 & \cdots & 0 \\ \vdots & \ddots & \ddots & \\ & & & 0 \\ x_{M+1} & & & x_1 \\ \vdots & \ddots & & \vdots \\ x_M & & & \\ 0 & \ddots & & \\ \vdots & \ddots & & \\ 0 & \cdots & 0 & x_M \end{bmatrix}. \tag{5.58}$$

This allows us to conclude that the posterior probability of h is a multivariate Gaussian with mean vector μ and with covariance matrix R. The latter probability is easy to sample according to $h = \mu + Q\varepsilon$, where ε is a normalized Gaussian white noise and Q^T is a square root matrix of R (that is, such that $R = QQ^T$), such as the one resulting from the Cholesky decomposition.

(c) Re-sampling of the hyperparameter σ

Given $P(\sigma^2) = 1$, it is also true that

$$P(\sigma^2|z, x, h, \lambda) \propto P(z|\sigma^2, x, h)\,. \tag{5.59}$$

As a function of σ^2, Eq. (5.46) takes the form

$$P(z|\sigma^2, x, h) \propto \frac{1}{(\sigma^2)^{\alpha+1}} \exp(-\beta/\sigma^2)\,,$$

up to a multiplicative constant, with $\alpha = (N + M - 1)/2 - 1$ and $\beta = \|z - h * x\|^2/2$, which means that the posterior probability of σ^2 follows an inverse gamma distribution of parameters (α, β). The latter can be easily sampled by taking the inverse of a gamma random generator output with the same parameters.

(d) Re-sampling of the hyperparameter λ

The reflectivity sequence x gathers all the information about λ contained in (z, x, h, σ^2), that is, $P(\lambda|z, x, h, \sigma^2) = P(\lambda|x)$. Following [65], let us remark that the Bernoulli sequence q can be retrieved from x with probability one according to $q_k = 1$ if $x_k \neq 0$, $q_k = 0$ otherwise. Thus, $P(\lambda|x) = P(\lambda|q)$, the latter being proportional to $P(q|\lambda)$ since we assumed a flat prior $P(\lambda) = 1$. Finally, according to Eq. (5.40), we get

$$P(\lambda|z, x, h, \sigma^2) \propto \lambda^n (1 - \lambda)^{M-n}\,, \tag{5.60}$$

which belongs to the family of beta probability densities $\mathcal{B}(\alpha, \beta)$ with $\alpha = n + 1$ and $\beta = M - n + 1$.

Chapter 6

Application I: Quantum inversion

For the application of our model we consider the single and coupled channels inversion using the Gaussian potential, smooth square-type potential and multi-layered potential.

6.1 Single channel inversion

In what follows we calculate the reflection and transmission coefficients as well as the $B-$functions for the Gaussian, smooth square-type and multi-layered potentials and reconstruct the potentials from these data.

6.1.1 Gaussian potential

The quality of our inversion model is demonstrated by reconstructing the potential from the calculated reflection coefficient for the Gaussian potential. For the numerical calculation of the reflection coefficient $R(k)$, it is advantageous to start in region III, (see Fig. (2.1)) where the wave function will be a multiple of e^{ikx} and integrate in the negative x-direction. After arriving at the point $x = 0$ both $R(k)$ and $T(k)$ can easily be worked out. The real and imaginary parts of the reflection and transmission coefficients represent the properties of a system within and outside the interval $[0, a]$. The real and imaginary parts of the reflection and transmission coefficients, $R(k)$ and $T(k)$, are depicted in Figs. (6.1) and (6.2) respectively. The Fourier transform of

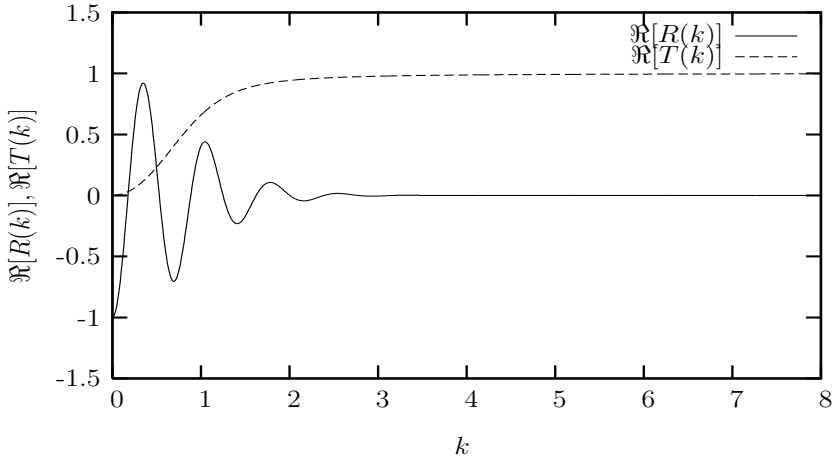

Figure 6.1: The real parts of the reflection and transmission coefficients for the Gaussian potential.

$R(k)$, that is, Eq. (4.6), has been calculated by applying the FFT algorithm [37]. The $B-$function, Eq. (4.6), which is the reflected wave, is plotted in Fig. (6.3). Fig. (6.4) depicts the reconstructed potential and its original potential while Fig. (6.5)

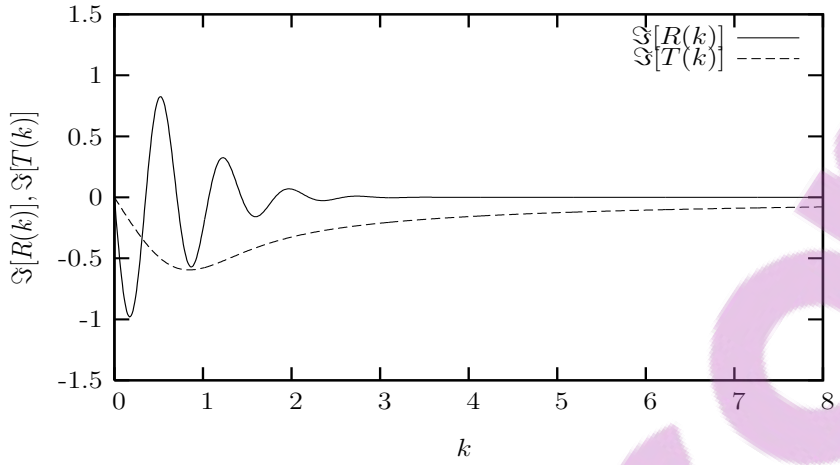

Figure 6.2: The imaginary parts of the reflection and transmission coefficients for the Gaussian potential.

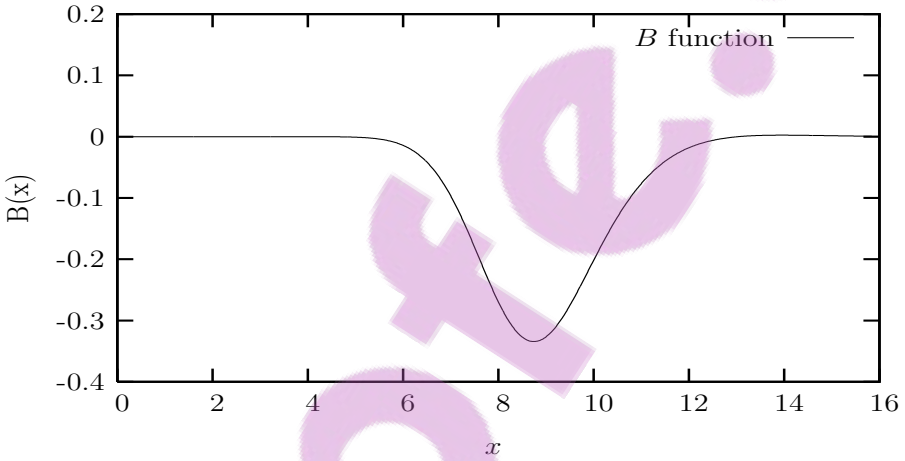

Figure 6.3: The $B-$function for the Gaussian potential.

gives the deviation of the reconstructed potential from the original potential. The number of integration points n_i and the number of Chebyshev points n_{ch} are 20 and 40 respectively for the Gaussian potential. The quality of the inversion is quite good and the input and reconstructed potentials are, for all practical purposes, identical.

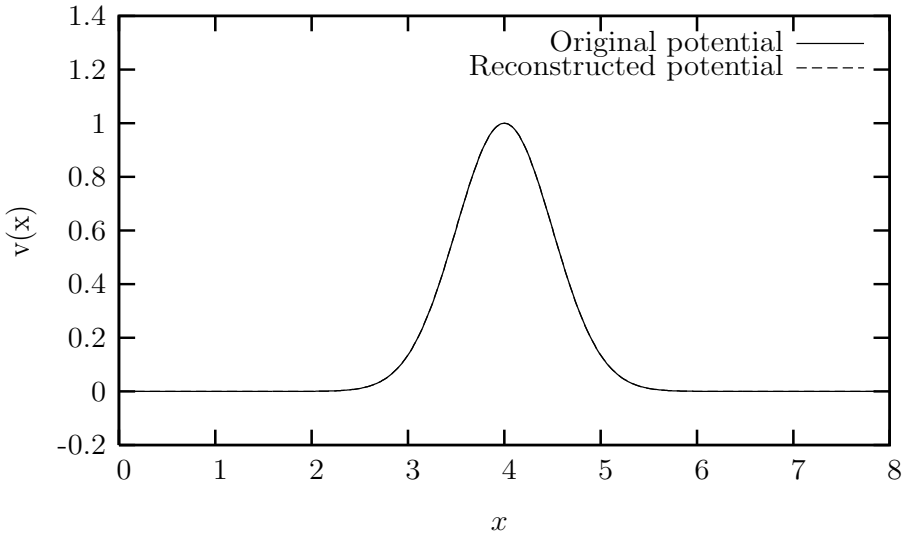

Figure 6.4: Comparison between the reconstructed and original Gaussian potentials. To all practical purposes, the two potentials coincide.

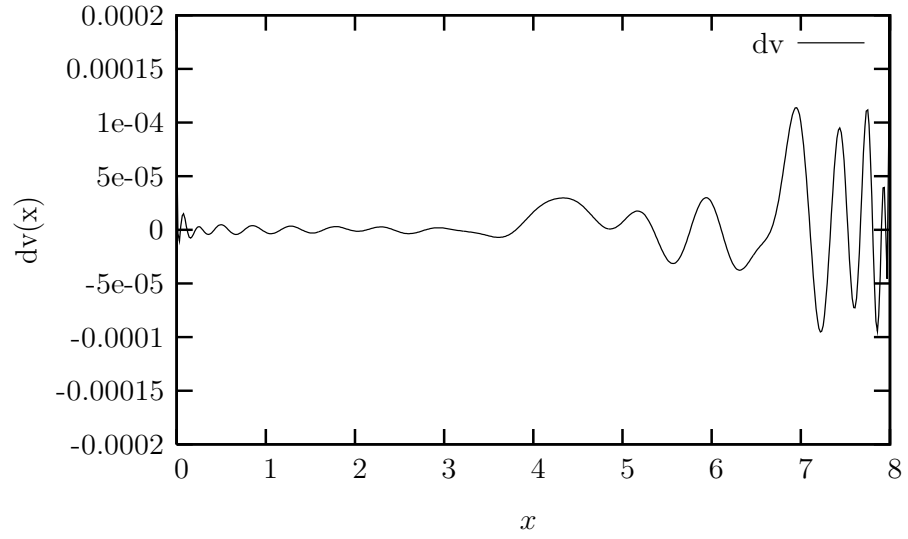

Figure 6.5: The difference between the reconstructed and original Gaussian potentials.

6.1.2 Smooth square-type potential

The procedure used in section 6.1.1 to calculate for the real and imaginary parts of the reflection and transmission coefficients, the reconstructed potential as well as the difference between the smooth square-type potentials has been followed. The number of integration points n_i and the number of Chebyshev points n_{ch} are both 100. The quality of the inversion model is again quite good. Figs. (6.6) and (6.7) depict the real and imaginary parts of the reflection and transmission coefficients. The B-function of the smooth square-type potential is shown in Fig. (6.8) while the reconstructed potential is shown in Fig. (6.9) and its deviation from the original potential is depicted in Fig. (6.10).

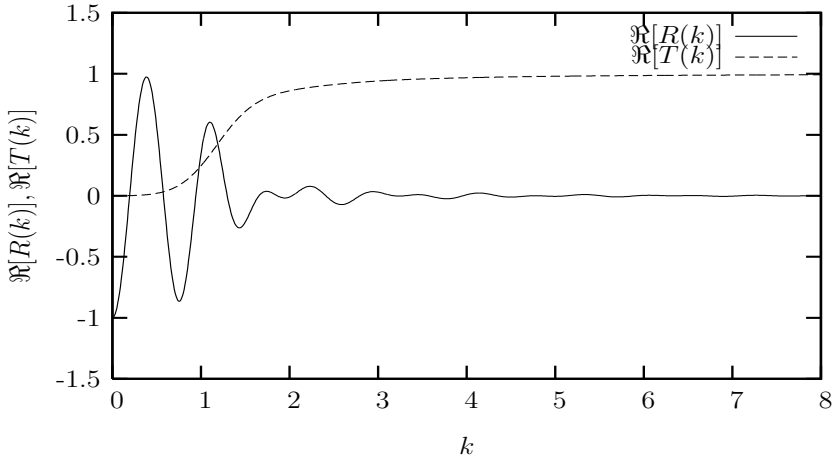

Figure 6.6: The imaginary parts of the reflection and transmission coefficients for the smooth square-type potential.

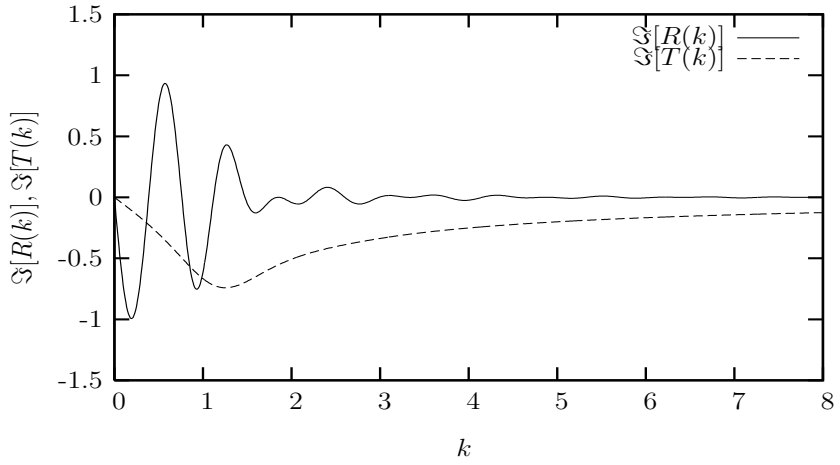

Figure 6.7: The imaginary parts of the reflection and transmission coefficients for the smooth square-type potential.

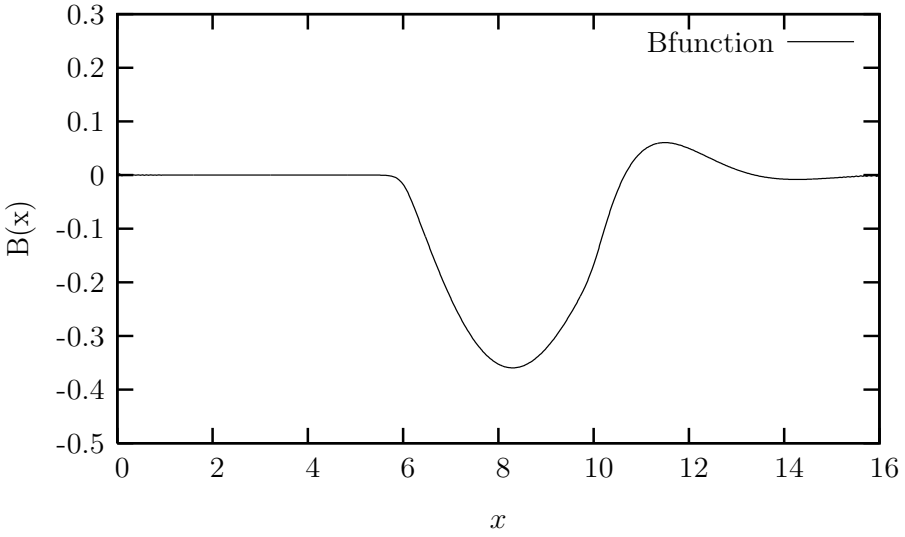

Figure 6.8: The $B-$function for the smooth square-type potential.

6.1.3 Multi-layered potential

To test the quality of the inversion method used in sections 6.1.1 and 6.1.2 we applied it to a much more structured potential (multi-layered potential) which shows several

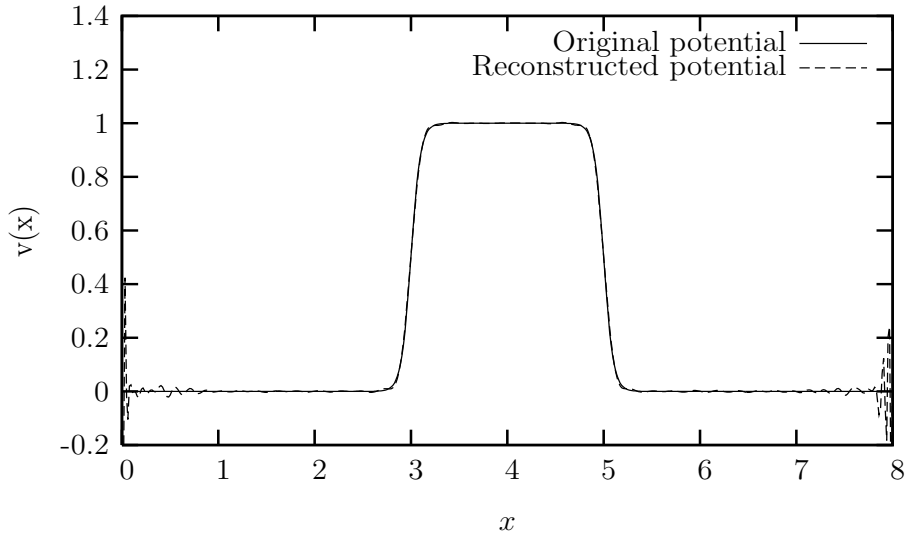

Figure 6.9: Comparison between the reconstructed and original smooth square-type potentials.

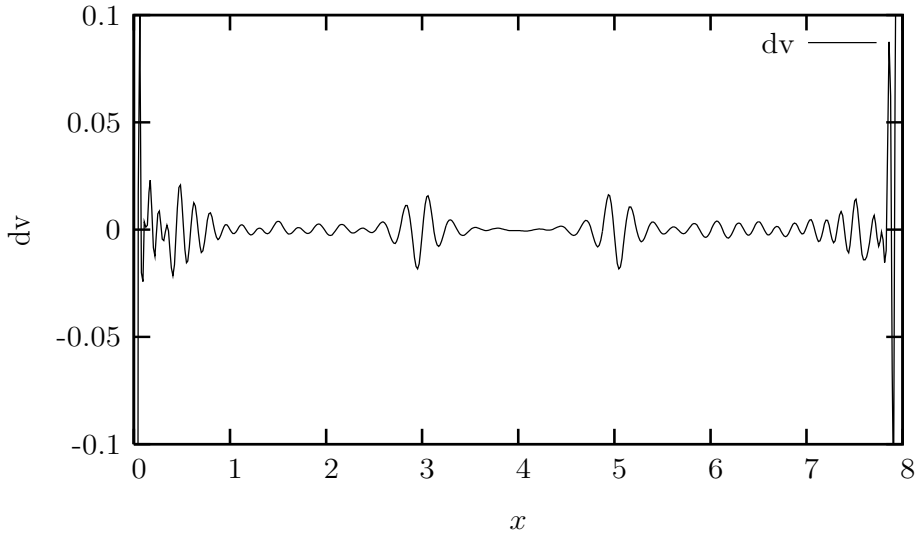

Figure 6.10: The difference between the reconstructed and original smooth square-type potentials.

layers. The real and imaginary parts of the reflection and transmission coefficients, the B-function, the reconstructed potential and the difference between the reconstructed and original potentials are shown in Figs. (6.11–6.15) respectively. The number of integration points n_i and the Chebyshev points n_{ch} are 200 and 300 respectively. The quality of the inversion method is also quite good for the multi-layered potential.

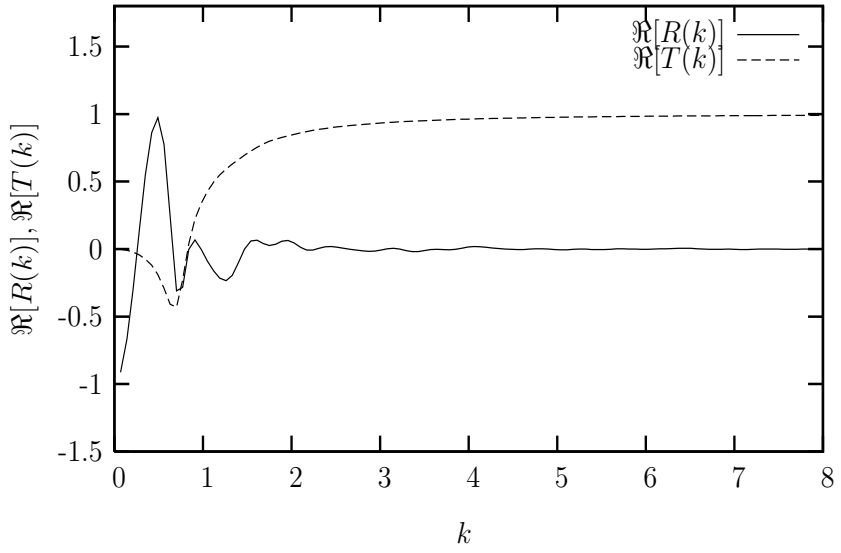

Figure 6.11: The real parts of the reflection and transmission coefficients for the multi-layered potential.

6.2 Coupled channel inversion

In what follows we calculate the elements of the reflected waves, the reconstructed potentials and their deviations from the original potentials.

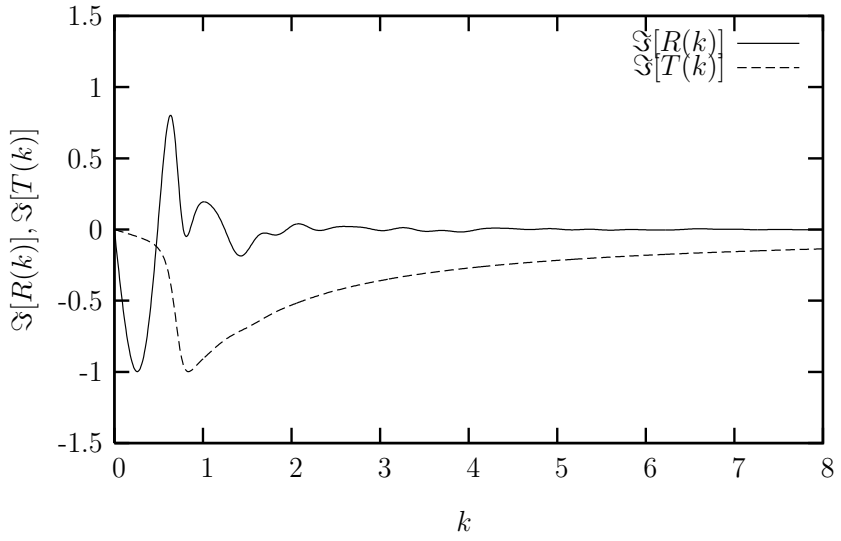

Figure 6.12: The real parts of the reflection and transmission coefficients for the multi-layered potential.

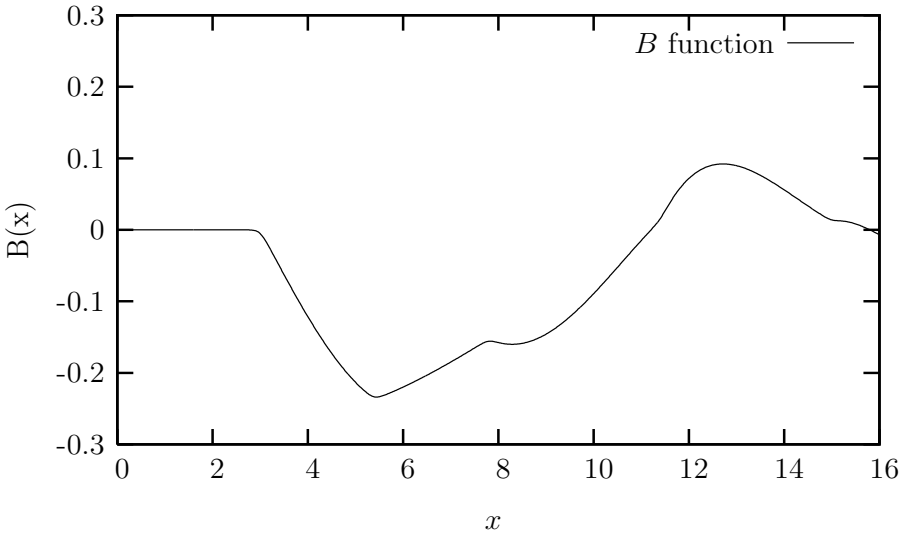

Figure 6.13: The $B-$function for the multi-layered potential.

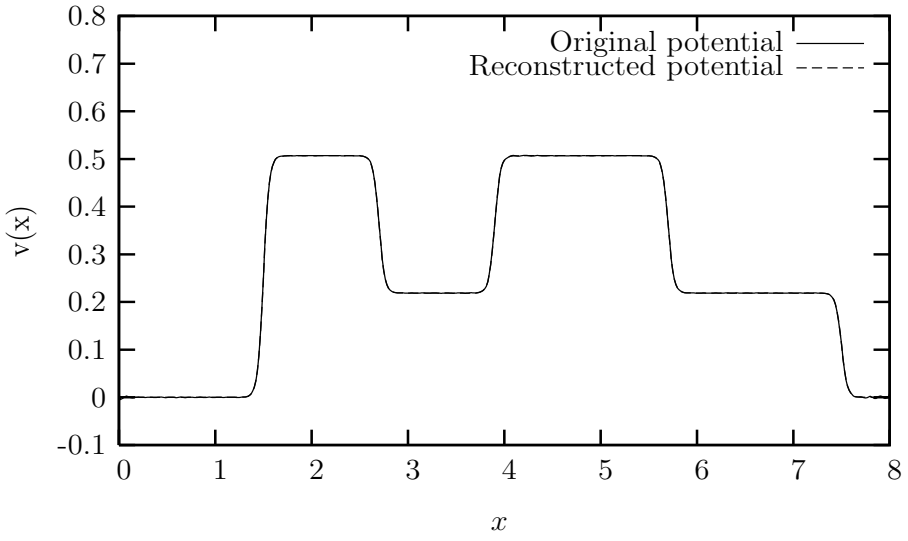

Figure 6.14: Comparison between the reconstructed and the original multi-layered potentials.

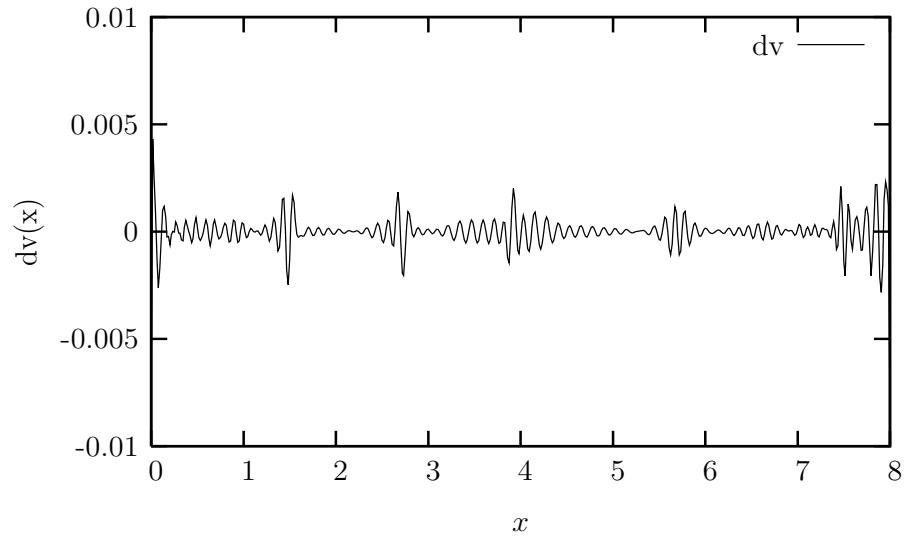

Figure 6.15: The difference between the reconstructed and the original multi-layered potentials.

6.2.1 Gaussian potential matrix

The description given for the single channel is also applicable to the coupled channel by using Eq. (2.17) for the Schrödinger equation and Eq. (5.15) for the Marchenko integral equation. Figs. (6.16–6.24) show the matrix elements of the reflected wave, reconstructed and original smooth square-type potential matrix as well as the difference between the reconstructed and original smooth square-type potential matrix respectively. The number of integration points n_i and the number of Chebyshev points n_{ch} used for the Gaussian potential matrix are 20 and 40 respectively. The quality of the inversion is quite good.

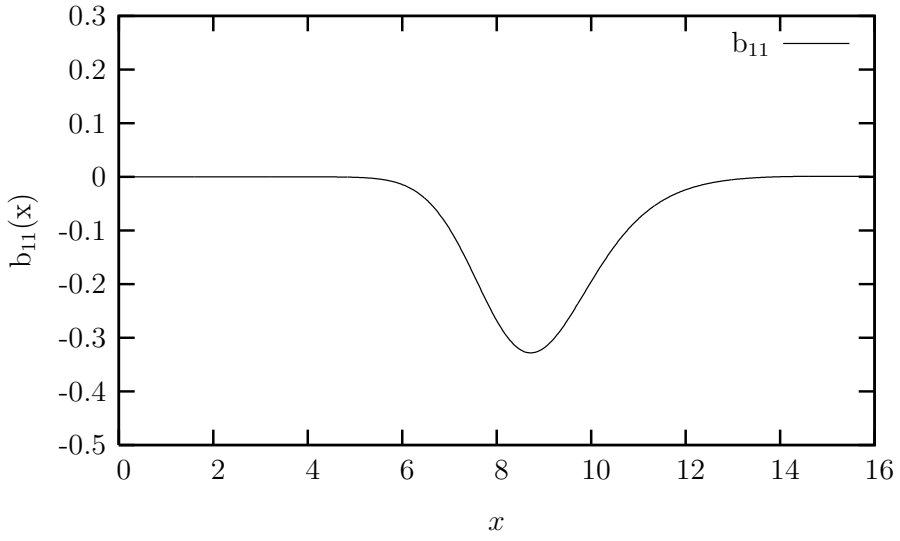

Figure 6.16: The $b_{11}-$function for the Gaussian potential matrix.

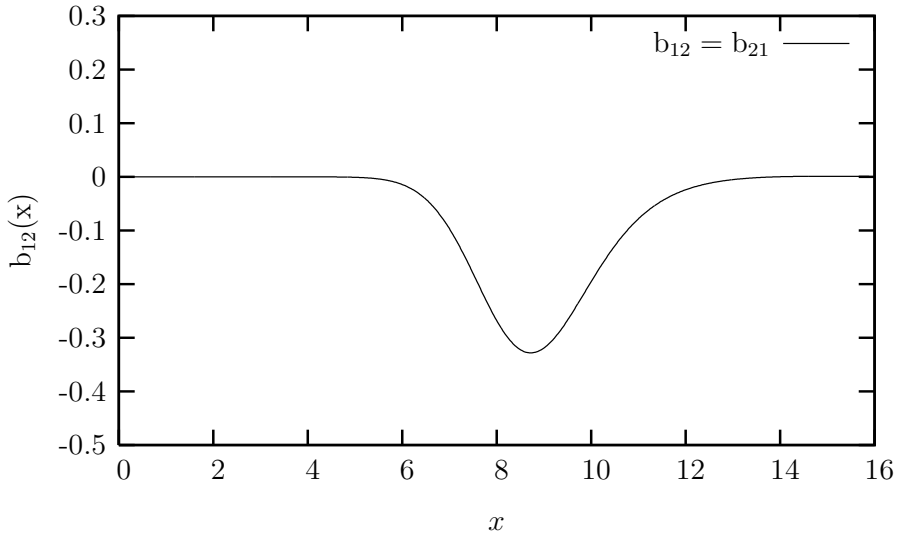

Figure 6.17: The $b_{12} = b_{21}-$function for the Gaussian potential matrix.

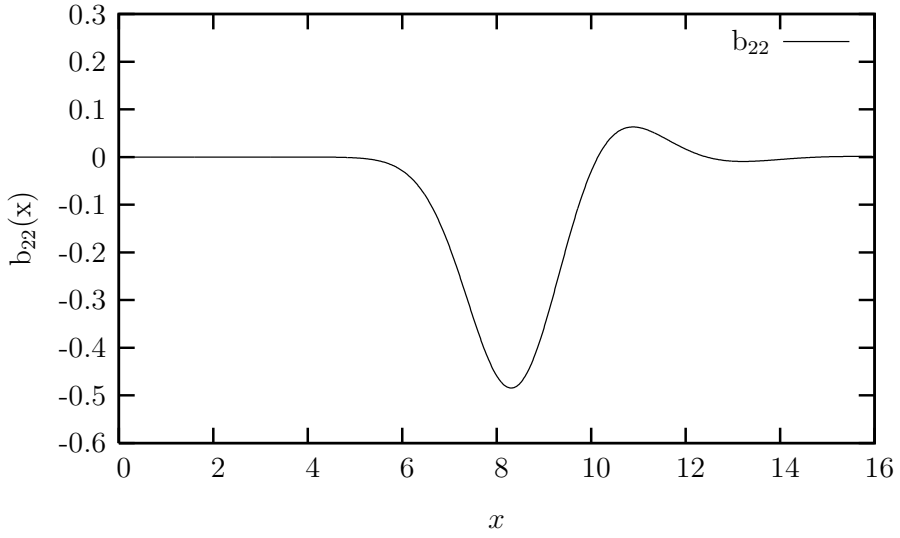

Figure 6.18: The $b_{22}-$function for the Gaussian potential matrix.

6.2.2 Smooth square-type potential matrix

The matrix elements (b_{11}, $b_{12} = b_{21}$, b_{22}) of the reflected waves for the smooth square-type potential are depicted in Figs. (6.25–6.27) while the reconstructed potential

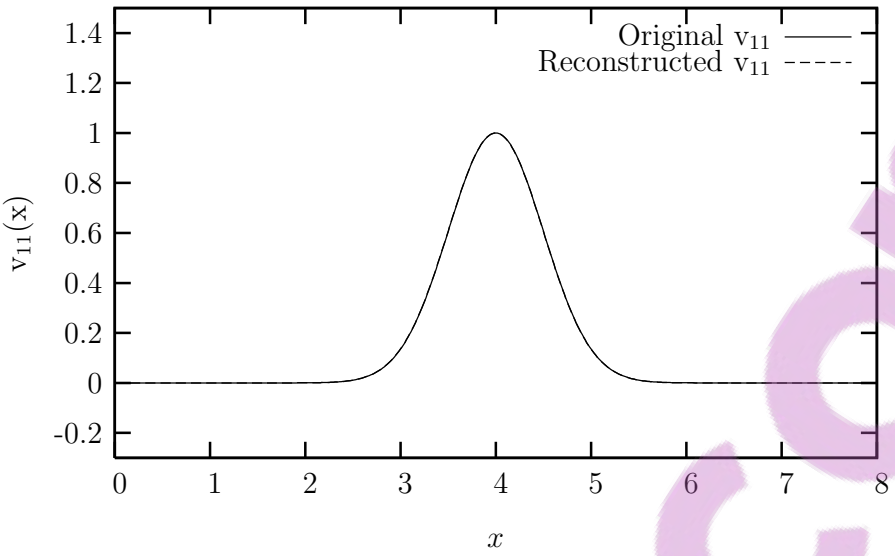

Figure 6.19: The comparison between the reconstructed and original Gaussian potential matrix elements v_{11}.

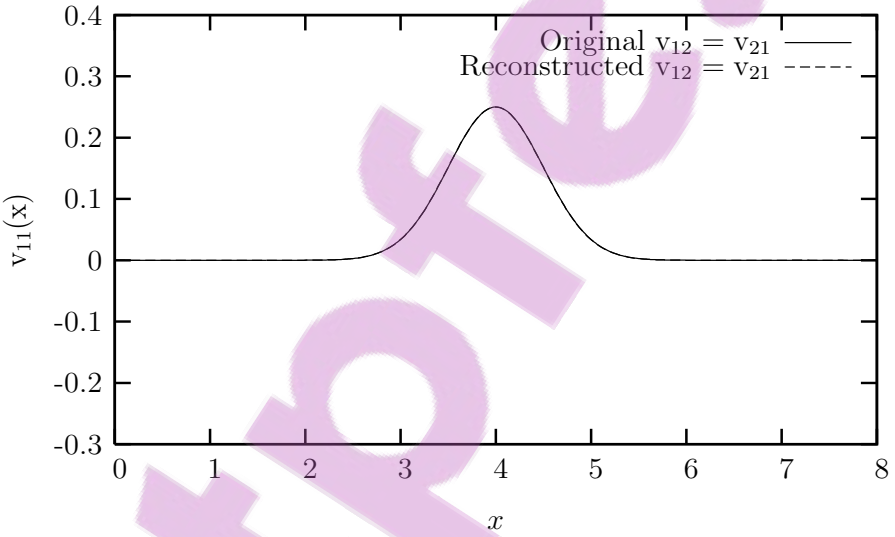

Figure 6.20: The comparison between the reconstructed and original Gaussian potential matrix elements $v_{12} = v_{21}$.

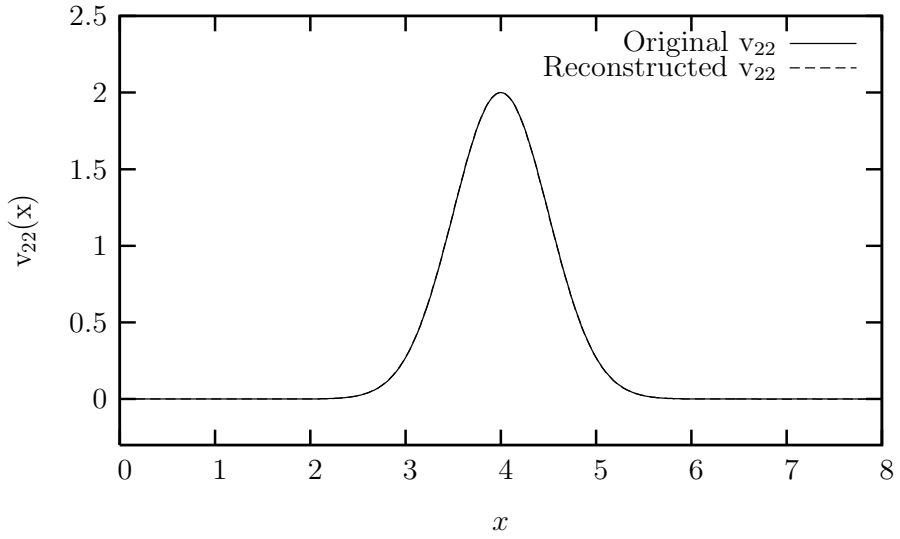

Figure 6.21: The comparison between the reconstructed and original Gaussian potential matrix elements v_{22}.

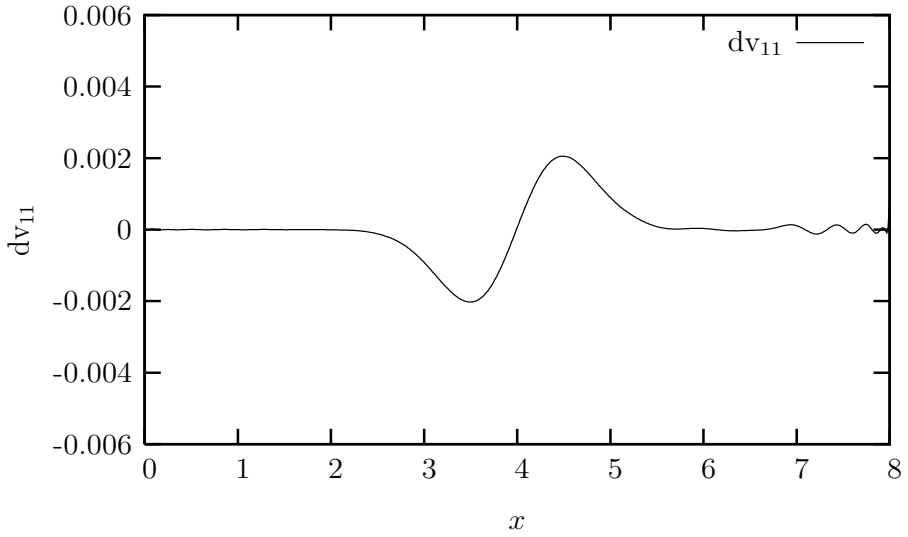

Figure 6.22: The difference between the reconstructed and the original Gaussian potential matrix elements v_{11}.

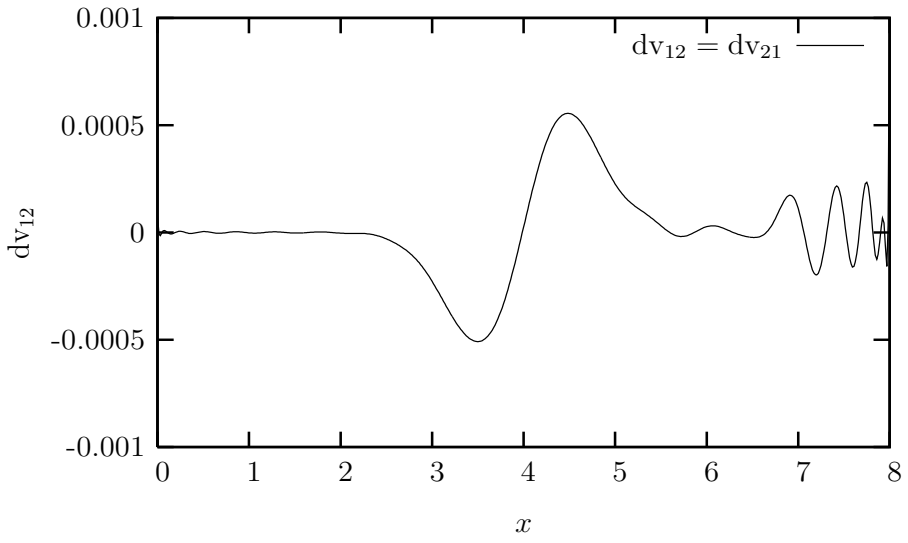

Figure 6.23: The difference between the reconstructed and original Gaussian potential matrix elements $v_{12} = v_{21}$.

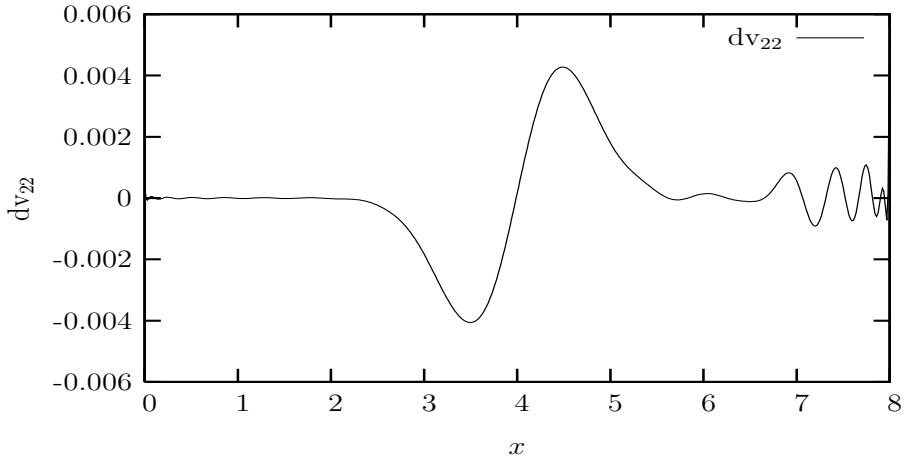

Figure 6.24: The difference between the reconstructed and original Gaussian potential matrix elements v_{22}.

matrix elements (v_{11}, $v_{12} = v_{21}$, v_{22}) are shown in Figs. (6.28–6.30). Figs. (6.31–6.33) show the difference between the multi-layered potential matrix elements (dv_{11},

$dv_{12} = dv_{21}$, dv_{22}). The number of integration points n_i and the number of the Chebyshev points n_{ch} are both 100 as in the single channel inversion. The quality of the inversion model is quite satisfactory.

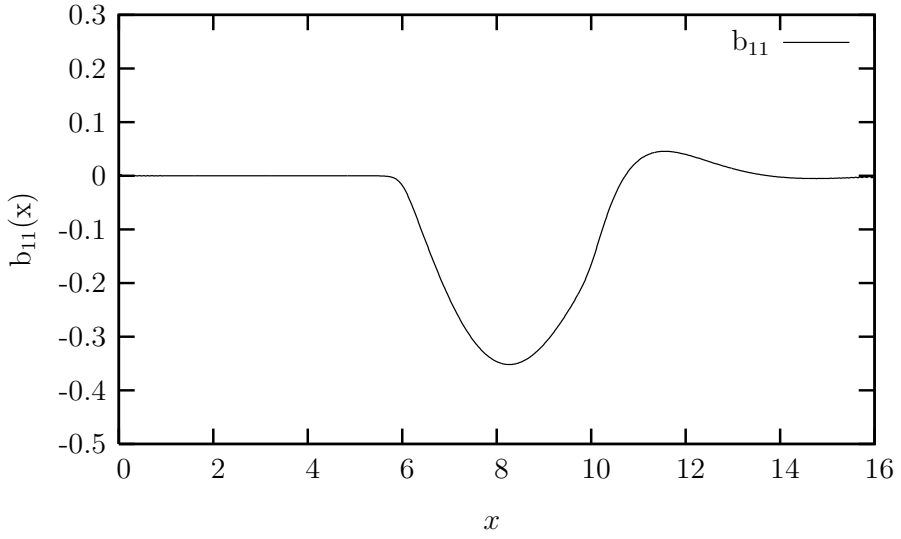

Figure 6.25: The $b_{11}-$function for the smooth square-type potential matrix.

6.2.3 Multi-layered potential matrix

Figs. (6.34–6.42) show the matrix elements of the reflected wave, reconstructed and original multi-layered potential matrix as well as the difference between the reconstructed and original multi-layered potential matrix in the coupled channel inversion respectively. The number of integration points n_i and the number of Chebyshev points n_{ch} used for the multi-layered potential matrix are 200 and 300 respectively. The quality of the inversion is still quite good.

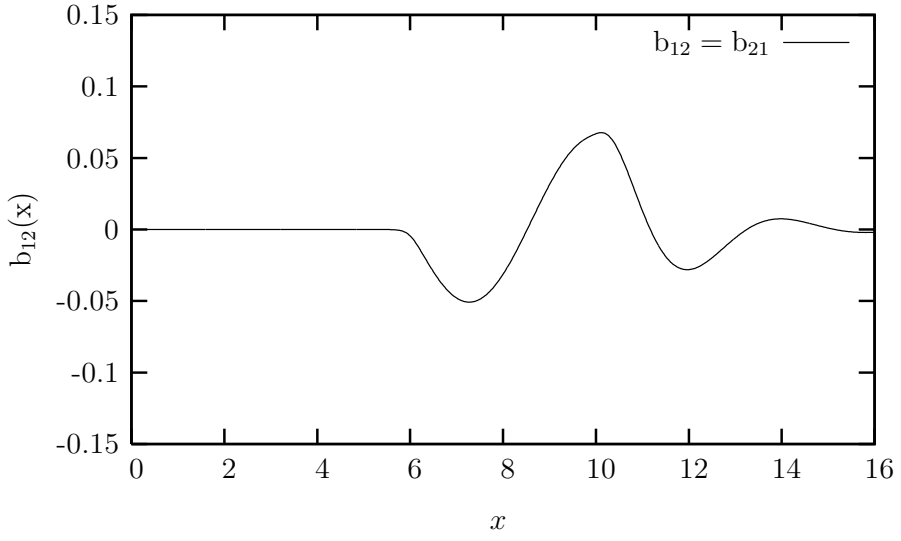

Figure 6.26: The $b_{12}-$function for the smooth square-type potential matrix.

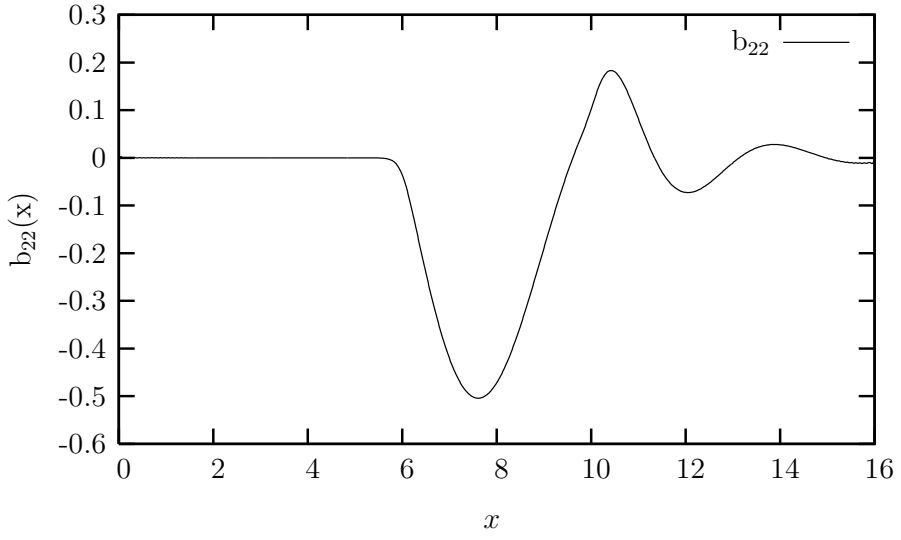

Figure 6.27: The $b_{22}-$function for the smooth square-type potential matrix.

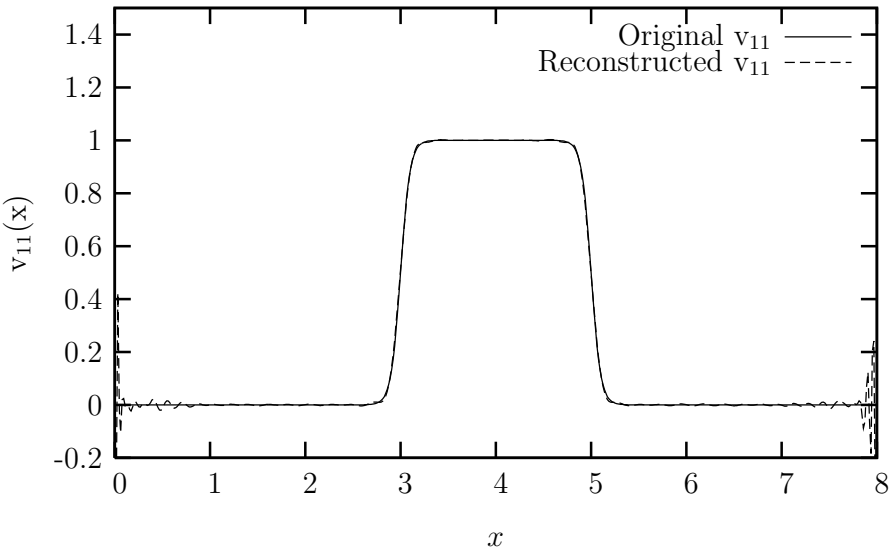

Figure 6.28: The comparison between the reconstructed and original smooth square-type potential matrix elements v_{11}.

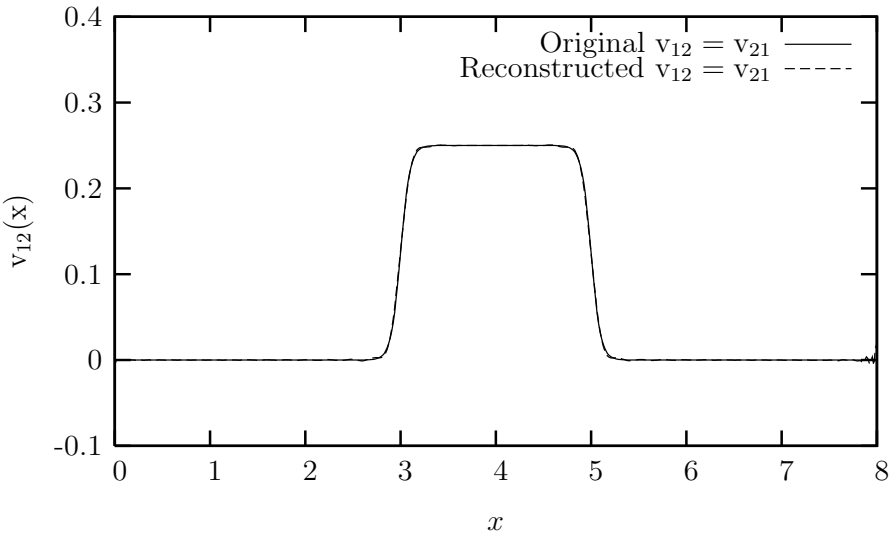

Figure 6.29: The comparison between the reconstructed and original smooth square-type potential matrix elements $v_{12} = v_{21}$.

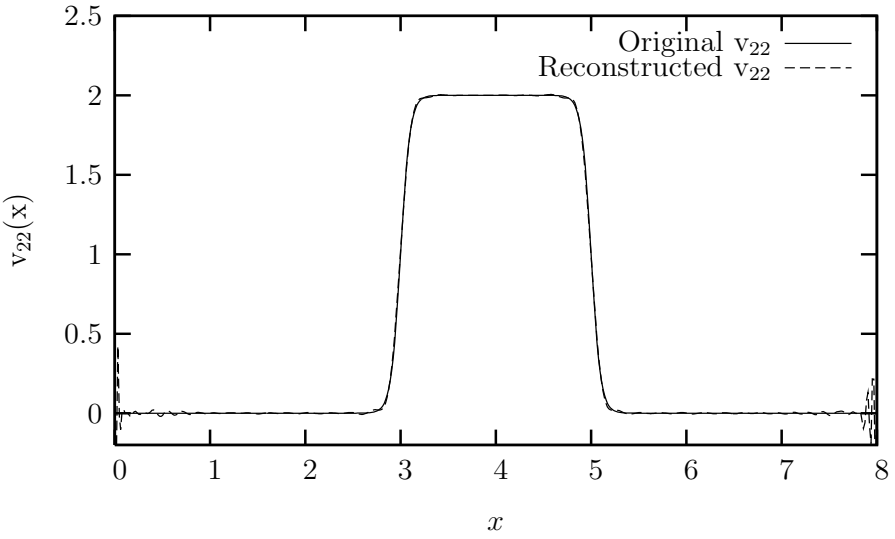

Figure 6.30: The comparison between the reconstructed and original smooth square-type potential matrix elements v_{22}.

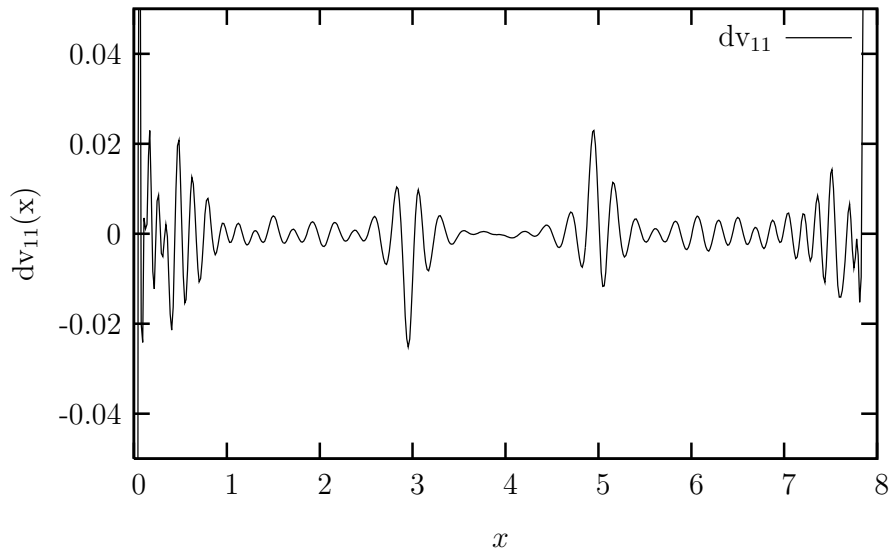

Figure 6.31: The difference between the reconstructed and the original smooth square-type potential matrix elements v_{11}.

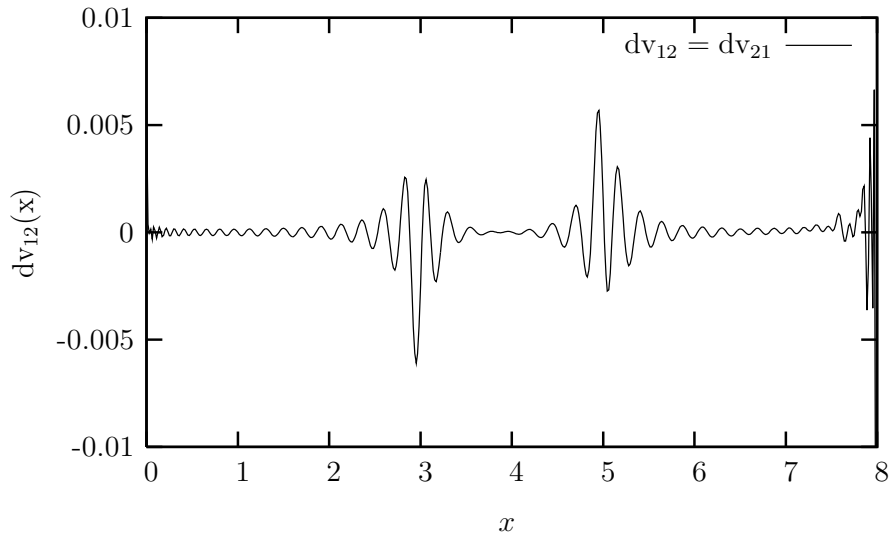

Figure 6.32: The difference between the reconstructed and original smooth square-type potential matrix elements $v_{12} = v_{21}$.

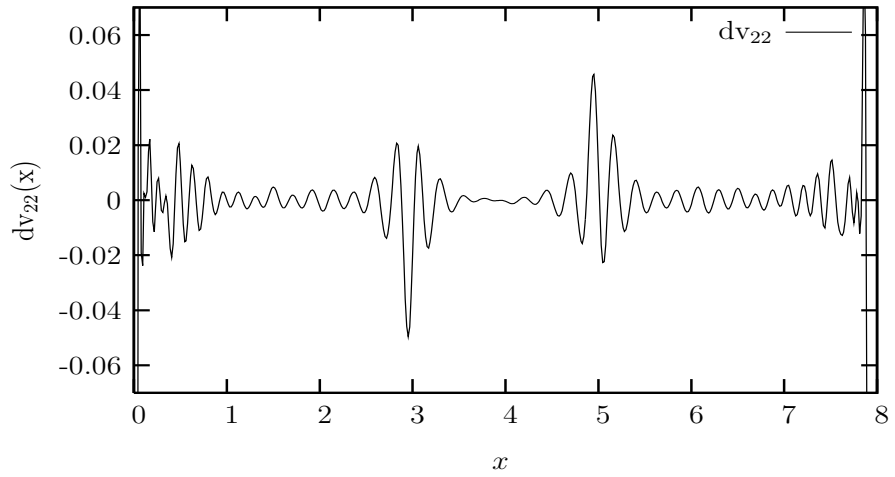

Figure 6.33: The difference between the reconstructed and original smooth square-type potential matrix elements v_{22}.

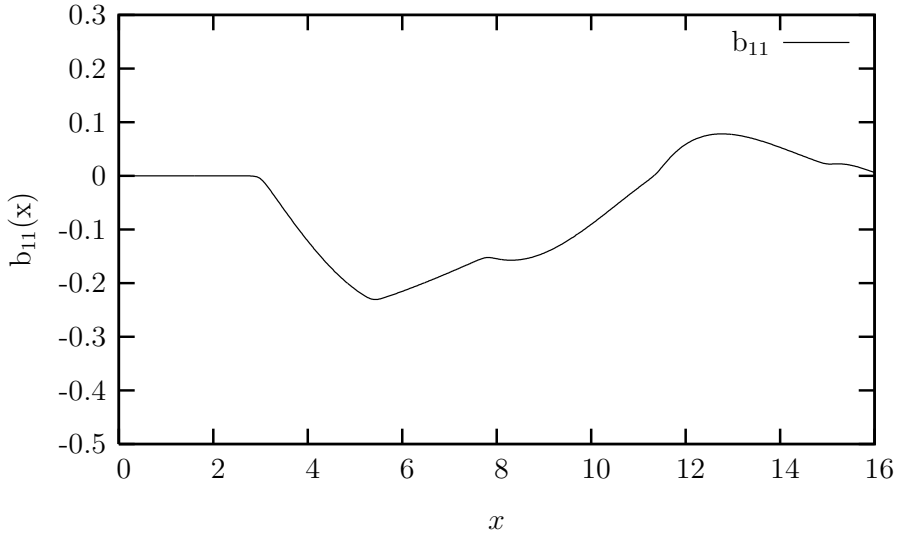

Figure 6.34: The $b_{11}-$function for the multi-layered potential matrix.

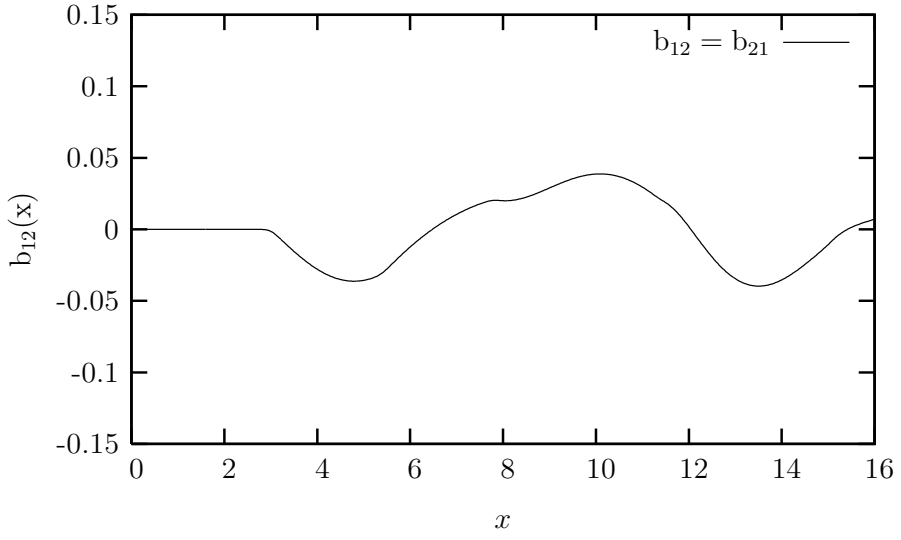

Figure 6.35: The $b_{12}-$function for the multi-layered potential matrix.

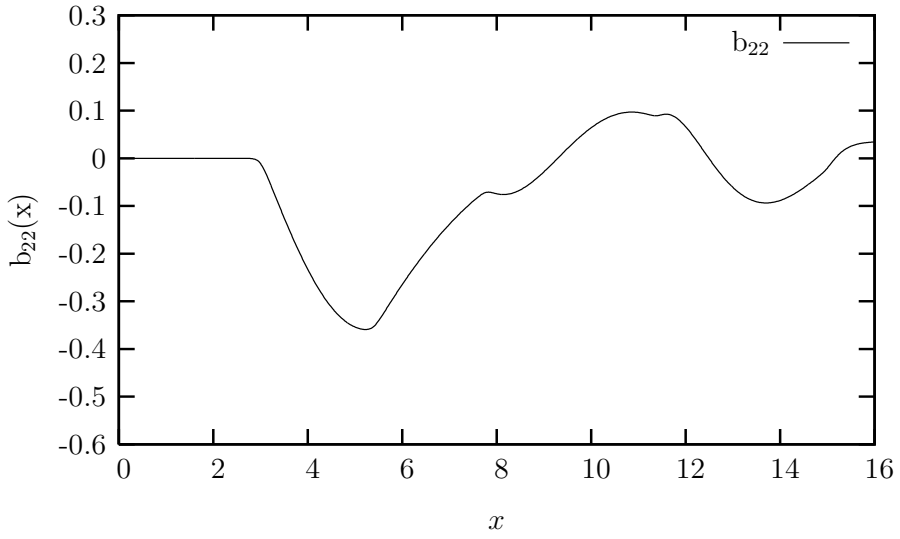

Figure 6.36: The $b_{22}-$function for the multi-layered potential matrix.

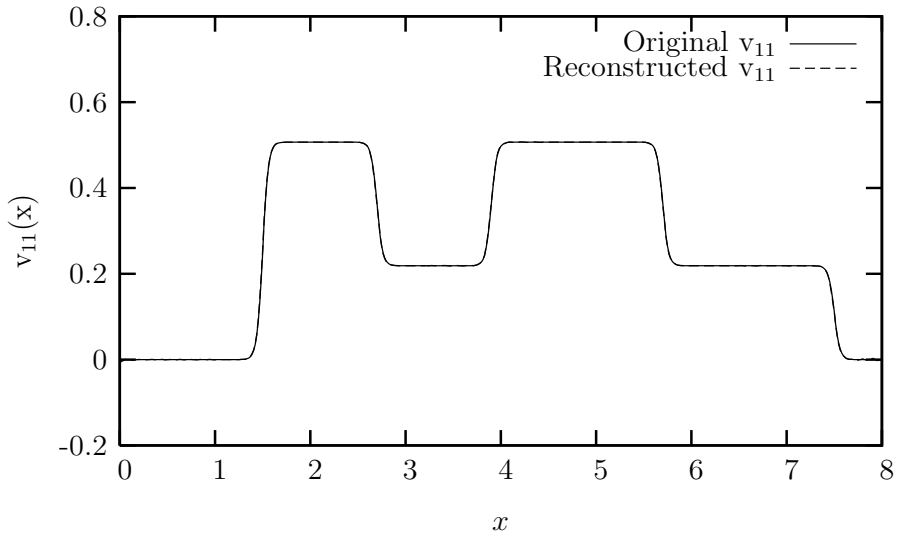

Figure 6.37: The comparison between the reconstructed and original multi-layered potential matrix elements v_{11}.

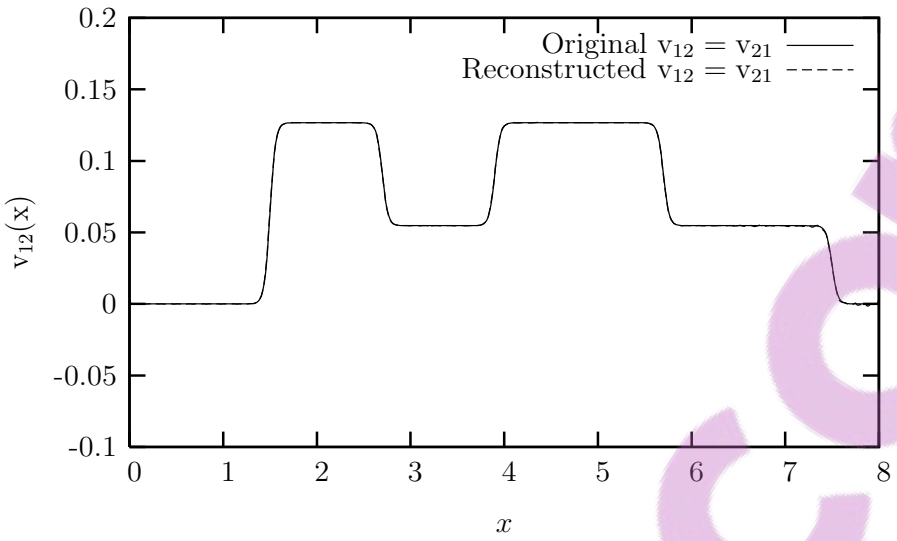

Figure 6.38: The comparison between the reconstructed and original multi-layered potential matrix elements $v_{12} = v_{21}$.

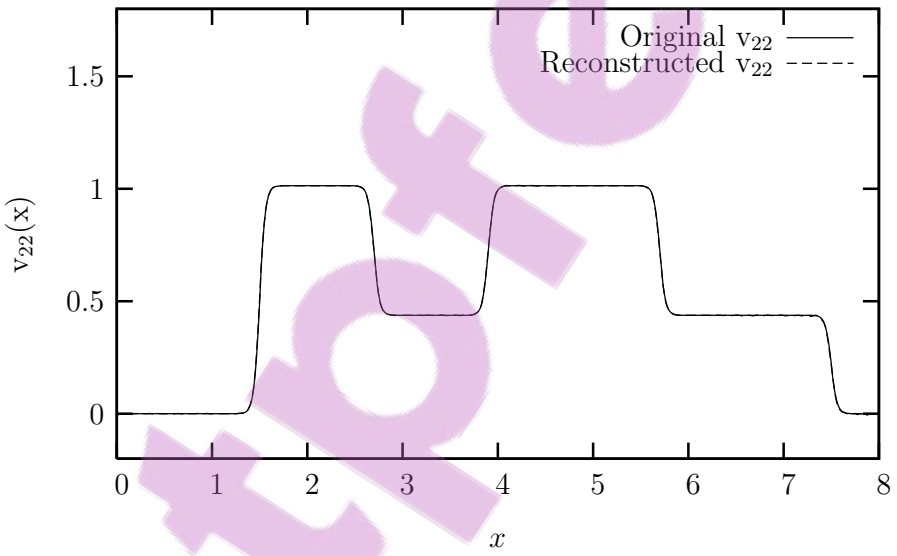

Figure 6.39: The comparison between the reconstructed and original multi-layered potential matrix elements v_{22}.

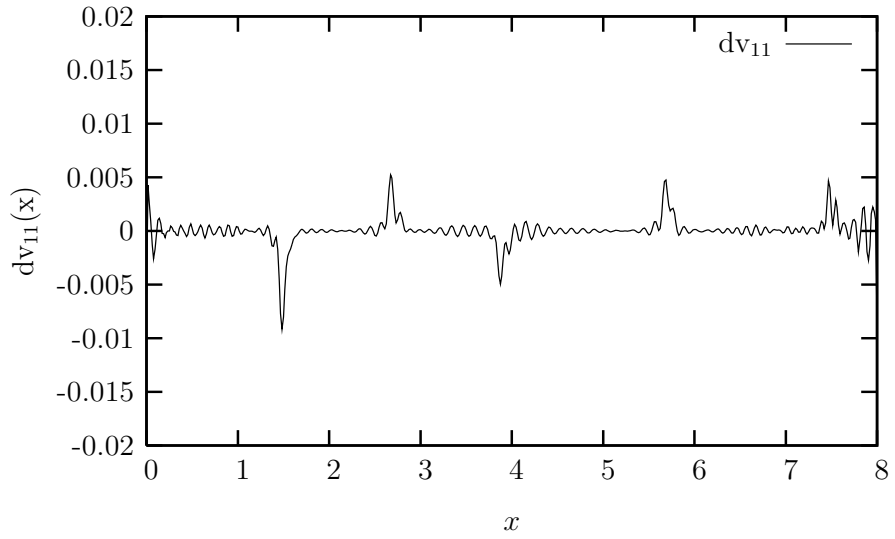

Figure 6.40: The difference between the reconstructed and the original multi-layered potential matrix elements v_{11}.

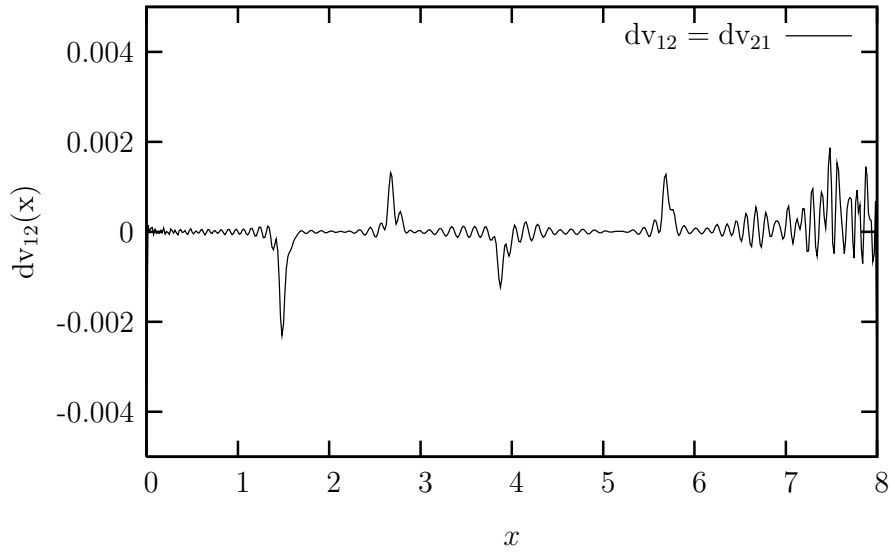

Figure 6.41: The difference between the reconstructed and original multi-layered potential matrix elements $v_{12} = v_{21}$.

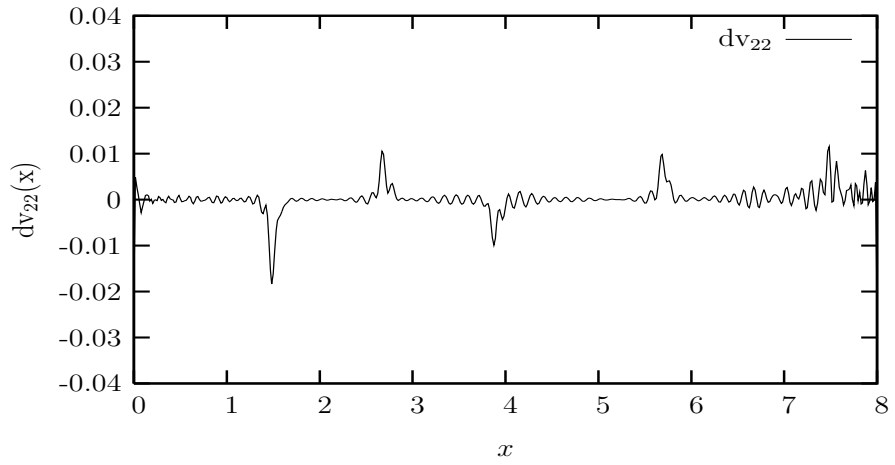

Figure 6.42: The difference between the reconstructed and original multi-layered potential matrix elements v_{22}.

Chapter 7

Application II: Seismic inversion

In the geophysical exploration process, the seismic waves are used for the search for oil, gas and mineral deposits. This process uses a seismic wave which is partially reflected and partially transmitted when it encounters the interface. The objective is to recover the seismic impedance from the observed seismic reflection data. In this chapter we reconstruct a slab-type seismic impedance by using the $B-$function, as obtained from our simulation, as input into the Marchenko integral equation.

7.1 Slab-type seismic impedance

7.1.1 Reconstruction of impedance using the ray series

(a) Single-interface problem

After transformation of Eqs. (3.39)–(3.43) to the travel-time domain, Gaussians of widths b, $3b$, $5b$, $7b$ and $9b$ are obtained yielding

$$\begin{aligned} B(\xi) &= \frac{R_{12}}{\sqrt{\pi}b}\mathrm{e}^{-\frac{(\xi-2\xi_1)^2}{b^2}} \\ &+ \frac{1}{\sqrt{\pi}b}R_{23}\mathrm{e}^{-\frac{(\xi-2\xi_2)^2}{b^2}} - \frac{1}{\sqrt{3\pi}b}R_{12}^2R_{23}\mathrm{e}^{-\frac{(\xi-2\xi_1))^2}{3b^2}} \\ &+ \frac{1}{\sqrt{3\pi}b}R_{23}^2R_{21}\mathrm{e}^{-\frac{(\xi-(4\xi_2-2\xi_1))^2}{3b^2}} - \frac{1}{\sqrt{5\pi}b}R_{12}^2R_{23}^2R_{21}\mathrm{e}^{-\frac{(\xi-(4\xi_2-2\xi_1))^2}{5b^2}} \\ &+ \frac{1}{\sqrt{5\pi}b}R_{23}^3R_{21}^2\mathrm{e}^{-\frac{(\xi-(6\xi_2-4\xi_1))^2}{5b^2}} - \frac{1}{\sqrt{7\pi}b}R_{12}^2R_{23}^3R_{21}^2\mathrm{e}^{-\frac{(\xi-(6\xi_2-4\xi_1))^2}{7b^2}} \\ &+ \frac{1}{\sqrt{7\pi}b}R_{23}^4R_{21}^3\mathrm{e}^{-\frac{(\xi-(8\xi_2-6\xi_1))^2}{7b^2}} - \frac{1}{\sqrt{9\pi}b}R_{12}^2R_{23}^4R_{21}^3\mathrm{e}^{-\frac{(\xi-(8\xi_2-6\xi_1))^2}{9b^2}} . \end{aligned} \quad (7.1)$$

Eq. (7.1) is now in effect finite due to a truncation of the ξ-domain. Thus, the higher terms do not contribute in the numerical treatment.

We demonstrate the reliability of the proposed method by using model seismic experiments. As a first example, we consider a single reflection in a two-layered medium with impedances $\eta_1 = 1$ and $\eta_2 = 1.5$. The reflected signal is assumed to be of Gaussian form with $\xi = 3$ and is the result of one bounce at the (first) interface. The $B(\xi)$ is given by Eq. (3.57) or the first term in Eq. (7.1) and the reflection coefficient R_{12} by Eq. (3.15). The b in this case was chosen as 0.5.

The signal used and the recovered impedance are shown in Figs. (7.1) and (7.2) respectively. It is seen that the reproduction of the seismic impedance of the reflecting medium is excellent. Outside the transition region, the values of η_1 and η_2 are recovered to about 4 decimals.

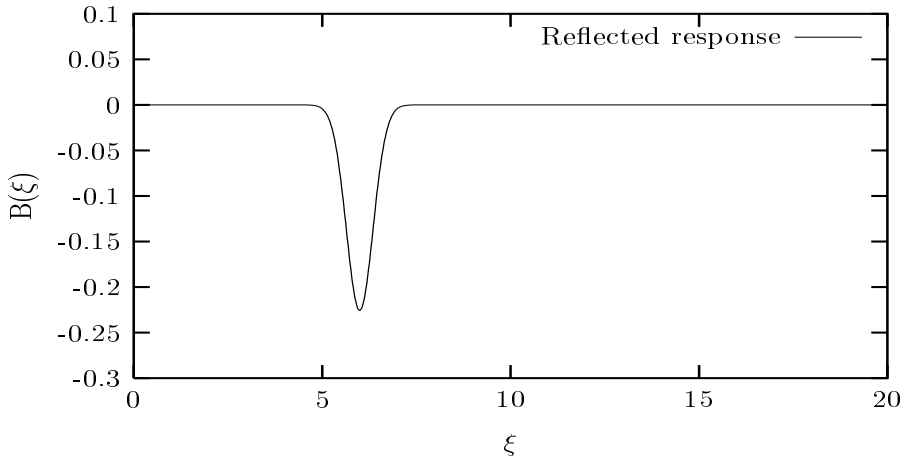

Figure 7.1: The single reflected signal in a two-layered medium.

(b) Double-interface medium

The second example considered is the one with a three-layered medium with interfaces at travel-times $\xi_1 = 3$ and $\xi = 5$, resulting in the reflected Gaussians being centred at $t_1 = 2\xi_1 = 6$, $t_2 = 2\xi_2 = 10$, $t_3 = 4\xi_2 - 2\xi_1 = 14$, $t_4 = 6\xi_2 - 4\xi_1 = 18$ and $t_5 = 8\xi_2 - 6\xi_1 = 22$. The seismic impedances of the layers are assumed to be $\eta_1 = 1$, $\eta_2 = 1.5$ and $\eta_3 = 0.9$. The reflected signal together with the recovered impedance, are shown in Figs. (7.3) and (7.4). The recovery of the impedances is, once more, excellent.

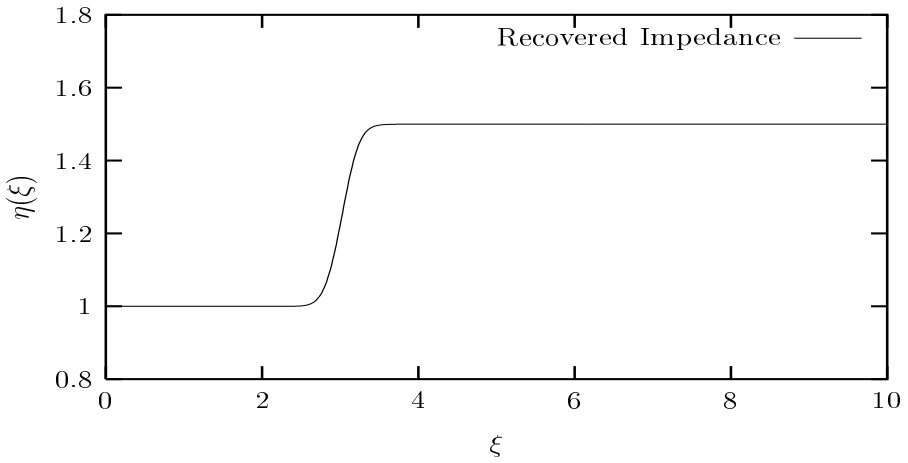

Figure 7.2: The recovered impedance. The input impedances are $\eta_1 = 1$ and $\eta_2 = 1.5$ for a single scattering in Fig. (7.1) in a two-layered medium.

.

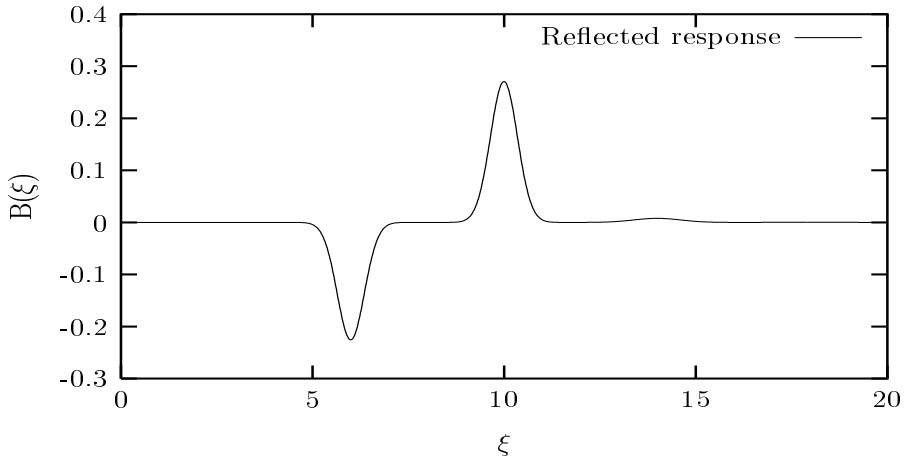

Figure 7.3: The reflected pulse at the second interface for five reflections in a three-layered medium.

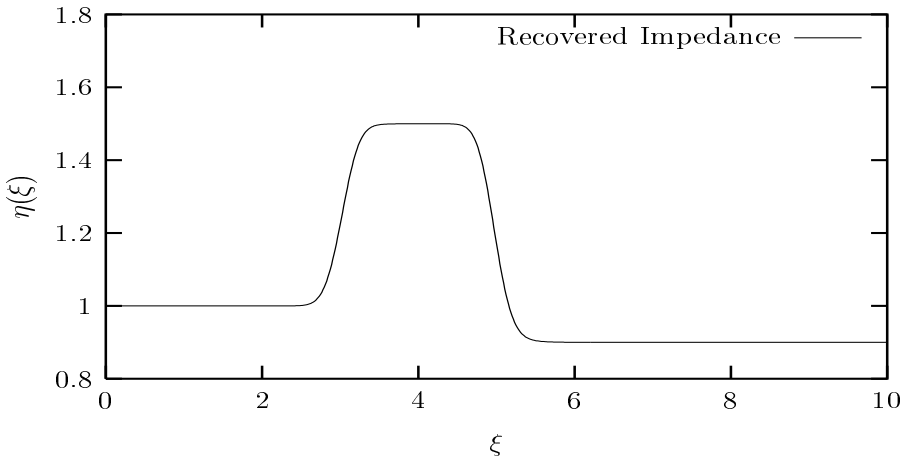

Figure 7.4: The reconstructed impedance from the input reflected signal shown in Fig. (7.3).

7.1.2 Recovery of impedance using the recursive relation

Here we simulate the reflected signals by applying the recursive equation of $\tilde{R}_{12}$ from Eq. (3.55) and the Gaussian forms. We use $\tilde{R}_{12}$ because it contains the effects of the whole stack of layers below interface at d_1. Eq. (3.31) can be replaced by

$$R_{i,i+1}(k) = R_{i,i+1}\mathrm{e}^{-\frac{b^2k^2}{4}}\,, \tag{7.2}$$

for a constant width b, otherwise

$$R_{i,i+1}(k) = R_{i,i+1}\mathrm{e}^{-\frac{b_i^2k^2}{4}}\,, \tag{7.3}$$

for a varying width b. Therefore, from Eq. (3.27), the reflection coefficient $R(k)$ (Eq. (3.28)), required for the Marchenko integral equation, can be obtained from Eqs. (3.39)–(3.43).

(a) Multi-interface media with a common width

We assume that a more appropriate simulation of a reflected signal received by the hydrophone can be modeled in the same form as the $B-$function

$$B(\xi) = \frac{1}{2\pi}\int_{-\infty}^{\infty} R(k)\mathrm{e}^{-ik\xi}dk\,, \tag{7.4}$$

where $R(k)$ is given by Eq. (3.34).

The equation applicable for an $N-$layered medium is given by Eq. (3.55). For such a system, 1 is the index of the top layer. The recursive application of Eq. (3.55) starts at the layer with index $N-1$ next to the bottom and then proceeds recursively towards the top layer, yielding the desired total reflection coefficient (Eq. (7.5)), which is given in terms of the nested reflection coefficients [50].

For the application of Eq. (7.4) we calculate the seismic impedances from the three-layered medium through to the six-layered medium. The reflection coefficient for the three-layered medium is recursively calculated using Eq. (3.55) as

$$\tilde{R}_{12}(k) = \frac{R_{12}(k) + \tilde{R}_{23}(k)\mathrm{e}^{2ik_2(d_2-d_1)}}{1 + R_{12}(k)\tilde{R}_{23}(k)\mathrm{e}^{2ik_2(d_2-d_1)}}\,. \tag{7.5}$$

where

$$\tilde{R}_{23}(k) = R_{23}(k)\,, \tag{7.6}$$

because there is no any other layer lower than the third layer. The reflected wave or $B-$function and its corresponding seismic impedance for the three-layered medium are depicted in Figs. (7.5–7.6). For the six-layered medium, the reflection coefficient R_{12}

is recursively determined using Eq. (3.55) as

$$\tilde{R}_{12}(k) = \frac{R_{12}(k) + \tilde{R}_{23}(k)\mathrm{e}^{2ik_2(d_2-d_1)}}{1 + R_{12}(k)\tilde{R}_{23}(k)\mathrm{e}^{2ik_2(d_2-d_1)}}\,. \tag{7.7}$$

$$\tilde{R}_{23}(k) = \frac{R_{23}(k) + \tilde{R}_{34}(k)\mathrm{e}^{2ik_2(d_3-d_2)}}{1 + R_{23}(k)\tilde{R}_{34}(k)\mathrm{e}^{2ik_2(d_3-d_2)}}\,, \tag{7.8}$$

$$\tilde{R}_{34}(k) = \frac{R_{34}(k) + \tilde{R}_{45}(k)\mathrm{e}^{2ik_2(d_4-d_3)}}{1 + R_{34}(k)\tilde{R}_{45}(k)\mathrm{e}^{2ik_2(d_4-d_3)}}\,, \tag{7.9}$$

$$\tilde{R}_{45}(k) = \frac{R_{45}(k) + \tilde{R}_{56}(k)\mathrm{e}^{2ik_2(d_5-d_4)}}{1 + R_{45}\tilde{R}_{56}(k)\mathrm{e}^{2ik_2(d_5-d_4)}}\,, \tag{7.10}$$

and

$$\tilde{R}_{56}(k) = R_{56}(k)\,. \tag{7.11}$$

It can be noted that $\tilde{R}_{56}(k) = R_{56}(k)$ because there is no any other layer lower than the sixth layer. Here, the width b is also 0.5 and the seismic impedances are given as $\eta_1 = 1.0$, $\eta_2 = 1.5$, $\eta_3 = 0.9$, $\eta_4 = 1.3$, $\eta_5 = 1.0$ and $\eta_6 = 1.7$ for all the six layers described above. The results are plotted in Figs. (7.7–7.8). The reconstruction method of seismic impedances is excellent.

(b) Multi-interface medium with various widths

We test our model for only the three- and the six-layered media. In this case the widths are chosen as $b_1 = 0.5$, $b_2 = 0.7$, $b_3 = 0.6$, $b_4 = 0.3$, $b_5 = 0.8$ and $b_6 = 0.4$ while the designed seismic impedances resemble those given in the previous section. Figs. (7.9) and (7.10) depict the results of the three-layered medium while Figs. (7.11) and (7.12) show the results of the six-layered medium. The results are excellent. By comparing Figs. (7.5) and (7.9) as well as Figs. (7.7) and (7.11) we observe that the amplitudes

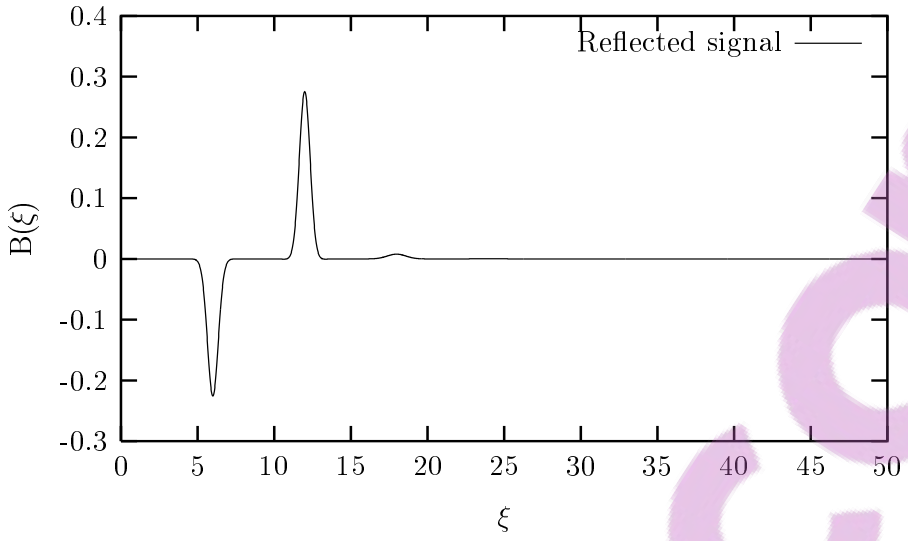

Figure 7.5: The reflected pulse for the three-layered medium with width $b = 0.5$.

of the positive side of the graphs are not equal. One can also compare the tails of Figs. (7.7) and (7.11) which also differ slightly. The deviations are the result of the various widths used for Figs. (7.9) and (7.11) as opposed to the common width used for Figs. (7.5) and (7.7).

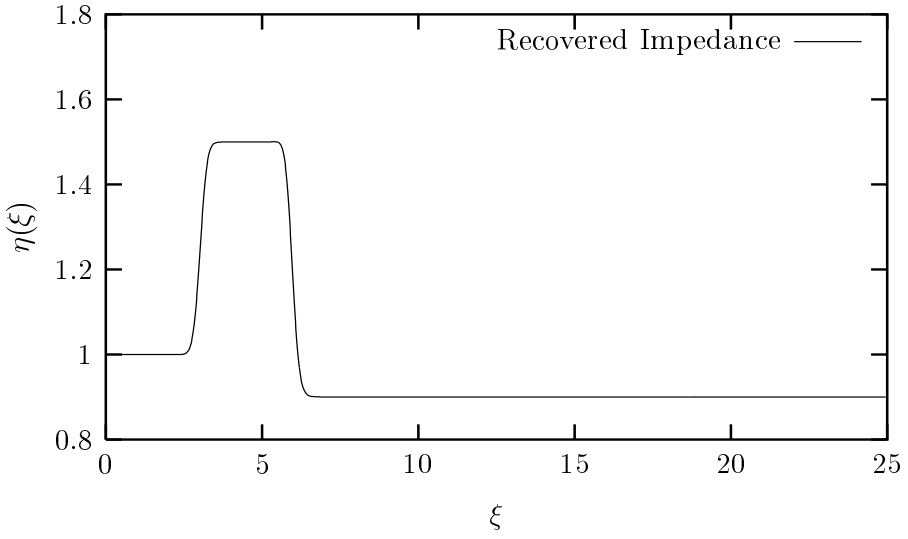

Figure 7.6: The reconstructed impedances from the input reflected signal of Fig. (7.5).

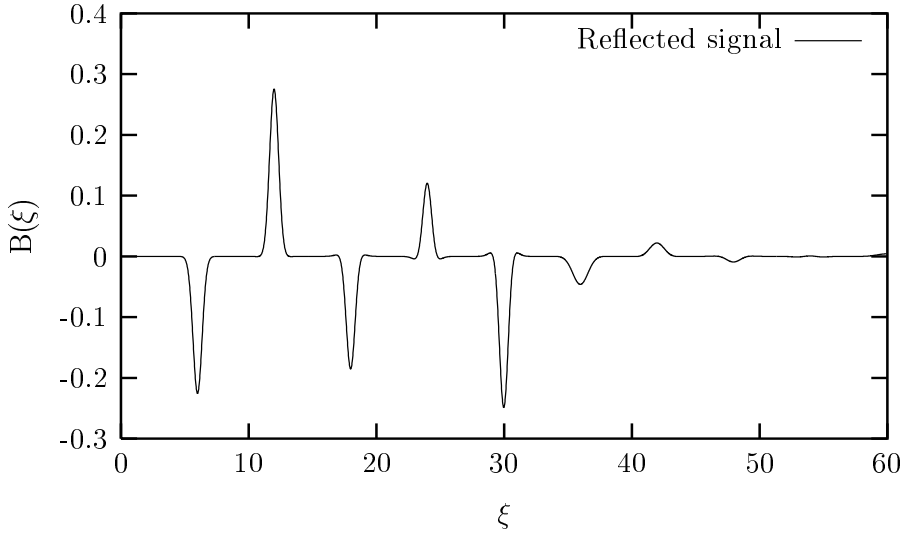

Figure 7.7: The reflected pulse for the six-layered medium with a common width $b = 0.5$.

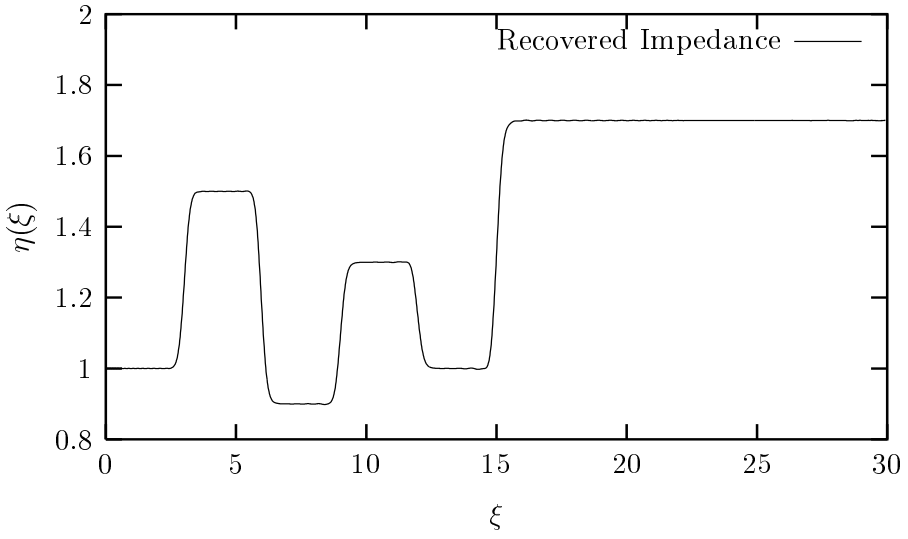

Figure 7.8: The reconstructed impedances from the input reflected signal of Fig .(7.7).

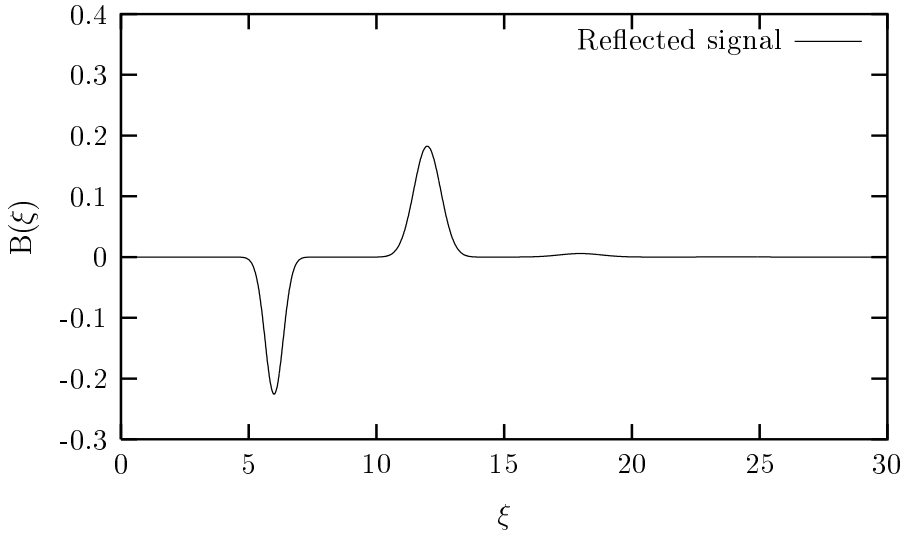

Figure 7.9: The reflected pulse for the six-layered medium with various widths.

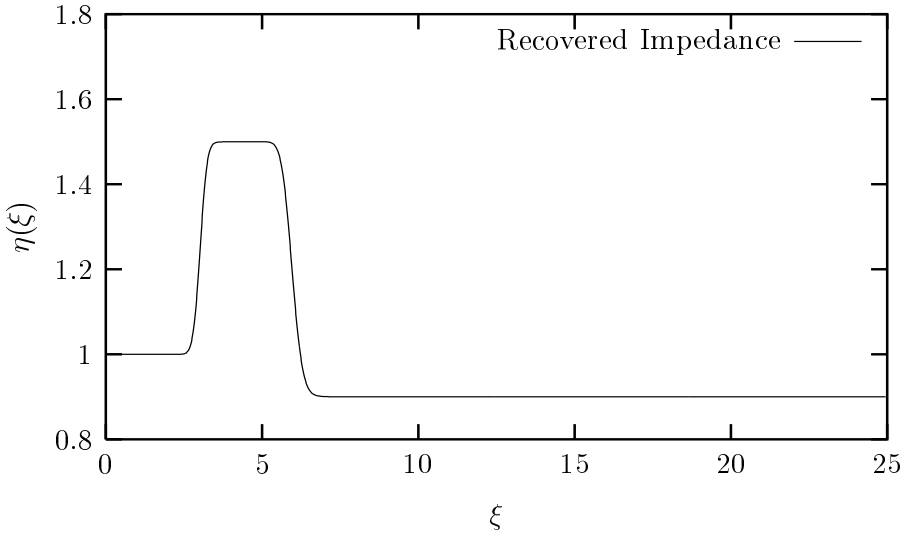

Figure 7.10: The recovered impedances from the input reflected signal of Fig. (7.9).

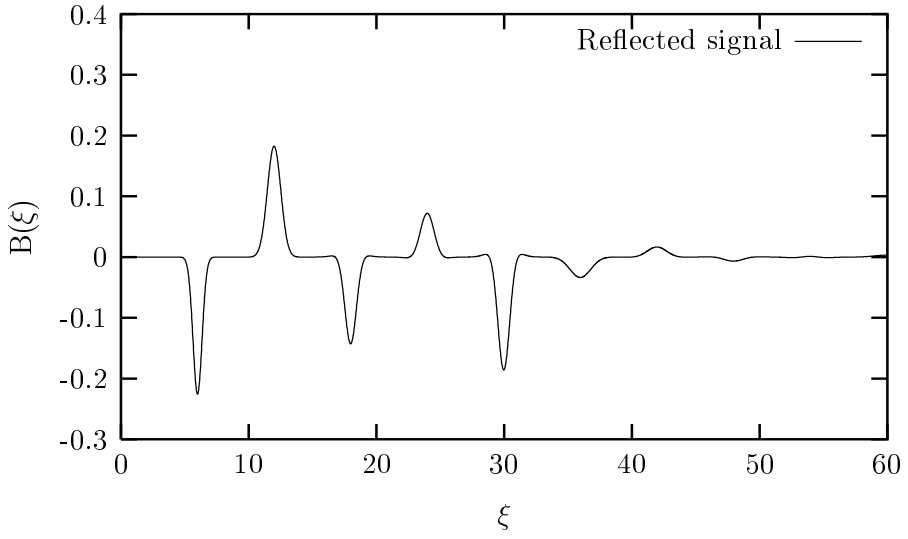

Figure 7.11: The reflected pulse for the six-layered medium with various widths.

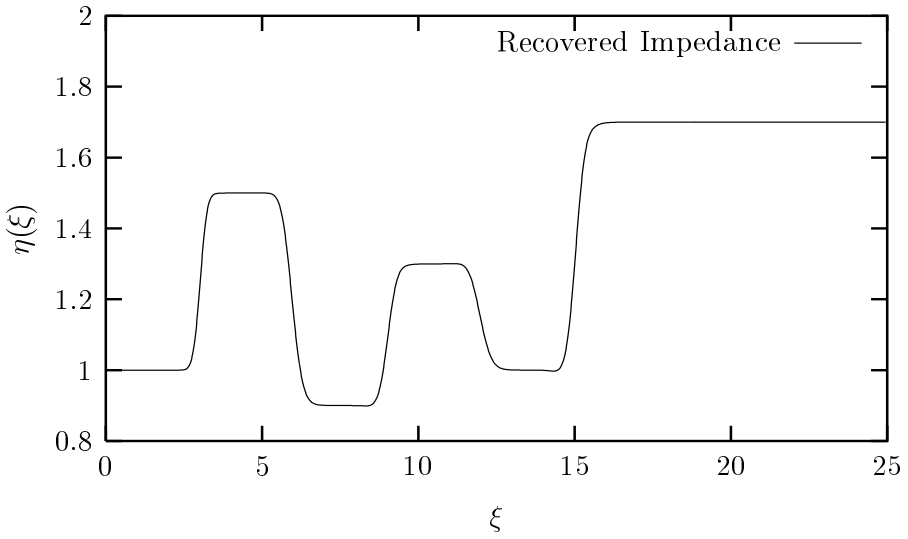

Figure 7.12: The recovered impedances from the input reflected signal of Fig. (7.11).

Chapter 8

Application III: Marine data

To examine the quality of our inversion model for obtaining the seismic impedance, we consider seismic reflection data from a deep water location in the North sea in which the seismic source was tracked by a ship which also dragged a multi-trace streamer consisting of array of hydrophones. These hydrophones record the seismic reflected traces after an airgun signal is sent to probe the layered Earth. The geophysical structure of the Earth can then be investigated through an analysis of the reflectivity sequence which describes the most important interfaces from the deep layers of the Earth.

8.1 Estimation of seismic impedance

In order to use the seismic reflection data for our purpose, the reflection events for different offsets at the same interface need to be reduced such that they coincide. This is the principle of normal move-out correction. Move-out correction generally assumes that the uncorrected reflection events lie along hyperbolic curves. This is true if the Earth is a constant velocity medium above the reflection.

The equation for the hyperbola is given by Ref. [53] (or any standard textbook).

$$\frac{v^2 t_x^2}{4z^2} - \frac{x^2}{4z^2} = 1\,, \tag{8.1}$$

from which

$$t_x = \sqrt{\frac{x^2}{v^2} + \frac{4z^2}{v^2}}\,, \tag{8.2}$$

where x represents the source-receiver offset, z denotes the thickness of the layer, v is the velocity of seismic waves and t_x stands for the two-way travel-time for offset distance x. Eq. (8.2) provides the travel-time curve of the reflections for the different offsets between source and receivers. For the two-way normal incidence time (t_0) we can write

$$t_0 = \frac{2z}{v}\,. \tag{8.3}$$

Upon using Eq. (8.3) we can write Eq. (8.2) in the form

$$t_x = \sqrt{t_0^2 + \frac{x^2}{v^2}}\,, \tag{8.4}$$

which is known as the normal move-out equation with t_0 being the zero-offset time. We illustrate the use of the blind deconvolution method on recorded marine seismic

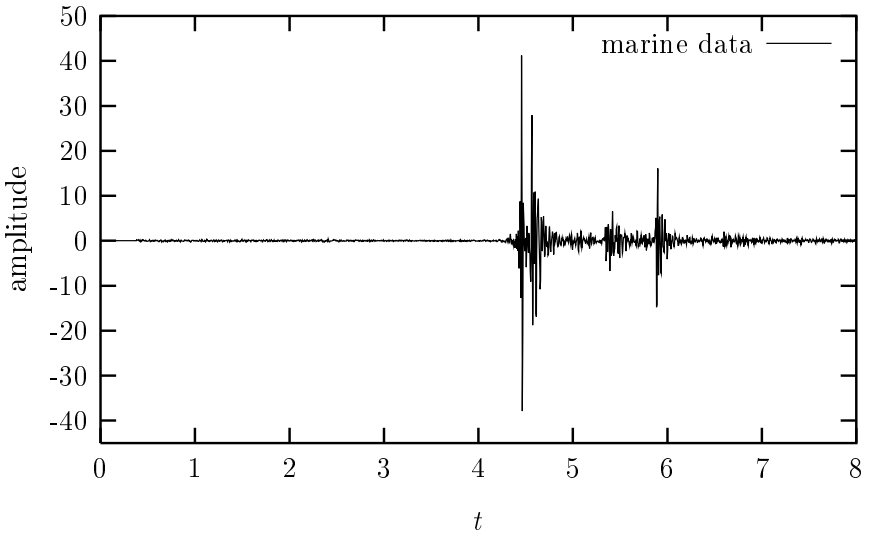

Figure 8.1: 1*st* seismic trace.

reflection data derived from a seismic survey in a deep water location in the North sea. We use linear interpolation to sample the traces at t-values not on the grid. The seismic reflection data used were collected with a streamer containing 240 hydrophone groups. The group interval is 15 m. The source-receiver offsets range from 940 m to 6069 m for a total of 240 seismic traces in the same axes. The sampling rate is 4 m s and the total length is 8 s. Each trace is composed of 2001 samples as shown in Figs. (8.1)–(8.4). Depicted in Fig. (8.5) is the seismic data-set of 240 recorded seismic traces. The seismic traces show only the travel-times. The individual seismic reflection data form a hyperbola. The hyperbolas on the far offset seismic traces are closer together as opposed to those on the near offsets. Thus, by using the normal move-out correction method we transform the offset seismic traces to zero-offset seismic traces. The migrated traces give the result shown in Fig. (8.6). The main modification as

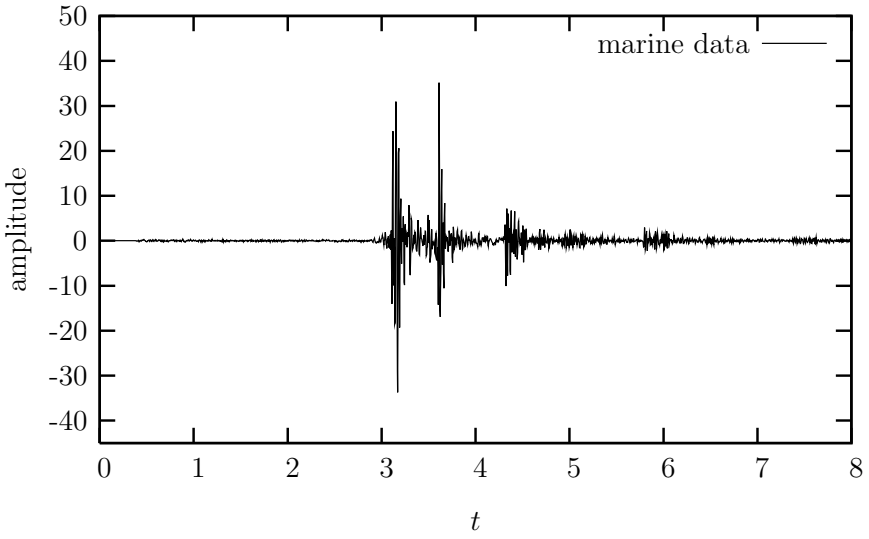

Figure 8.2: 90*th* seismic trace.

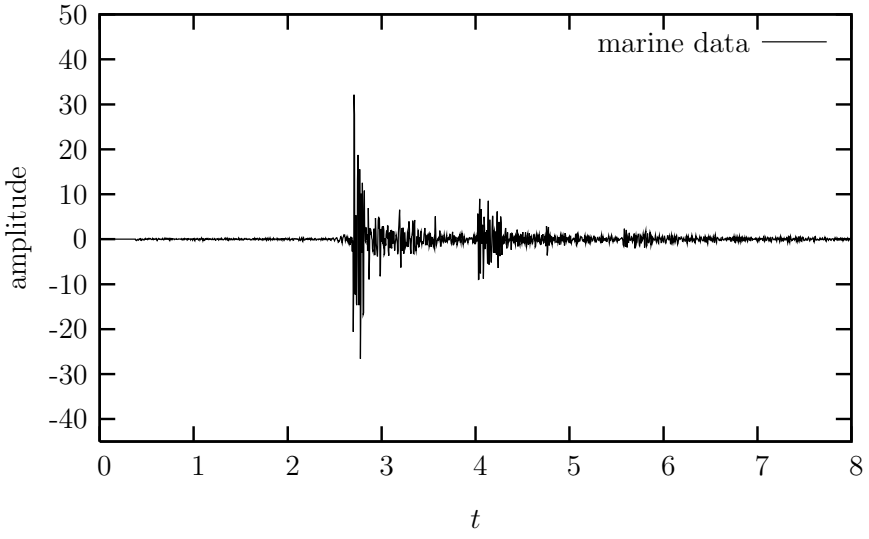

Figure 8.3: 120 *th* seismic trace.

compared to Chen's version [65] is that we assume a shape given by

$$s = [0.1,\ 0.4,\ 1.0,\ 0.4,\ 0.1]\,, \tag{8.5}$$

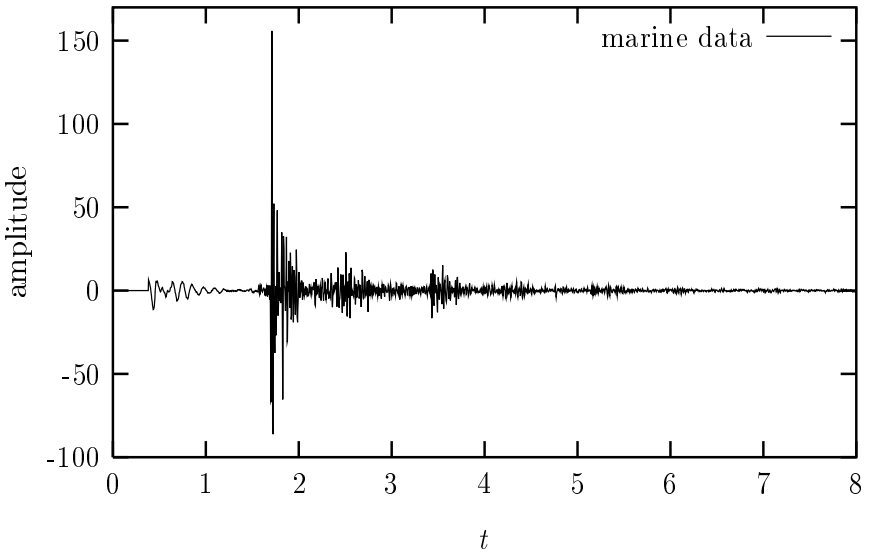

Figure 8.4: 240*th* seismic trace.

instead of pure spikes in order to obtain a narrow bell-shaped form to facilitate the numerical solution of the Marchenko inversion. This means that the observation model, Eq. (5.34), now becomes

$$z = h * s * x + n\,, \tag{8.6}$$

where s is a known shape. If the shape s is equal to unity then of course the original equation (Eq. (5.34)) is recovered. We use in our calculations the seismic data-set from Fig. (8.6). In addition we used all 150 migrated traces collectively as observed reflection data and modified the MCMC algorithm accordingly. Shown in Fig. (8.7) is the seismic wavelet extracted from the migrated seismic reflection data in Fig. (8.6). Fig. (8.8) depicts the statistically estimated reflection sequence corresponding to the seismic wavelet in Fig. (8.7). The estimated seismic impedance is shown in Fig. (8.9).

We also note that the observed seismic reflection data are not calibrated, that is, they only provide relative amplitudes. The details of the source of the signal, that is, the

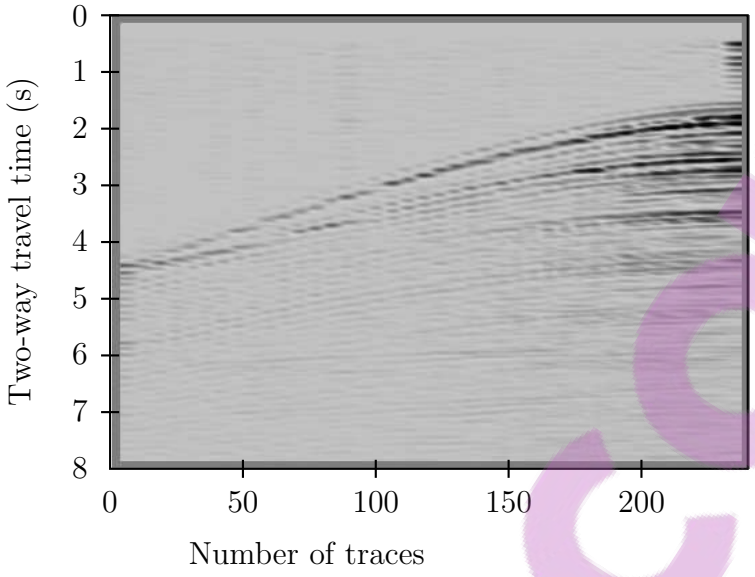

Figure 8.5: The seismic data without move-out correction.

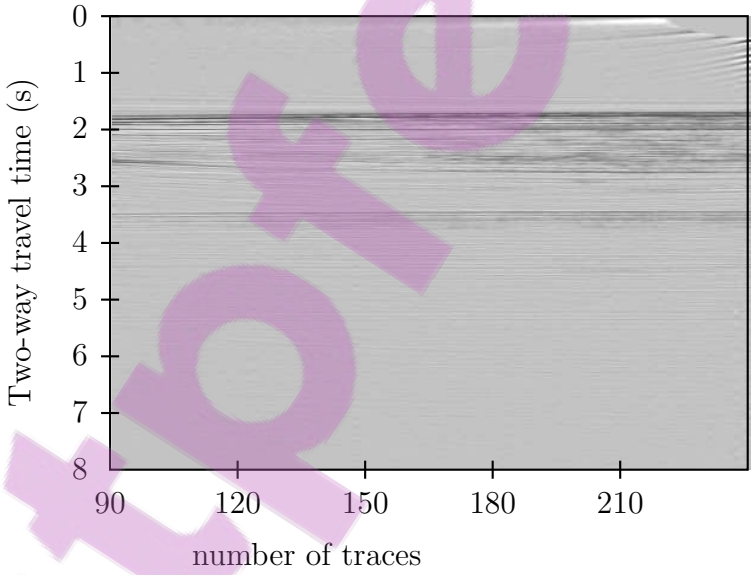

Figure 8.6: The seismic reflection data with move-out correction.

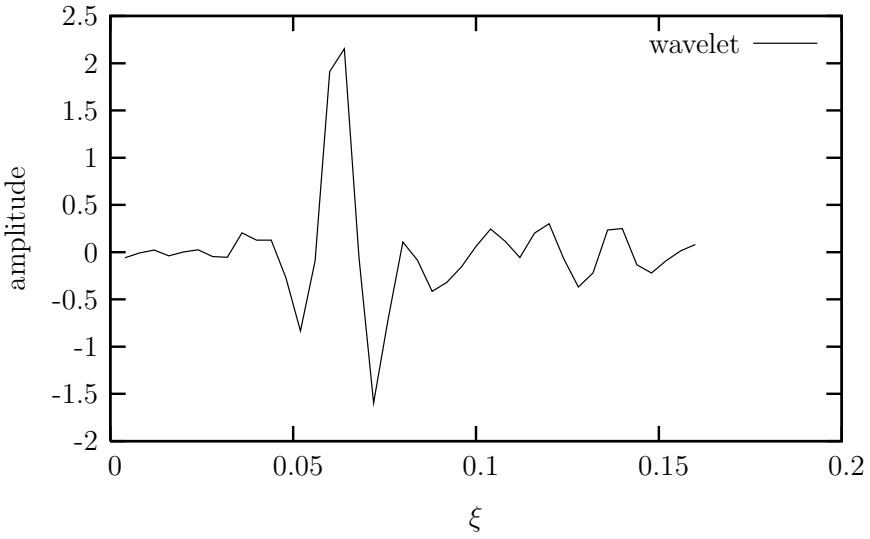

Figure 8.7: Seismic wavelet statistically estimated from a data-set in Fig. (8.6).

airgun, are also not known. Therefore, the reflectivity sequence that we obtain from the statistical procedure will be related to the unit response of the medium by a suitable factor. This calibration problem can be solved by using additional information, such as the seismic impedance jump at the ocean bottom if known via other means.

8.2 Scaling factor

8.2.1 (a) Sea bottom consisting of clay

As a first example we assume a sea bottom consisting of clay. For our purpose we model the sea floor as fluid so that only the compressional seismic wave can be supported. We assume that while the density changes, the velocity of $1500\,\mathrm{m\,s^{-1}}$ remains constant,

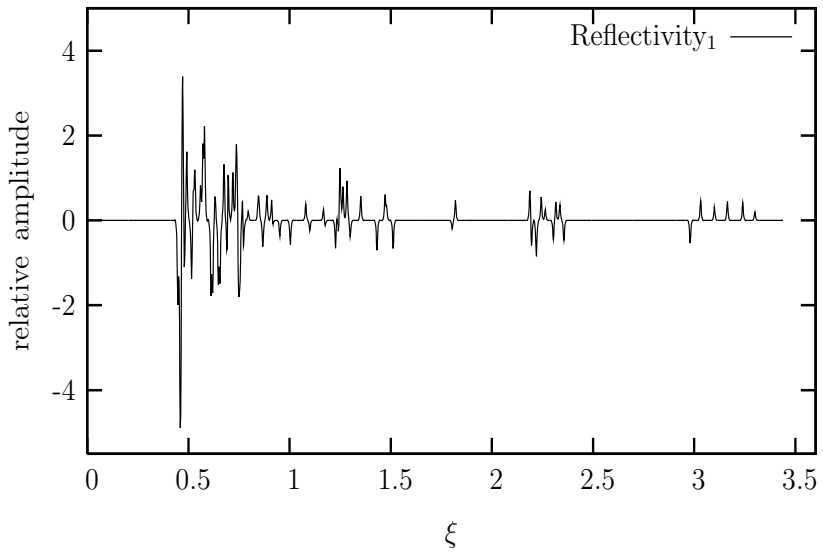

Figure 8.8: Statistically estimated reflectivity sequence corresponding to a seismic wavelet in Fig. (8.7).

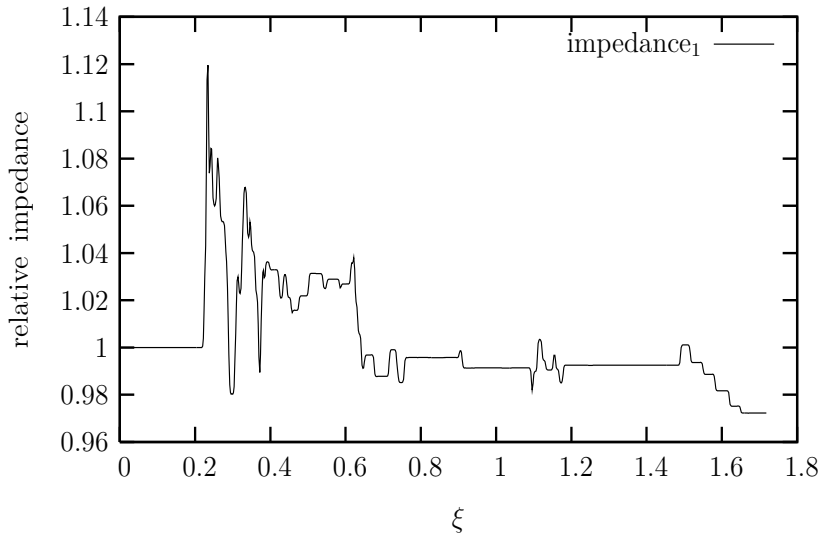

Figure 8.9: Estimated seismic impedance corresponding to a statistically estimated reflectivity sequence in Fig. (8.8).

that is, [50, 68, 69]

$$\frac{\rho_2}{\rho_1} = 1.5\,, \tag{8.7}$$

and

$$\frac{c_2}{c_1} = 1.0\,, \tag{8.8}$$

where $\rho_1 = 1000\,\mathrm{kg\,m^{-3}}$ is the density of the sea water, $\rho_2 = 1500\,\mathrm{kg\,m^{-3}}$ is the density of clay, $c_1 = 1500\,\mathrm{m\,s^{-1}}$ is the velocity of the seismic compressional wave in sea water and $c_2 = 1500\,\mathrm{m\,s^{-1}}$ is the velocity of the seismic compressional wave in clay. Thus, from Eqs. (8.7) and (8.8) we express the ratio of the seismic impedances as

$$\frac{\eta_2}{\eta_1} = \frac{\rho_2 c_2}{\rho_1 c_1} = 1.5\,, \tag{8.9}$$

where η_1 is the seismic impedance of the sea water and η_2 is the seismic impedance of clay. Assuming this value of the ratio η_2/η_1 we proceed to re-scale the amplitude of the estimated reflectivity sequence by a suitable factor of 3.53. This factor is obtained by scaling the amplitude of the input kernel into the Marchenko equation, such that the inversion procedure yields a first jump approximately equal to $\eta_2/\eta_1 = 1.5$. Figs. (8.10) and (8.11) show the reflectivity sequence scaled by a suitable factor of 3.53 and the corresponding estimated seismic impedance respectively.

8.2.2 (b) Sea bottom consisting of silt

If we assume that the sea bottom consists of silt (fine sand or soil) and that the density changes much more than the velocity (which does not change much), then the above procedure can be followed from which the value 1.785 of the ratio of the seismic impedances is obtained [50, 68, 69]. In Figs. (8.12) and (8.13) we show the reflectivity

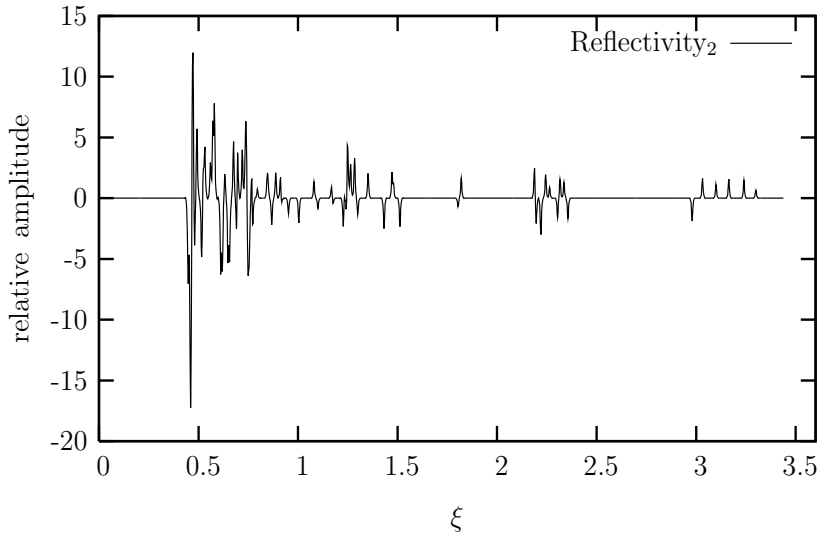

Figure 8.10: Scaled reflectivity sequence version of Fig. (8.8) when the sea bottom consists of clay.

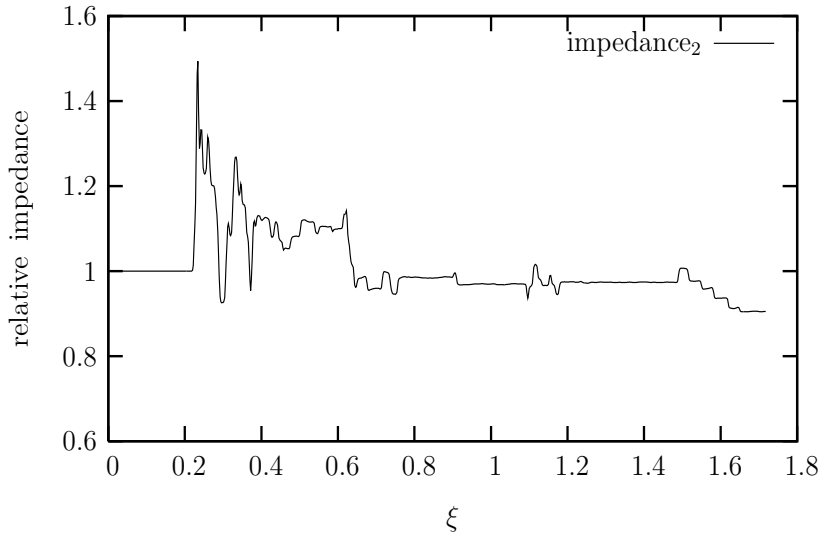

Figure 8.11: Estimated seismic impedance corresponding to the scaled reflectivity sequence in Fig. (8.10).

sequence and its corresponding estimated seismic impedance for this scaling factor respectively.

In Figs. (8.14) and (8.15) we observe the invariance of peak ranking and location of

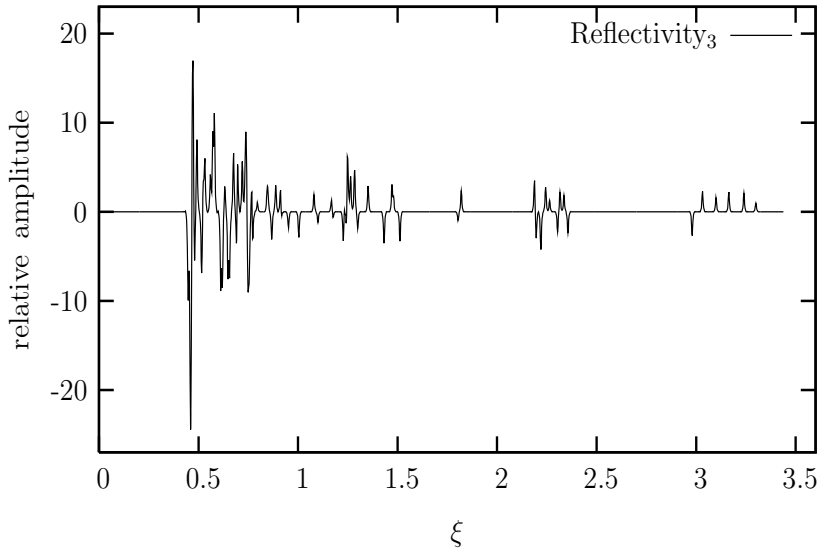

Figure 8.12: Scaled reflectivity sequence version of Fig. (8.8) for the case where the sea bottom consists of silt.

peaks between the estimated seismic impedances with and without a scaling factor. We also observe the same between the scaled seismic impedances as depicted by Fig. (8.16). Thus, we conclude that a lot of information can be retrieved even without knowledge of the proper scaling factor. The procedure has been implemented in Matlab codes using the freely available Octave software compatible with Matlab.

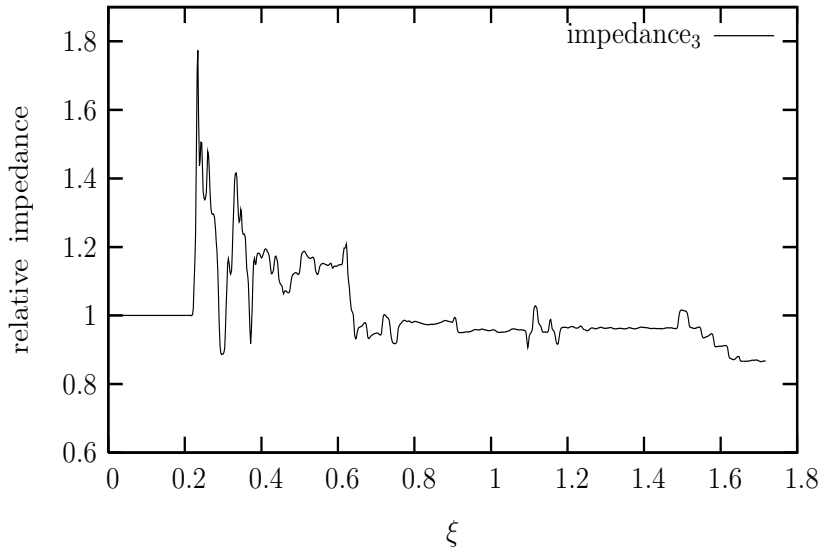

Figure 8.13: Estimated seismic impedance corresponding to the scaled reflectivity sequence in Fig. (8.12).

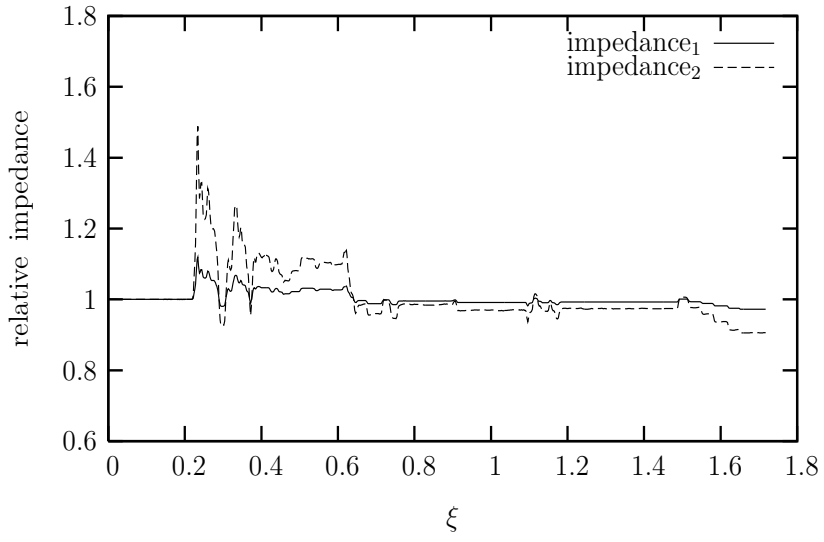

Figure 8.14: Comparison between the seismic impedance with a scaling factor (Fig. 8.11) and that without a scaling factor (Fig. (8.9).

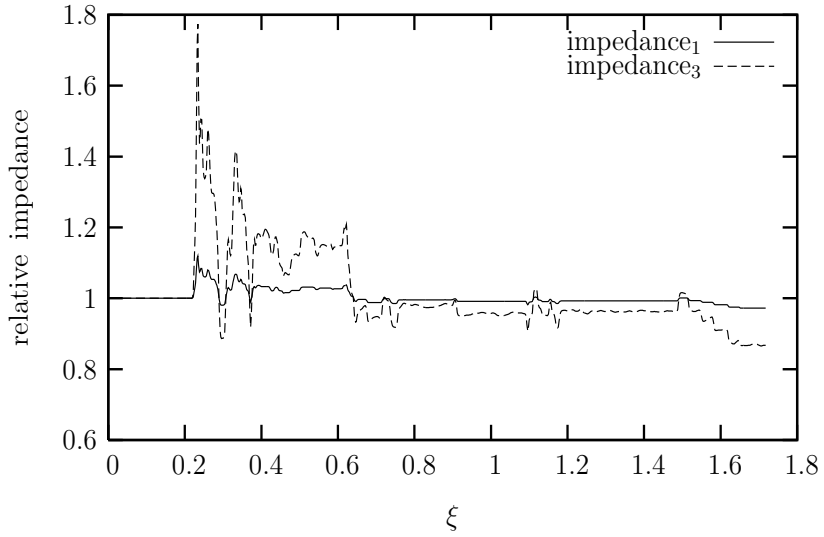

Figure 8.15: Comparison between a seismic impedance with a scaling factor (Fig. 8.13) with that without a scaling factor (Fig. (8.9).

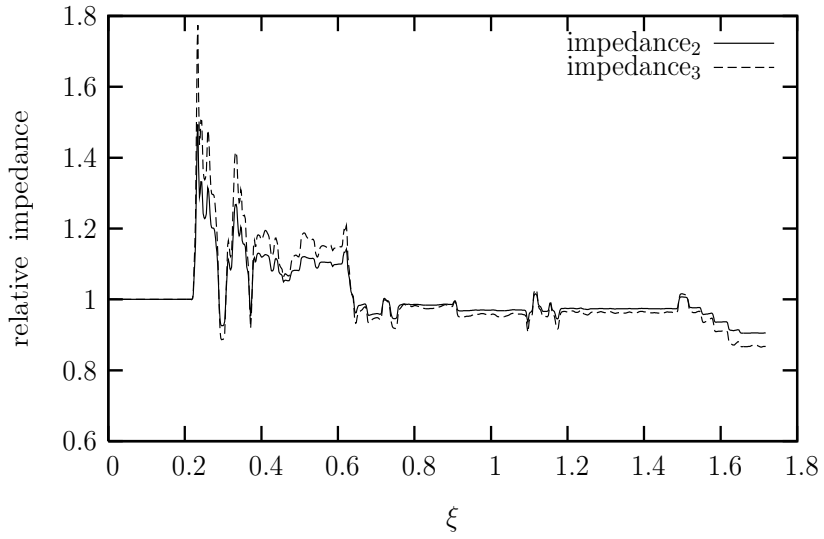

Figure 8.16: Comparison between the scaled seismic impedances in Figs. (8.11) and (8.13).

Chapter 9

Conclusions and directions for future work

In the following sections we summarize our results for the single and coupled channel inversion, synthetic seismic reflection data and marine seismic reflection data.

9.1 Single and coupled channel inversions

The solution of the inverse problem is to find the scattering potential from known scattering information. This presupposes the solution of the Marchenko integral equation in a reliable way. We have employed the Hermite interpolation polynomials and the collocation method to solve the MIE. These piecewise polynomials are nowadays widely employed in solving ill-posed integral and differential equations due to the fact that

they are analytically known, and that the underlying boundary conditions are easy to be rigorously included. The suitability of the collocation method is demonstrated by strong agreement between the reconstructed potentials and the original potentials in both the single and coupled channel cases. In all cases, the deviation of the reconstructed potential from the original potential is very small. The Marchenko integral equation has been solved numerically for a Gaussian potential, smooth square-type potential and a multi-layered potential in which the numerical algorithms have proved to be accurate, robust and efficient.

9.2 Synthetic seismic reflection data

Further to the above we have shown that our numerical method is suitable to obtain the seismic impedance of substrates by using reflection travel-time data in a one-dimensional medium. We have transformed the one-dimensional seismic wave equation into the one-dimensional Schrödinger-like equation.

As an application of our method we treated model cases with two-layered, three-layered and multi-layered media. The performance of the Marchenko inversion is illustrated through numerical experiments in these media with seismic impedances ranging from 0.9 to 1.7 for comparison with the reconstructed seismic impedances. Various reflection coefficients have been calculated from the known seismic impedances of the media. We have simulated the synthetic reflected field in a Gaussian form from the source placed in the surface of the layered medium. The values of the seismic impedances have been recovered to at least four decimals which is a good measure of the success of the

collocation method.

9.3 Marine seismic reflection data

We presented an MCMC method for estimating the seismic wavelet and reflectivity sequence under the Bayesian approach. The method involves the Bernoulli-Gaussian white sequence model for the reflectivity sequence. The method makes it thus possible to simultaneously estimate a plausible seismic wavelet and reflectivity sequence. However, because the marine seismic reflection data are not calibrated and the details of the source signal are not known, we related the acquired $B-$function (reflectivity sequence) to the unit response of the Earth medium by a suitable scaling factor. The Marchenko inversion has been found to be robust and provided satisfactory seismic impedance estimates. We observe the invariance of peak ranking and location of peaks which is an indication that a lot of information is available even without knowledge of the scaling factor.

Since our reconstructed reflectivity sequence and the seismic wavelet appear geophysically reasonable, the blind deconvolution of marine reflection data can be considered successful. Reconstruction of such a reflectivity sequence of Earth substrates might pave the way to a quantitative approach to geology and petrophysics for geophysicists and seismologists.

The field examples have demonstrated the practicability of our approach. The benefits

which may accrue from it are better reconstruction of seismic impedances and improved resolution of thin layers. The results we have obtained indicate that the extraction of the information about the seismic impedances that are coded into the measured seismic reflection traces is possible.

9.4 Directions for future work

In this thesis there are questions that remain to be investigated. We used equidistant points for our collocation method. Would it be better if values of the potential $V(x)$ were used to guide the partitioning? Do we need more points in areas where $V(x)$ varies rapidly and fewer points in areas where $V(x)$ varies slowly?

In seismic inversion the reflected wave is measured through a convolution model involving the seismic wavelet. Thus, the blind deconvolution is used, when the seismic wavelet is not provided, to simultaneously recover the reflectivity sequence and seismic wavelet. It would be good if the inversion procedure could also be applied to the handling of seismic reflection data from other seismic surveys.

Bibliography

[1] L.D. Faddeev, *Uspekhi Matem. Nauk* **14**, II, 57; English translation: *J. Math. Phys.* **4**, 72 (1963).

[2] I. Kay, *The inverse Scattering Problem*. New York: University Research Report, EM-74, 1955.

[3] I. Kay, *Comm. Pure Appl. Math* 13, 1960, p.371.

[4] Z. S. Agranovich and V. A. Marchenko *The Inverse Problem of Scattering Theory*. New York: Gordon and Breach, 1963.

[5] D. N. Gosh Roy, in *Methods of inverse problems of scattering Theory* , Gordon and Beach N.Y (1963) p.2, 4. D. N. Gosh Roy, in *Methods of inverse problems in Physics*, CRC Press, Boston, (1991).

[6] K. Chadan & P. C. Sabatier, *Inverse Problems in Quantum Scattering Theory*. Berlin, Heidelberg,

[7] F. Calogero and A. Degasperis, *Spectral Transform and Solitons*. Amsterdam, New York, OXFORD: North-Holland Publishing Co. 1, 1982.

[8] W. T. Wei, X. Xing and L. R. Xun, *Inverse Problems*, 3: 143-148, 1987.

[9] M. Korvi, *Numerical Algorithms for one-dimensional inverse scattering and Imaging*. Hilger, Bristol, Philadelphia, New York: Editors, M. Bertero & E.R. Pike, Eds. 1992.

[10] K. Chadan and P.C. Sabatier, in *Inverse Problems in Quantum Scattering Theory*, 2nd edition, Springer, Berlin, Heidelberg, N.Y (1982 and 1989).

[11] R.G. Newton, in *Scattering of waves and particles*, 2nd edition, Springer-Verlag Berlin, Heidelberg, N.Y (1982).

[12] D. L. Colton and R. Kress, *Inverse Acoustic and Electromagnetic Scattering Theory*. Berlin: Springer-Verlag, 1992.

[13] A. G. Ramm, *Multidimensional Inverse Scattering Problems*. New York: Longman Scientific and Wiley, 1992.

[14] K. Chadan, D. L. Colton, L. Paivarinta and W. Rundell, *An Introduction to Inverse Scattering and Inverse Spectral Problems*. Philadelphia: SIAM, 1997.

[15] I. Kay, *Comm. Pure Appl. Math*, **13**, 371 (1960).

[16] C.E. Frodberg, *Phys. Rev.* **72**, 519 (1947).

[17] E.A. Hylleraas, *Phys.Rev.* **74**, 48 (1948).

[18] V. Bargmann, *Rev. Mod. Phys.* **21**, 488 (1949).

[19] V. Bargmann, *Phys.Rev.* **75**, 301 (1949a).

[20] N. Levinson, *Kgl. Danske Videnskab. Selskab, Mat. Fys. Medd.* **25**, no. 9 (1949).

[21] V.A. Marchenko, *Dokl. Akad. Nauk S.S.S.R.* **72**, 47 (1950).

[22] V.A. Marchenko, Trudy Moscov. Matem. **1**, 327 (1952).

[23] R. Jost and W. Kohn, *Phys. Rev.***87**, 977 (1952), *Phys. Rev.* **88**, 382 (1952a).

[24] G. Borg, *11th Proc. Congress of Scandinavian Mathematics*, held at Trondheim, August, 1949, p.276.

[25] B. Holmberg, *Nuovo Cim.* **9**, 597 (1952).

[26] I.M. Gel'fand and B.M. Levitan, *Izvestia Akad. Nauk S.S.S.R Ser. Math.* **15**, 309 (1951).

[27] R. Jost and W. Kohn, *Kgl. Danske Videnskab. Selskab, Mat. Fys. Medd.***27**, 9 (1953).

[28] K.I. Hopcraft, in *An introduction to electromagnetic inverse scattering*, p. 2-3.

[29] R. Lipperheide, G. Reiss, H. Fiedeldey, S. A. Sofianos & H. Leeb, *Physica B* **190**, 1993 p 377-382.

[30] R. Lipperheide, G. Reiss, H. Leeb & S. A. Sofianos *Phys. Rev B*, 51, 1995, p.11032.

[31] M. Braun, S. A. Sofianos & R. Lipperheide, *Inverse Problems*, 11, 1995, L1-L3.

[32] S. A. Sofianos, M. Braun and H. Leeb, *Lecture notes in physics*, 488, 54, 1997.

[33] E. Kreyszig, in *Advanced Engineering Mathematics*, fifth edition, John Willey and Sons, 1983, p 844.

[34] K. Burrage, *A special family of Runge-Kutta methods for solving stiff differentials*, BIT, 18, 1978, p.22-41.

[35] G. J. Cooper, R. C. Butcher, *An iteration scheme for the implicit Runge-Kutta methods*, IMA J. Numer. Anal. 3, 1983, p. 127-140.

[36] E. Hairer, G. Wanner, *Algebraically stable and implementable Runge-Kutta methods of high order*, SIAM J. Numer. Anal. 18 1981, p. 1098-1108.

[37] W.H. Press, B.P. Flannery, S.A. Teukolsky and W.T. Vetterling, in *Numerical Recipes*, Cambridge University Press, (1989), p. 143-144, 147-152, 390-395.

[38] D. Bilgeri and A. Carlini, *Non-linear estimation of reflection coefficients from seismic data, Geophysical prospecting*, 1981, 29, 672-686.

[39] M. T. Silvia and E. A. Robinson, in *Deconvolution of geophysical time series in the exploration for oil and natural gas*, Elsevier Scientific Publishing Company, Amsterdam, 1979, p.IX, 1, 56-58.

[40] J. M. Mendel, *Optimal seismic deconvolution: An estimate-based approach*. New York: Academic, 1993.

[41] J. M. Mendel, *Maximum-Likelihood deconvolution: A journey into model-based signal processing*,. Berlin, Germany: Springer-Verlag, New York, Berlin, 1990, p. 4-15.

[42] J. Idier and Y. Goussard, *Multichannel seismic deconvolution*, IEEE Trans. Geosci. Remote Sensing, vol. 31, p.961-979, 1993.

[43] T. -J. Yu, P. C. Müller, G. -Z. Dai, and C. -F. LIn, *Minimum-variance deconvolution for noncausal wavelets*, IEEE Trans. Geosci. Remote Sensing, vol. 32, p. 513-524, 1994.

[44] J. Wang and N. Zabaras, *Hierarchical Bayesian models for inverse problems in heat conduction*, Inverse Problems 21, 2005, p. 183-206.

[45] C. Andrieu, N. D. Freitas, A. Douchet and M. I. Gordan, *An introduction to MCMC for machine learning* Mach. Learning, 50, 2003, p. 5-43.

[46] C. P. Robert, *The Bayesian choice*, New York: Springer-Verlag, 1994.

[47] A. Buland and H. Omre, *Bayesian wavelet estimation from seismic and well data*, Geophysics, Vol. No. 6, November-December 2003, p. 2000-2009.

[48] S. Geman and D. Geman, *Stochastic relaxation, Gibbs distribution and the Bayesian restoration of images*, IEEE Trans. Pattern. Anal. Mach. Intell., vol. 6 1984, p721-741.

[49] M. Wadati and T. Kamijo, *On the extension of inverse scattering method*, Progress of theoretical Physics, vol. 52, no. 2, August 1974, p. 397-414.

[50] F. B. Jensen, W. A. Kuperman, M. B. Porter, H. Schmidt, in *Computational ocean acoustics*, American Institute of Physics, New York, 1994, p. 41-54.

[51] *Plane wave propagation in a 2-half space medium*, http://utam.geophysics.utah.edu/ebooks/yuegg522/basicphysics /node8.html.

[52] K. Aki and P. G. Richards, in *Quantitative Seismology theory and Methods*, Vol. 2, W. H. Freeman and Company, San Francisco, 1980, p 4659-672.

[53] J. M. Reynolds, *An introduction to Applied and Environmental Geophysics*, John Wiley & Sons, Singapore, 1997, p. 218,226, 233, 360.

[54] W. C. Chew, in *Waves and fields in inhomogeneous media*, Van Nostrand, Reinhold, New York, 1990, p.49-52,532-547.

[55] I Tolstoy, in *Wave propagation*, McGraw-Hill, Inc.,1973, p.90.

[56] J. F Claerbout, in *Fundamental of Geophysical Data Processing* McGraw-Hill, New York, 1976, chaps. 8-9.

[57] H. R. Harrison and T Nettleton, in *Advanced Engineering dynamics*,John Wiley and Sons, New York, 1977, p. 128-129, 132-133.

[58] M. B. Dorbin, *Introduction to Geophysical prospecting*, 3rd edition, McGraw-Hill international book company, 1976, p.32-36.

[59] R. Burridge, in *Wave motion 2*, North-Holland Publishing Company, 1980, p.305-323.

[60] R. Caroll and F. Santosa, *On complete recovery of geophysical data*, Math. Methods Appl. Sci. 1981.

[61] S. Nettel, in *Wave Physics, Oscillations - Solitons - Chaos*. Berlin, Heidelberg: Springer-Verlag, 1992.

[62] I. Kay, *The inverse scattering problem when the reflection coefficient is a rational function* Inverse scattering papers: 1955-1963, Math. Sci. Press, 1982, p.219-241

[63] E. Anderson *et. al*, *LAPACK Users' Guide*, 3rd edition, Society for Industrial and Applied Mathematics, 1999.

[64] J. Kormylo and J. M. Mendel, Maximum-likelihood detection and estimation of Bernoulli-Gaussian processes, IEEE Trans. Inform. Theory, vol. IT-28, p.482-488, 1982.

[65] Q. Cheng, R. Chen, and T. -H. Li, *Simultaneous wavelet estimation and deconvolution of reflection seismic signals* IEEE Trans. Geosci. and Remote sensing, vol. 34, no. 2, March 1996, p. 377-384.

[66] A. Papoulis, Probability, random variables and stochastic processes. McGraw-Hill, New York, 1965 and 1984.

[67] S. V. Vaseghi, Advanced signal processing and digital noise reduction, John Wiley and Teubner, Chichester, New York, 1996 p. 66-67, 71-72.

[68] E. L, Hamilton, *Geoacoustic modeling of the sea flour*, J. Acoust. Soc. Am. Vol. 68, 1980, p. 1313-1340.

[69] E. L. Hamilton, *Acoustic properties of sediments*, in Acoustics and Ocean Bottom, edited by A. Lara-Sáenz, C. Ranz-Guerra and C. Carbió-Fité (C.S.I.C, Madrid, Spain, 1987), p. 3-58.